AN ABSTRACT OF THE THESIS OF

William E. Nichols for the degree of Master of Science in Civil Engineering presented on October 24, 1989.

Title: Land Surface Energy Balance and Surface Soil Moisture Variation in HAPEX-MOBILHY

Abstract approved: Redacted for Privacy

Dr. Richard H. Cuenca

The HAPEX-MOBILHY regional experiment provided an significant opportunity to analyze the partition of energy and distribution of water over land surfaces. The combination of remotely sensed data and ground instrument networks over the large-scale *in situ* experiment allowed investigation of spatial and temporal variation of such hydrologic parameters as the latent heat flux and surface soil moisture.

A literature review provided the fundamental physical theory for remote sensing detection of surface energy balance components and surface soil moisture. In instances where ground-based instruments were incorporated into the remote sensing approach, or were specifically of interest in the study, the appropriate theoretical background was also presented. The review identifies the approaches necessary for future attempts to model evaporative flux directly with combined remote-based and ground-based data collection systems.

Sensors and equipment used in the HAPEX-MOBILHY Program to monitor land surface hydrologic processes are identified and described. Algorithms were developed for use in computer processing of data collected by a passive microwave sensor, the Push Broom Microwave Radiometer.

The variation of the surface energy balance was examined through the use of the evaporative fraction, a ratio found to be relatively stable for daylight periods. The behavior of the evaporative fraction was examined with respect to location and meteorological conditions to determine its suitability for remote sensing applications.

Surface soil moisture variation was examined for two intensely instrumented ground sites in the HAPEX-MOBILHY experiment grid using passive microwave remote sensing. The relationship between passive microwave measurements and ground truth data was examined to attempt to calibrate the remote sensor. Factors which resulted in a weak relationship were examined.

The association between surface energy balance and soil moisture was examined using several soil moisture measurement techniques. This resulted in an understanding of the limitations of passive microwave remote sensing for use in measuring a state variable, moisture, as it pertains to evaporative flux estimation by remote-sensing techniques.

Several suggestions for additional research priorities in this field were made with future large-scale *in situ* experiments in mind. Opportunities to combine these research efforts with ongoing or planned projects are noted.

Land Surface Energy Balance and Surface Soil Moisture Variation in HAPEX-MOBILHY

by

William E. Nichols

A THESIS

submitted to

Oregon State University

in partial fulfillment of

the requirements for the degree of

Master of Science

Completed October 24, 1989

Commencement June 1990

APPROVED:

Redacted for Privacy

Associate Professor of Civil Engineering

Redacted for Privacy

Head of Department of Civil Engineering

Redacted for Privacy

Dean of Graduate School

Thesis presented by William E. Nichols

Date thesis is presented October 24, 1989

ACKNOWLEDGEMENTS

Many talented people contributed to the research that is embodied in this paper and deserve recognition. The most significant support came from Dr. Richard H. Cuenca (Associate Professor, Oregon State University). It was Dr. Cuenca who attracted me to graduate study, guided my education, and stimulated my interest in scientific research. His vision, encouragement, and example will guide my career for many years to come.

I am also deeply indebted to Dr. Thomas J. Schmugge for his cooperation in obtaining the remote sensing data crucial to this research. Also to his agency, the USDA Agricultural Research Service National Hydrology Laboratory, for funding this investigation. This study would not have been possible without this financial and scientific support.

My graduate committee, Dr. Peter Klingeman, Dr. David Myrold, and Dr. David Thomas, all merit appreciation for their time and suggestions.

Thanks are due to Dr. Larry Mahrt (Professor, Dept. of Atmospheric Sciences, Oregon State University) and Wayne Gibson (Research Assistant, Dept. of Atmospheric Sciences, Oregon State University) for extending services and VAX computer time for transfer of the remote data examined in this paper. Also to Dr. Joel Noilhan (Centre National Recherche Météorologique, Toulouse, France) for reviewing the thesis manuscript and for his insightful suggestions.

Finally, for editing the manuscript as well as for enduring the long road to a graduate degree, I owe my eternal thanks to my wife, Michelle.

Some work was completed at the USDA-ARS National Hydrology Laboratory. The bulk of the research effort was completed at Oregon State University using the facilities of the Water Resources Engineering Team. This investigation was funded under USDA-ARS Specific Cooperative Agreement Number 58-3K47-9-006, "Water Budget Studies With HAPEX-MOBILHY."

TABLE OF CONTENTS

LIST OF FIGURES

LIST OF TABLES

Land Surface Energy Balance and Surface Soil Moisture Variation in HAPEX-MOBILHY

1 INTRODUCTION

1.1 Background

Evaporative flux from land surfaces constitutes an important component of the hydrologic cycle, second only to precipitation in total quantity (Linsley *et al.*, 1982). Quantifying evaporative flux is essential for many hydrologic management and planning requirements at scales ranging from regional to field or local. Meeting the challenges imposed by increasing population and the specter of global climate change requires an improved understanding of this hydrologic process at several scales.

The largest scale of interest is regional, which allows for examination of global processes (Eagleson, 1986). Concern over potential global climatic change resulting from the "greenhouse effect" has revealed the need for better understanding of land surface processes on a regional scale. Tools such as General Circulation Models (GCM's) require that hydrologic processes be quantified on the regional scale. These models are used in the scientific community to predict future climate trends and rates of change, and to assess the potential impact of large scale environmental changes. Atmospheric modeling efforts are also conducted at this scale, where land surface fluxes constitute the lower boundary condition. To reduce the large uncertainty in such models, several large-scale field experiments have been conducted and more are planned (André *et al.*, 1986; Sellers *et al.*, 1989; NASA, 1988).

At the watershed scale, quantification of hydrologic processes, including water flux from land surfaces, is necessary to provide information for constructive basin management decisions. The hydrologic response characteristics of an entire watershed are largely determined by evaporation at this scale.

In agricultural regions where irrigation is used to enable or enhance food and fiber production, quantification of evaporative flux at field scales is central to improving irrigation system design and operation. As a major water consumer, the agricultural community will

most likely have to make optimum use of water resources in the presence of increased demand for limited, potentially shrinking supplies. Achieving this requires improved irrigation system design and operation, which in turn requires accurate information about crop water consumption.

Modern interest in quantification of the natural phenomena of evaporation from land surfaces began with the Penman equation (Penman, 1948). This combination method used aerodynamic and energy balance approaches to estimate evaporation with measured meteorological parameters. Since Penman's development, many improvements and advances have been made following this general approach with surface data. Some of these methods are reasonably accurate and have high temporal resolution, but suffer from a poor spatial resolution. In general, accuracy of an evaporation estimate improves in proportion to the number of physically significant data parameters required by the estimating method. For this reason, obtaining modest accuracy in such an estimate requires relatively expensive instrumentation. This expense prevents the spatial replication necessary to use these techniques on a field by field basis.

Remotely sensed data have the potential to extend point measurements to a larger spatial scale. Technology used to collect required data exists and is well understood. Techniques to apply this knowledge to obtain accurate measurements of evaporative flux are needed and have been the focus of extensive research. This study is directed toward analysis of both remote- and ground-based data to develop the potential of remotely sensed data for land surface hydrologic measurements.

1.2 Objectives

This project's overall objective is to examine the partition of land surface energy in order to better quantify evaporative flux using remote- and ground-based data. The specific objectives of this project are:

1. Analyze the proportion of surface energy used for evaporation at overflight times as measured with ground instruments. Determine if this proportion is suitable for extension of remotely sensed instantaneous measurements of land surface fluxes to daily values. Distinguish between ideal and non-ideal surface energy balance conditions in the analysis to determine strength of the relationship with respect to irregular energy availability.
2. Examine the spatial and temporal variability of surface soil moisture in HAPEX-MOBILHY, focusing on its constraining influence on the partition of surface energy.
3. Determine if a relationship exists between surface soil moisture detected by passive microwave remote sensing sensors and the surface energy balance. If no relationship, or a weak one, is found examine other soil moisture data to explain this result.

The first objective is undertaken because of the considerable interest that exists in inferring the quantity of evaporation over a period of time from instantaneous remote sensing measurements. Soil moisture is an important variable to study because the surface energy partition is directly affected by moisture availability. The potential for passive microwave to monitor soil moisture is an important area of hydrologic research requiring more investigation. The third objective is aimed at determining the strengths, or weakness, of using passive microwave remote sensing to measure a state variable (moisture) for quantifying energy-vapor transport processes over land surfaces. The focus of attention is on the effects of vegetation on moisture availability and the surface energy balance. Accomplishing these objectives will expand the ability to monitor land surface processes with remote sensing techniques.

1.3 Data

Data collected in the HAPEX-MOBILHY Program[1] provide the opportunity to examine land surface energy fluxes. This program was directed at the study of the hydrologic budget

1 Hydrologic Atmospheric Pilot Experiment - Modélization du Bilan Hydrique. A large-scale field experiment conducted in southwest France. See André *et al.*, 1986; 1988 for an overview of the program.

and evaporation flux at the scale of a GCM grid square, i.e., 10^4 km^2 (André *et al.*, 1988; 1989). The location of the experimental area in southwest France is shown in Figure 1.1. Extensive ground and remotely sensed data, both aircraft and satellite based, were collected during the Special Observation Period (SOP) of 7 May to 15 July 1986.

Three characteristics of the HAPEX-MOBILHY database make it particularly appropriate for the objectives of this research. These characteristics include diversity of surface cover, large spatial scale, and extent of coordinated ground and remote data. The first characteristic, diversity of surface cover, is important because it facilitates improved understanding of physical phenomena in heterogeneous conditions. In HAPEX-MOBILHY the project area included both forested and agricultural regimes, and instrumented ground sites included four different crop covers. The second characteristic, large spatial scale, is essential because such scales are characteristic of remote sensing. The GCM-scale of HAPEX-MOBILHY was commented on previously, and is suitable in this respect. The final characteristic, extent of coordinated ground and remote data, is crucial to the calibration and verification of remote sensing techniques. In HAPEX-MOBILHY, the extent of coordinated remote- and ground-based data is evident in the variety of instruments employed in monitoring the experiment area. Mesoscale networks of ground instruments were used to sample surface fluxes. Among these were twelve SAMER[2] stations used to monitor the surface energy balance on a 15-minute interval (André *et al.*, 1988). Another ground network consisted of fourteen neutron probe access tube sites used to monitor soil profile moisture content on a weekly interval (Cuenca and Noilhan, 1988; Goutorbe *et al.*, 1989). All twelve SAMER station sites coincided with neutron probe monitoring locations. Remote and atmospheric sensing instruments were carried aboard a National Atmospheric and Space Administration (NASA)[3] C-130 aircraft, a National Center for Atmospheric Research (NCAR) King-Air aircraft, and several satellite platforms available during the experiment. The platform of interest in this study is the NASA C-130, configured for HAPEX-MOBILHY with the NS001 Thematic Mapper

---

2 Systéme Automatique de Mesure de l'Evapotranspiration Réele. See Bessemoulin *et al.*, 1986 for a complete overview of the SAMER network.

3 NASA C-130 Research Aircraft. Some aircraft characteristics include 6,100 m (20,000 ft) maximum altitude, and 7.0 hour flight endurance (NASA, 1988).

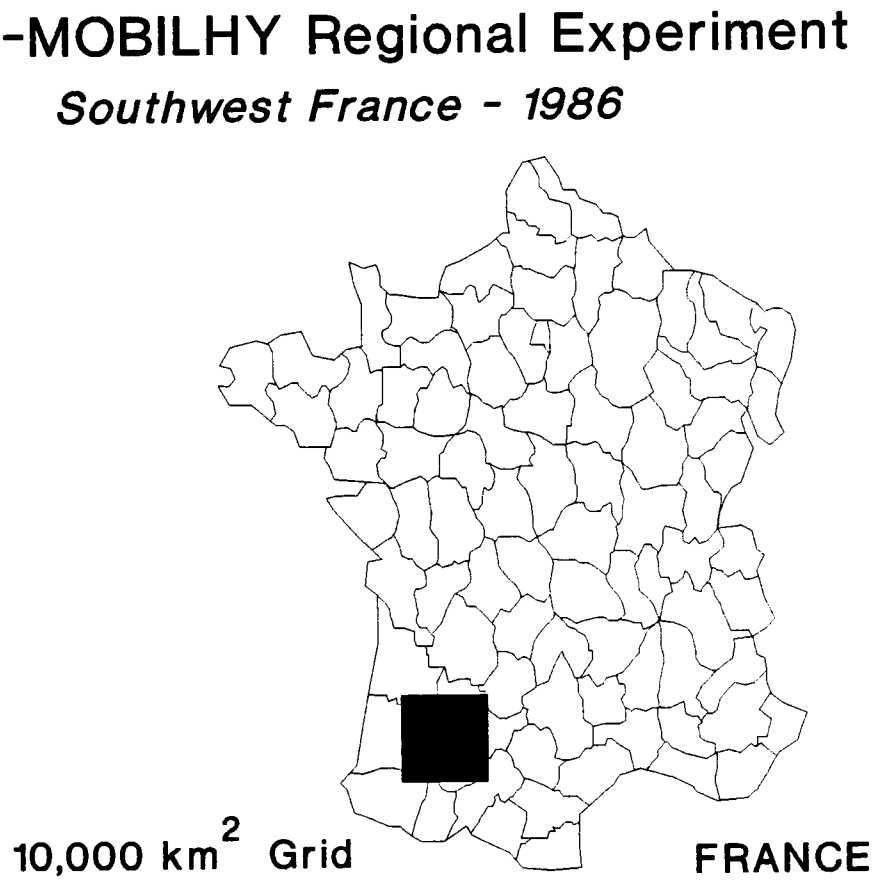

Figure 1.1 Location of the HAPEX-MOBILHY 10^4 km^2 experiment grid in Southwest France.

Simulator (TMS), the Push Broom Microwave Radiometer (PBMR), the Thermal Infrared Multispectral Scanner (TIMS), the PRT-5 Micron Non-scanning Radiometer, and a 9-inch color infrared nadir-viewing video camera (Schmugge and Janssen, 1988).

The promise of this diverse, large-scale, coordinated data collection for study of evaporative flux from land surfaces is evident in the above discussion. The task of this study is to use the data available from the HAPEX-MOBILHY Program to examine the surface energy partition and fulfill the outlined objectives.

2 REVIEW OF LITERATURE

Significant research has been devoted to the use of remote sensing techniques to monitor land surface processes. Part of the interest in use of remote sensing is due to the difficulty that has been experienced in the use of ground-based methods to measure quantities that have a high spatial variability. This section presents a review of fundamental theory and research related to quantification of evaporative flux using remote sensing techniques.

Remote-based measurements are not a replacement for ground-based measurements. Remote sensing techniques require calibration and validation using "ground truth." In the measurement of land surface fluxes, it is impossible to measure several key variables, such as incident solar radiation, using remote sensors. Such key variables can be measured accurately with ground-based instruments and may be extrapolated on a limited basis. Ground-based sensors can accurately measure all variables required for evaporative flux estimation, but only for a local area. Thus each method suffers from a scale resolution problem: ground-based methods may have high temporal resolution but are essentially a spatial point measurement. Conversely, remote sensing methods may have high spatial resolution but are instantaneous point measurements in time.

Spatial and temporal resolution are functions of the particular instrumentation and methods applied. For ground-based methods the temporal resolution may range from minutes to days or weeks. For remote sensing methods the spatial resolution is a function of the optical-mechanical properties of the sensor and the altitude of the sensor above the Earth. For example, the Thematic Mapper (TM) carried aboard LandSat 4 and LandSat 5[4], orbits at an nominal altitude of 705-km providing a resolution of 30-m. The Thematic Mapper Simulator (TMS) is a nearly identical aircraft-borne version of this sensor which provides a 3.75-m resolution when flown at 1.5-m altitude. Geostationary satellites are an exception to the limited temporal resolution of remote sensing. These satellites provide continuous coverage of a single portion of the Earth. To attain a geostationary position however requires that the

4 LandSat 4, 5 - Earth resources monitoring satellites. These satellites are equipped with the older Multispectral Scanner (MSS) used in earlier LandSat satellites and Thematic Mapper (TM) multispectral sensor. LandSat 4 and 5 are in sun-synchronous orbits at a 705-km nominal altitude, with a 16 day repeat cycle (Lillesand and Kiefer, 1986).

satellite orbit at high altitude, e.g. 36,000-km for an equator-synchronous orbit, resulting in very low spatial resolution. These sensors are mostly used for meteorological purposes and in snow extent mapping.

Measuring land surface fluxes with high spatial *and* temporal resolution requires both remote- and ground-based measurements. In this Review of Literature ground-based and remote-based methods are reviewed separately for convenience, but the combined use of these methods will play an important role in future resource analyses.

2.1 Ground Based Measurement Methods

The ground based approach for measuring evaporative flux can be segregated into four different methods (Hatfield, 1988). These are (a) combination methods with canopy resistance, (b) surface energy balance, (c) eddy correlation, and (d) soil water simulation models. All four methods were applied in one manner or another in the HAPEX-MOBILHY Program. Interest here focuses on the surface energy balance and soil water simulation methods which were employed in HAPEX-MOBILHY by the SAMER stations, and the hydrologic balance model employing neutron probe data (Cuenca, 1988a).

2.1.1 Surface Energy Balance

The energy balance of the Earth's surface can be assumed to be comprised of four major fluxes. Energy available at the Earth's surface is derived from absorbed solar and terrestrial radiation, the combination of which is termed net radiation. Net radiation is taken as positive when absorbed radiation components exceed emitted and reflected components. Energy transfer to or from the Earth is termed soil heat flux, and is taken as positive when the soil is warming. Energy transfer to or from the atmosphere not associated with water vapor movement is termed sensible heat flux, taken as positive when the atmosphere is warming. Finally, energy transfer that is associated with water vapor movement is termed latent heat flux,

taken as positive when water vapor is transported from the surface to the atmosphere. The mathematical relationship encompassing these four terms is given by the surface energy balance equation

$$R_n = L_e E + H + G \tag{2-1}$$

where

R_n = net radiation, $W \cdot m^{-2}$, positive downward

L_e = latent heat of evaporation/condensation, $\approx 2.45 \times 10^3 J \cdot g^{-1}$

E = evaporation/condensation rate, $g \cdot m^{-2} \cdot s^{-1}$, positive when evaporation is occurring.

H = sensible heat flux, $W \cdot m^{-2}$, positive when air is warming.

G = soil heat flux, $W \cdot m^{-2}$, positive when soil is warming.

The product $L_e E$ is the latent heat flux, expressed in $W \cdot m^{-2}$.

A well known term in the study of evaporative flux is the Bowen ratio, defined as the ratio of the sensible heat flux to the latent heat flux;

$$\beta = \frac{H}{L_e E} \tag{2-2}$$

where

β = Bowen ratio, dimensionless

H = sensible heat flux, $W \cdot m^{-2}$

$L_e E$ = latent heat flux, $W \cdot m^{-2}$

The Bowen ratio is known to vary over a very wide range (Ayra, 1988). Another parameter derived from sensible and latent heat fluxes is the evaporative fraction (Shuttleworth *et al.*, 1989), defined as

$$EF = \frac{L_e E}{H + L_e E} \tag{2-3}$$

where

EF = evaporative fraction, dimensionless

$L_e E$ = latent heat flux, $W \cdot m^{-2}$

H = sensible heat flux, $W \cdot m^{-2}$

The EF is presented by FIFE[2] researchers to characterize the surface energy balance over the FIFE project area. Shuttleworth *et al.* (1989) found a strong correlation between the value of the evaporative fraction at midday and the daytime average value for the four "golden days" of the FIFE study in 1987. This result is considered "potentially useful from a remote sensing standpoint, since it implies that the daytime average evaporative fraction might be an entity which is adequately deduced from a single, instantaneous (remote sensing) measurement."

The common approach for ground based measurement systems is to measure R_n, H, and G first and then compute the latent heat, or evaporative flux, as a residual. Two fluxes, net radiation and soil heat flux, can be directly measured. Net radiation is sometimes calculated based on measured solar radiation or sunshine hours, coupled with the saturated vapor pressure deficit of the atmosphere and air and surface temperatures (Cuenca, 1989). It is occasionally measured using a net radiometer. The soil heat flux is measured with a soil heat flux plate or a combination of a soil heat flux plate and thermocouples. Few methods exist for directly measuring sensible heat flux. One of these is the eddy correlation method. In place of

---

2 FIFE - First ISLSCP Field Experiment. ISLSCP is an acronym for the International Satellite Land Surface Climatology Program. The FIFE program involved a detailed study over a 15-km by 15-km grassland area in the Konza Prairie Reserve, Kansas. The objective was to determine the extent to which surface parameters could be determined from remotely sensed data (Sellers *et al.*, 1989)

a direct measurement of sensible heat flux, several methods are available. These include the bulk transfer method, the gradient or aerodynamic method, and the profile method (Ayra, 1988). The approach used for the data available to this study involved an aerodynamic method. The sensible heat flux can be represented by a Newtonian rate equation;

$$H = \frac{\rho c_p (T_s - T_a)}{r_{ah}} \tag{2-4}$$

where

ρ = density of air, $kg \cdot m^{-3}$

c_p = volumetric heat capacity of air, $J \cdot kg^{-1} \cdot K^{-1}$

T_s = surface temperature, $°C$

T_a = air temperature, $°C$

r_{ah} = aerodynamic resistance for sensible heat transfer, $s \cdot m^{-1}$

The driving force of heat transfer in equation (2-4) is the temperature gradient from the surface to the atmosphere, and the resistance to heat transfer is expressed by r_{rh}. Direct use of equation (2-4) to compute H requires surface and air temperature measurements and some means of measuring or estimating the aerodynamic resistance.

The aerodynamic resistance is dependent on wind speed and surface roughness. This dependence makes this parameter the most difficult to evaluate, limiting the utility of equation (2-4). However, measurement of these parameters can be avoided by using a gradient or aerodynamic method. This involves making measurements at two or more heights well above the top of the roughness regime but within the atmospheric surface layer. The sensible heat flux is computed from the heat flux across the gradient, taking into account the stability conditions of the atmosphere. This is the method used by the SAMER stations in HAPEX-MOBILHY. The SAMER system's aerodynamic approach to computing sensible heat flux is discussed more fully in Section 3.1.1, SAMER System.

2.1.2 Soil Water Balance

The energy balance discussed in the previous section is required to obtain measurement of surface fluxes in small time increments, such as in 15-minute or daily intervals. A different approach based on a long-term water balance can be used to provide an independent check on evaporative flux from a site. This approach involves application of the classical principal of conservation of mass which states that the mass can not be created or destroyed. Mathematically;

$$\frac{d(\delta m)}{dt} = 0 \tag{2-5}$$

where

m = mass, kg

t = time, s

When the mass conservation principal is applied to water, the technique is traditionally identified as a hydrologic balance. The soil water balance approach is a hydrologic balance which treats precipitation and irrigation as inputs, soil moisture as a storage term, and drainage, deep percolation, runoff, and evaporation as outputs. The normal approach is to measure or estimate all other terms and compute evaporation as a residual. The hydrologic balance over a particular time period is expressed as

$$W_a + E + D + \Delta\Theta_v = 0 \tag{2-6}$$

where

W_a = applied water, either precipitation or irrigation

E = evaporation from the soil and canopy surface

D = drainage, deep percolation, and runoff

$\Delta\Theta_v$ = change in soil moisture during the time period

All of the above terms are expressed as volumes or equivalent depth of water. The applied water term is commonly measured with a rain gage or similar device. Prior knowledge of soil characteristics, particularly field capacity, allow estimates of drainage, deep percolation, and runoff to be made with a certain degree of confidence. Soil moisture can be measured using a variety of techniques including tensiometric, gypsum block, or neutron scattering (Cuenca *et al.*, 1988; Cuenca and Noilhan, 1988). Neutron scattering was the method employed in HAPEX-MOBILHY. Evaporation is computed as the residual when the other terms are summed.

2.2 Remote Sensing Measurement Methods

Remote sensing in this paper is broadly defined as collecting and interpreting information about a target, in this case the Earth's surface, without being in physical contact with the object. This definition is restricted to methods that employ electromagnetic energy as the means of detecting and measuring target characteristics. In general, the remote sensing technique involves aircraft or satellite borne electronic sensors that acquire data in a specific wavelength portion of the electromagnetic spectrum. Interpretative methods are used to apply the data.

The resolution of sensor instruments is an important consideration in remote sensing techniques. Resolution is defined as the ability to discern difference with respect to distance, and is a function of the sensors optical-mechanical characteristics and of the distance between the sensor and the target. The same sensor carried on an aircraft platform will have a finer resolution, and view a smaller total area, than if it were carried on a satellite platform. Though not necessarily suitable for practical application, smaller platforms have been used for research purposes. For example, model aircraft flown at 200 m above the mean ground level (MGL) have been used to study evaporative flux from a single tree canopy (Balek *et al.*, 1986). Helicopters have carried microwave radiometers for low altitude coverage in several French experiments (Bernard *et al.*, 1986; Perry and Carlson, 1988). The present study uses information obtained with sensors flown in aircraft at altitudes of 300-m and 1500-m, providing

considerably higher resolution than is possible with satellite imagery. This higher resolution allows better use of ground data. The results of this basic research could possibly be extended for future use with Earth-orbiting platforms.

2.2.1 The Electromagnetic Spectrum

Remote sensing involves electromagnetic radiation which can be detected using a variety of sensors. From basic physics, wavelength and frequency of electromagnetic radiation are inversely related (Tipler, 1982);

$$c = \upsilon\lambda \tag{2-7}$$

where

c = speed of light, a constant $\approx 3.0 \times 10^8$

υ = frequency, Hz

λ = wavelength, m

Figure 2.1 depicts the general regions of the electromagnetic spectrum. Though energy is emitted by the sun throughout the spectrum, only certain portions of the spectrum are useful for remote sensing on Earth due to energy interactions in the form of scattering and absorption in the atmosphere. Those portions of the spectrum for which energy is readily transmitted through Earth's atmosphere are commonly called *atmospheric windows*. Atmospheric windows are the regions of the spectrum where the remote sensing of Earth features is feasible. Table 2.1 describes several regions of the electromagnetic spectrum, and the usefulness of each for remote sensing. For natural resources work, the portions of the electromagnetic spectrum that have been identified as most useful are the visible, near infrared, thermal infrared, and microwave (Lillesand and Kiefer, 1987).

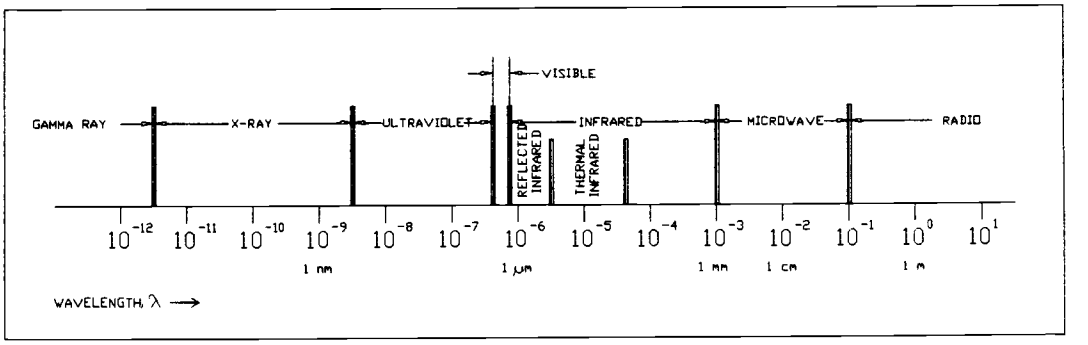

Figure 2.1 The electromagnetic spectrum.

Before developing remote sensing techniques for hydrologic applications it is appropriate to present several tools and concepts that are commonly used in many diverse remote sensing applications. These are presented here to minimize confusion and standardize the notation.

Table 2.1 Electromagnetic spectral regions (Sabins, 1987).

Region	Wavelength	Remarks
Gamma ray	< 0.03-nm	Incoming radiation is completely absorbed by the upper atmosphere and is not available for remote sensing.
X-ray	0.03 to 3.0-nm	Completely absorbed by atmosphere. Not employed in remote sensing.
Ultraviolet	0.03 to 0.4-μm	Incoming wavelengths less than 0.3-μm are completely absorbed by ozone in the upper atmosphere.
Photographic UV band	0.3 to 0.4-μm	Transmitted through atmosphere. Detectable with film and photodetectors, but atmospheric scattering is severe.
Visible	0.4 to 0.7-μm	Imaged with film and photodetectors. Includes reflected energy peak of Earth at 0.5-μm.
Infrared	0.7 to 100-μm	Interaction with matter varies with wavelength. Atmospheric transmission windows are separated by absorption bands.
Reflected IR band	0.7 to 3.0-μm	Reflected radiation that contains no information about thermal properties of materials. The band from 0.7 to 0.9-μm is detectable with film and is called the *photographic IR band*.
Thermal IR band	3 to 5-μm, 8 to 14-μm	Principal atmospheric windows in the thermal region. Images at these wavelengths are acquired by optical-mechanical scanners and special vidicon systems but not by film.
Microwave	0.1 to 30-cm	Longer wavelengths can penetrate clouds, fog, and rain. Images may be acquired in the active or passive mode.
Radar	0.1 to 30-cm	Active form of microwave remote sensing. Radar images are acquired at various wavelength bands.
Radio	> 30-cm	Longest wavelength portion of electromagnetic spectrum. Some classified radars with very long wavelength operate in this region.

2.2.1.1 Spectral Indices

Researchers have employed spectral indices in a variety of applications to integrate the information of two or more spectral bands into a single ratio. The two indices most commonly referred to in work with land surfaces covered with vegetation are the Vegetative Index (VI) and the Normalized Difference Vegetative Index (NDVI), both of which are computed from multispectral digital data by the following relations (Greegor and Norwine, 1986; Baucsh and Neale, 1987)

$$VI = \frac{DIN_R}{DIN_{IR}} \tag{2-8}$$

and

$$NDVI = \frac{DIN_R - DIN_{IR}}{DIN_R + DIN_{IR}} \tag{2-9}$$

where

VI = vegetative index

$NDVI$ = normalized difference vegetation index

DIN_R = digital index number, red band

DIN_{IR} = digital index number, near infrared band

The term DIN represents the Digital Index Number, the value recorded by a sensor for a particular band. The DIN for TMS data is an 8-bit number, i.e., ranging from 0 to 255. Given the appropriate gain and offset these values can be converted to spectral radiances. In theory, the value of NDVI ranges from -1.0 to 1.0. For Earth observations values typically range from -0.1 to 0.7 (Greegor and Norwine, 1986).

These indices are used in applications such as spectral crop coefficients (Bausch and Neale, 1987), crop and land-use classification (Lillesand and Kiefer, 1987), and estimation of ground heat flux in regression against net radiation (R. D. Jackson *et al.*, 1987; see Section 2.2.2.3, Soil Heat Flux).

2.2.2 Multispectral Remote Sensing

The use of multispectral reflectance measurements, defined here for convenience as visible through thermal infrared bands, to determine land surface fluxes is common to many research efforts. Past efforts are reviewed here because the results of the current study will further the work of evaporative flux modelling with remote sensing data.

Several authors have demonstrated that remotely sensed data together with some ground-based measurements can be used to estimate or measure evaporative flux (Choudhury, 1986; Hatfield, 1983; Hatfield *et al.*, 1983; Gash, 1987; Seguin and Itier, 1983) In all cases, effective consideration of the processes involved requires that the researcher begin with the surface energy balance equation presented in equation (2-1). Rearranging equation (2-1) to express the energy balance with respect to the variable of interest, the latent heat flux, the surface energy balance equation is

$$L_e E = R_n - H - G \tag{2-10}$$

where

$L_e E$ = latent heat flux, $W \cdot m^{-2}$

R_n = net radiation, $W \cdot m^{-2}$

H = sensible heat flux, $W \cdot m^{-2}$

G = soil heat flux, $W \cdot m^{-2}$

In the ground based situation, net radiation, sensible heat flux, and soil heat flux can be directly measured. In the remote case this is not possible. Attention must be given to identifying which parameters can be measured, which estimated, and which safely neglected so that the latent heat flux may be determined with acceptable accuracy. In general, the larger number of relevant parameters that can be measured by remote means, the more accurate an areal evaporative flux measurement will be and the less the need to replicate expensive ground-based instrumentation to obtain the same information.

The three terms on the right hand side of equation (2-10) are now considered individually. Methods used by researchers to measure, estimate, or in some cases the rationale for neglecting some terms will be presented for each term.

2.2.2.1 Net Radiation

Net radiation at the surface of the Earth is the sum of the incident and reflected solar radiation (short-wave, $0.15 \, to \approx 0.4 \, \mu m$) and the incident sky and emitted terrestrial radiation (long-wave, $\approx 0.4 \, to \approx 1000 \, \mu m$) radiation. This may be expressed as

$$R_n = R_s^{\downarrow} - R_s^{\uparrow} + R_l^{\downarrow} - R_l^{\uparrow} \tag{2-11}$$

where

$R_s^{\downarrow}$ = incident solar radiation, $W \cdot m^{-2}$

$R_s^{\uparrow}$ = reflected solar radiation, $W \cdot m^{-2}$

$R_l^{\downarrow}$ = incident sky radiation, $W \cdot m^{-2}$

$R_l^{\uparrow}$ = emitted terrestrial radiation, $W \cdot m^{-2}$

The incident terrestrial (downward long-wave) term is given by the Stefan-Boltzmann equation:

$$R_l^{\downarrow} = \sigma \epsilon_a T_a^4 \tag{2-12a}$$

where

$R_l^{\downarrow}$ = incident sky radiation, $W \cdot m^{-2}$

T_a = air temperature, K

ϵ_a = effective emissivity for a cloudless sky

σ = Stefan-Boltzmann constant = 5.6703×10^{-8} $W \cdot m^{-2} K^{-4}$

Similarly for the emitted terrestrial (upward long-wave) term;

$$R_l^{\uparrow} = \sigma \epsilon_s T_s^4 \qquad \text{(2-12b)}$$

where

$R_l^{\uparrow}$ = reflected solar radiation, $W \cdot m^{-2}$

T_s = surface temperature, K

ϵ_s = surface emissivity

σ = Stefan-Boltzmann constant = 5.6703×10^{-8} $W \cdot m^{-2} K^{-4}$

Substituting equations (2-12a) and (2-12b) into equation (2-11) gives

$$R_n = R_s^{\downarrow} - R_s^{\uparrow} + \epsilon_a \sigma T_a^4 - \epsilon_s \sigma T_s^4 \qquad \text{(2-13)}$$

where

$R_s^{\downarrow}$ = incident solar radiation, $W \cdot m^{-2}$

$R_s^{\uparrow}$ = reflected solar radiation, $W \cdot m^{-2}$

T_a = air temperature, K

T_s = surface temperature, K

ϵ_a = effective emissivity for a cloudless sky

ϵ_s = surface emissivity

σ = Stefan-Boltzmann constant = 5.6703×10^{-8} $W \cdot m^{-2} K^{-4}$

By measuring, estimating, or treating as negligible these four radiation terms, the net radiation can be computed. Since remote sensing is the detection of reflected and emitted energy, it follows that remote sensing techniques should be capable of measuring $R_{s\uparrow}$ and $\epsilon_s \sigma T_s^4$ using multispectral data. The other terms are beyond the capabilities of remote sensing techniques and must hence be obtained by some other means.

$R_s^{\downarrow}$ can be measured using ground-based equipment, and is relatively independent of surface parameters and conditions, e.g. incident solar radiation is the same over adjacent corn and wheat fields, though reflected solar radiation probably is not. Hence, a ground based measurement can be extrapolated spatially for some distance. This is the reasoning used by R. D. Jackson *et al.* (1985) when they argue that the incident terms $R_s^{\downarrow}$ and $\epsilon_a \sigma T_a^4$ could best be measured with traditional ground-based instruments. The principal constraint of this approach is the assumption of uniformity in meteorological conditions, i.e., to what distance can measured ground terms be extrapolated, and with what degree of confidence? R. D. Jackson *et al.* (1985) found, based on calculations, that the limiting factor may be the extrapolation of air temperature and wind speed.

$R_l^{\downarrow}$ can be computed from $\epsilon_a \sigma T_a^4$ as indicated in equation (2-12a) above. Thus atmospheric emissivity and air temperature are required. Brutsaert (1982) derived an expression for the effective atmospheric emissivity to predict incident long-wave radiation at ground level under a clear sky and for a nearly standard atmosphere. The equation derived is

$$\epsilon_{ac} = 1.24\left(\frac{e_v}{T_a}\right)^{\frac{1}{7}} \qquad (2\text{-}14)$$

where

ϵ_{ac} = effective atmospheric emissivity

e_v = vapor pressure near surface, mb

T_a = air temperature near ground (usually at screen height), K

This reduces the data requirements for computing $R_l^{\downarrow}$ to air temperature and vapor pressure, both of which are readily available from many meteorological stations. Under relatively stable

meteorological conditions, the error introduced by the spatial extrapolation of $R_l^{\downarrow}$ from ground-based point measurements of air temperature and vapor pressure are acceptable (R. D. Jackson *et al.*, 1985).

$R_l^{\uparrow}$ is a function of surface temperature, and can be evaluated by data collected by the thermal channel of multispectral radiometers (R. D. Jackson, 1985). This is accomplished by equating the measured apparent surface temperature to $\epsilon_s \sigma T_s^4$, the last term in equation (2-13). The surface emissivity is incorporated into the apparent surface temperature if the radiometer channel is calibrated with reference to a blackbody whose emissivity is near zero.

$R_s^{\uparrow}$ is the final term required to compute the net radiation. R. D. Jackson (1985) described how a multispectral radiometer could be used to estimate reflected solar (upward short-wave) radiation over the entire spectrum. The method relied on a ratio of the radiation measured by a multispectral radiometer to the total reflected radiation, termed the partial/total (P/T) ratio. The ratio is essentially independent of surface conditions when the appropriate channels, or bands, are selected. Calculation of $R_s^{\uparrow}$ is performed as follows. The reflected energy for each channel is first computed, which is equal to the product of the voltage response of the multispectral radiometer and a calibration factor. The appropriate channels are then summed and divided by the P/T ratio to obtain the total reflected solar radiation, $R_s^{\uparrow}$. For low altitude aircraft platforms the P/T ratio is essentially independent of atmospheric scattering and mildly influenced by atmospheric water vapor.

2.2.2.2 Sensible Heat Flux

As in the ground-based measurement case, determination of the sensible heat flux begins with equation (2-4), restated here for convenience;

$$H = \frac{\rho c_p (T_s - T_a)}{r_{ah}} \tag{2-15}$$

where

H = sensible heat flux, $W \cdot m^{-2}$

ρ = density of air, $kg \cdot m^{-3}$

c_p = volumetric heat capacity of air, $J \cdot kg^{-1}K^{-1}$

T_s = surface temperature, $°C$

T_a = air temperature, $°C$

r_{ah} = aerodynamic resistance for sensible heat transfer, $s \cdot m^{-1}$

In general, the remote sensing approach to determine the sensible heat flux utilizes data collected from both ground- and remote-based sensors. The surface temperature can be measured using the thermal band of the electromagnetic spectrum. The air temperature can not be remotely sensed and hence requires ground-data. This parameter can not be extrapolated long distances as it is highly dependent on local and micro-meteorological conditions.

The aerodynamic resistance must be calculated with respect to atmospheric stability conditions. For neutral conditions, the aerodynamic resistance can be calculated from the expression:

$$r_a = \frac{\left\{\ln \frac{(z-d)}{z_0}\right\}^2}{(k^2 u)} \qquad (2\text{-}16)$$

where

r_a = aerodynamic resistance, $s \cdot m^{-1}$

z = reference height, m

d = zero plane displacement height, m

z_0 = surface roughness height, m

k = von Karman's constant = 0.38, dimensionless

u = wind speed at reference height, $m \cdot s^{-1}$

Neutral conditions translate into approximate equality of the surface and air temperatures, which is not a common condition when examining evaporative flux. To handle unstable conditions requires the use of a stability correction as suggested by Montieth (Hatfield *et al.*, 1983) in which the Richardson Number is included. Expressing this number in terms of temperature differences, and combining with equation (2-16) results in the expression:

$$r_{ac} = r_a \left[\frac{1 - n(z-d)g(T_c - T_a)}{T_0 u^2} \right] \qquad (2\text{-}17)$$

where

r_{ac} = stability corrected aerodynamic resistance, $s \cdot m^{-1}$

r_a = aerodynamic resistance, $s \cdot m^{-1}$, computed using equation (2-16)

n = empirical constant (Montieth suggested 5)

g = acceleration due to gravity, $\approx 9.81 m \cdot s^{-2}$

T_0 = average daily temperature (usually taken as air temperature), K

T_c = surface temperature, K

and the other terms are as defined in equation (2-16) above. The aerodynamic resistance is the most difficult term to determine in computing the sensible heat flux. Hatfield *et al.* (1983) examined the effects of wind speed and surface roughness in predicting evapotranspiration using remotely sensed surface temperatures in conjunction with ground measurements of net radiation, air temperature, wind speed, and surface roughness. From previous discussion in this Review of Literature, it has been shown that net radiation can also be computed using several remote sensing bands and certain ground data. Ground measurements are still required for wind speed, air temperature, and surface roughness, none of which can be extrapolated far from the measurement point. How far is still a question facing researchers, but the local scale may suffice as a temporary definition, i.e. on the order of 10-km.

2.2.2.3 Soil Heat Flux

In ground-based techniques, the soil heat flux is measured with sensors buried below the soil surface (see Section 2.1.1, Surface Energy Balance, for further discussion of ground measurement techniques). This flux is dependent on soil moisture and vegetation cover, thus a ground-based measurement is not appropriate for areal extrapolation. Since it is not possible to estimate soil heat flux with instantaneous remote measurements there is no method to measure the parameter with spatial resolution other than through replication of the ground-based measurement. The soil heat flux is generally small in magnitude compared to the other terms of equation (2-10), a fact that allows empirical estimations to be made without introducing a large error into the calculation of the latent heat flux.

An empirical approach based on unpublished data (Reginato *et al.*, 1985) assumed that the soil heat flux could be adequately estimated by a linear function of crop height and net radiation. The data indicated that the soil heat flux was approximately ten percent of net radiation for bare soil and less than ten percent for full canopies. The empirical relation based on these observation is

$$G = (0.1 - 0.042h)R_n \tag{2-18}$$

where

G = soil heat flux, $W \cdot m^{-2}$

h = crop height, m (assumed = 1.2 at maturity)

R_n = net radiation, $W \cdot m^{-2}$

This relationship was for a wheat canopy. This empirical relation has been used several times in remote sensing studies (Reginato *et al.*, 1985; R. D. Jackson, 1986).

Another relation used to estimate the soil heat flux is based on a vegetative index computed from multispectral data. R. D. Jackson *et al.* (1987) adopted this approach by relating a ratio of soil heat flux and net radiation to the NDVI. The relationship is

$$\frac{G}{R_n} = 0.583e^{-2.13(NDVI)} \tag{2-19}$$

where

G = soil heat flux, $W \cdot m^{-2}$

R_n = net radiation, $W \cdot m^{-2}$

$NDVI$ = Normalized Difference Vegetation Index, defined in equation (2-9)

Both of the above techniques for estimating soil heat flux are computationally efficient, though the second is preferable since ground measurements (i.e. crop height) are not required.

2.2.3 Microwave Remote Sensing

The microwave portion of the electromagnetic spectrum is useful for detection of soil moisture and has some significant advantages over the shorter wavelength bands used in remote sensing. The physics of microwave remote sensing are well understood in theory, though the impact of naturally occurring effects such as vegetation and surface roughness are not as well known.

2.2.3.1 Fundamentals of Microwave Remote Sensing

Microwave emissions are influenced primarily by the following Earth surface features: (1) surface roughness, (2) surface material density, and (3) electrical characteristics (Lillesand and Kiefer, 1987). The most significant of the these are the electrical characteristics, a physical property of the object or medium being sensed. A measure of an object's electrical characteristics is given by the dielectric constant, which quantifies the propagation characteristics of an electromagnetic wave in a medium such as soil. The characteristics of the wave include velocity, wavelength in the medium, and energy absorption by the medium. There is a large contrast in the dielectric constant of water (≈ 80) and dry soil (≈ 3.5), which

results from the ability of the electric dipole of a water molecule to align itself in response to electric field activity at microwave frequencies. The correlation between water presence and the magnitude of the dielectric constant makes the microwave region very useful for remote sensing in hydrologic work over land surfaces.

Another physical parameter, the concentration of salts in water, also affects the value of the dielectric constant. The dielectric constant of saline water mixed with soil, and of pure water mixed with soil differ. Fortunately, recent research has demonstrated that this effect is negligible in agricultural regimes, and that for general applications the effects of soil salinity can be ignored in interpreting microwave data for estimation of soil moisture (T. J. Jackson and O'Neill, 1987).

Microwave remote sensing techniques are generally characterized by the source of illumination; if the sensor detects ambient microwave signals, the sensor is termed *passive*, as opposed to an *active* sensor that incorporates an apparatus for transmitting a microwave signal and detecting the return signal. In passive microwave remote sensing, the sensor, generally a radiometer, observes variations in the thermal emission of an Earth surface due to changes in emissivity (T. J. Jackson and Schmugge, 1986). Active microwave sensors are called radar (radio detection and ranging), and tend to be used for position and/or velocity measurements. Active radar also has useful imaging applications in mapping areas of the Earth under constant cloud cover and/or heavy vegetation (Lillesand and Kiefer, 1987), and in vegetative observations (Krul, 1988). Passive microwave remote sensing is of principal interest in this study since this has been found to be the most promising for operational remote sensing of soil moisture (T. J. Jackson and Schmugge, 1986).

Use of the microwave portion of the electromagnetic spectrum originated in the military, and for security purposes that institution classified microwave regions with a letter scheme that has no significant meaning. The classification scheme is still in use, and is summarized in Table 2.2. The L-band has been shown to be the most sensitive to soil moisture variation (T. J. Jackson and Schmugge, 1986).

Thermal emission at the Earth's surface is commonly measured with the use of a microwave radiometer. To understand what the radiometer measures requires a short

Table 2.2 Microwave wavelengths and frequencies used in remote sensing (Sabin, 1987).

Band	Wavelength (λ), cm	Frequency, (υ), $, MHz$
Ka	0.8 to 1.1	40.0 to 26.5
K	1.1 to 1.7	26.5 to 18.0
Ku	1.7 to 2.4	18.0 to 12.5
X	2.4 to 3.8	12.5 to 8.0
C	3.75 - 7.5	8.0 to 4.0
S	7.5 to 15.0	4.0 to 2.0
L	15.0 - 30.0	2.0 to 1.0
P	30.0 to 100.0	1.0 to 0.3

examination of quantum physics. Planck's law, an empirical function developed in 1900 by the German physicist Max Planck (Tipler, 1982) to describe the radiation energy emitted from a blackbody is used to compute the energy emitted from a target;

$$E = \frac{hc/\lambda}{e^{hc/\lambda kT} - 1} \tag{2-20}$$

where

E = emitted energy, W

h = Planck's constant = $6.626 \times 10^{-34} J \cdot s$

c = speed of light (constant $\approx 3.80 m \cdot s^{-1}$)

λ = wavelength, m

k = Boltzmann's Constant = $1.38 \times 10^{-23} J \cdot K^{-1}$

T = temperature, K

At longer wavelengths, such as microwave, the intensity of the observed emission from a object is proportional to the product of the objects temperature and the emissivity of the object surface. This relationship is known as the Rayleigh-Jeans approximation to Planck's law (T. J. Jackson and Schmugge, 1986; Schmugge, 1988). This product of temperature and emissivity is commonly called the brightness temperature. When measured by a microwave radiometer a specific height above the surface, the brightness temperature is given by (T. J. Jackson and Schmugge, 1986)

$$T_B = \tau[R T_{sky} + (1 - R) T_{soil}] + T_{atm} \tag{2-21}$$

where

T_B = brightness temperature, K

τ = atmospheric transmission, dimensionless

R = surface reflectivity, dimensionless

T_{sky} = reflected sky thermal contribution, K

T_{soil} = thermal emission from the surface, K

T_{atm} = direct atmospheric thermal contribution, K

T_B is the equivalent temperature of the microwave radiation thermally emitted by an object (Foster, 1987). The individual terms of equation (2-21) require some elaboration. The reflected sky brightness temperature depends on atmospheric conditions and frequency, and is typically $5 \text{ to } 10\ K$, of which $3\ K$ is the contribution of constant cosmic background radiation. The direct atmospheric contribution is about $5\ K$. Atmospheric transmission is typically 99 percent. Thus, equation (2-21) reduces to (Schmugge, 1988)

$$T_B = (1 - R) T_{soil} = e T_{soil} \tag{2-22a}$$

for an isothermal soil and

$$T_B = e\int_{-\infty}^{0} T(z)\alpha(z)\exp[-\alpha(z')dz']dz \qquad (2\text{-}22b)$$

for a soil with temperature variation, where

T_B = brightness temperature, K

R = surface reflectivity, dimensionless

e = surface emissivity, dimensionless

T_{soil} = thermal emission from the surface, K

$T(z)$ = temperature at depth z in the soil, K

$\alpha(z)$ = absorptivity at depth z in the soil

The emissivity e describes the fraction of radiation transmitted into the air, and is the primary indicator of soil moisture content due to its sensitivity to water presence. The depth at which a microwave radiometer measures soil moisture is the thickness of the depth layer whose dielectric properties determine e. This depth is approximately a few tenths of a wavelength thick, based on early theoretical and experimental studies. For an L-band radiometer at 21 cm wavelength, this translates into a soil depth layer of 2 to 5 cm.

The complexity of sensing soil moisture increases in the presence of vegetative cover. The vegetative canopy attenuates and scatters the emission signal of the soil and its own emission is added to the total radiative flux. This is due to the water content of the vegetation itself. The effect is to change the slope of the relation between soil moisture and the passive microwave response. Because vegetative cover is highly complex and variable, empirical approaches have been adopted to deal with the attenuation effects of the vegetation. For example, (T. J. Jackson and Schmugge, 1986);

$$e = 1 + (e_s - 1)\exp(-b_2 Qm) \qquad (2\text{-}23)$$

where

e = observed emissivity

e_s = emissivity of soil under vegetation, i.e., what would be observed if vegetation were removed

Q = dry biomass, $100 \ \ kg \cdot ha^{-1}$

m = moisture content of the vegetation dry biomass, $g \cdot g^{-1}$

b_2 = coefficient incorporating parameters relating to wavelength, incidence angle, and plant shape (an empirical parameter)

Although an understanding of the physics reviewed above is important in understanding the basis for use of microwave technology, the central theme in this paper remains the application of remote sensing data to the problem of areal measurement of hydrologic parameters. Therefore more detailed discussion of microwave physics is not necessary as the fundamentals have been sufficiently established. With this groundwork, more recent research efforts directed toward the use of passive microwave remote sensing for hydrologic applications can be discussed.

2.2.3.2 Review of Microwave Remote Sensing Research

Investigation of hydrologic applications for remote sensing has been limited by the availability of operational sensors. With microwave radiometry, such instruments have only recently been available for natural resource applications. Remote sensing in the low-frequency microwave range has been established as a useful tool for surface soil water content (T. J. Jackson and Schmugge, 1986), and research has begun to focus on the use of microwave data for hydrologic studies.

Bernard *et al.* (1981) presented a methodology for estimating bare soil evaporation from microwave radar data that involved a numerical solution of the classical nonlinear Richard's equation. The equation is solved using soil moisture values estimated from radar data as the upper boundary condition. The authors simulated the radar data for testing the methodology and demonstrated that radar data could be used to define the surface conditions in a water transfer model for a bare soil.

Prevot *et al.* (1984) applied the above approach, using an implicit finite difference scheme to solve the Richard's equation with daily soil surface moisture data obtained from a C band scatterometer on bare soil. This confirmed that a soil water transfer model can estimate the soil water budget and evaporation when used with remotely sensed microwave data.

As airborne systems became more widely available for research, new concepts evolved with respect to the use of microwave data. Bernard *et al.* (1986) observed that use of the Richard's equation, though correctly describing the variation in time of bare soil surface moisture, was impractical for large-scale purposes. Water budget estimation from remote data using this methodology requires precise knowledge of the hydraulic characteristics of the soil in question, which can vary by orders of magnitude within short distances (de Marsily, 1986; Cuenca, 1989). Instead, Bernard *et al.* (1986) presented a simple two-layer physical model with a diffusivity type of water exchange between layers. The model was used for a water budget study using microwave data collected with the French ERASME[3] scatterometer and a Barnes PRT-5 infrared radiometer.

The lack of understanding of vegetative effects caused researchers to begin with bare soil studies. T. J. Jackson *et al.* (1986) assessed pre-planting soil moisture using airborne microwave sensors in Texas in 1984. This practical application demonstrated that microwave systems can provide an efficient means for mapping variations in soil moisture over large areas. The sensor used in this experiment was the Push Broom Microwave Radiometer (PBMR), the same sensor used in the HAPEX-MOBILHY Program.

More recently, the French helicopter-borne ERASME scatterometer was employed in a vegetated region of France to obtain soil water content data, which was then compared with thermal infrared surface temperature and surface moisture availability (Perry and Carlson, 1988). Thermal infrared surface temperatures are known to vary with soil moisture, and available moisture determines how sensible and latent heat fluxes are partitioned in the surface energy balance. Some interesting points were made. First, infrared measured surface temperatures reflected a desiccated surface layer, whereas the microwave measurements pertained to a deeper, wetter soil layer. Second, temporal variations in soil moisture may be

---

3 ERASME - Etude Radar des sols et de la mer, a helicopter-borne frequency-modulated continuous wave radar. It has a 5.3-GHz center frequency, horizontal polarization, and 11° incidence angle (Bernard *et al.*, 1986)

more readily detectable by infrared temperature measurements than by spatial variations. Third, analyzing spatial variations of soil moisture using infrared surface temperatures appears impractical. Microwave measurements thus appear to be the confirmed as the best remote-based technique for soil moisture determination at this time.

Active microwave is still under investigation for soil moisture variation detection as well. Soarés *et al.* (1988) used a C-band active microwave instrument to monitor spatial and temporal variations in soil moisture up to 5- or 10-cm below the soil surface. These authors claimed that if thermal infrared irradiance is measured simultaneously with microwave emissions, it may be possible to monitor actual evaporation and the soil water budget. Work was restricted to essentially bare soil in this study, reflecting the difficulty of dealing with vegetative cover.

Theis and Blanchard (1988) investigated the sensitivity of soil moisture estimates derived from passive microwave sensors with respect to 1) surface roughness and vegetation, and 2) measurement error due to noise. They presented a methodology for estimating measurement error due to vegetation in the form of a perpendicular vegetation index (PVI), a remotely sensed vegetation parameter derived from visible and infrared sensor data. This spectral index was not considered in the present study, though it should be examined in future extensions of this study.

Research conducted with the PMBR in FIFE over the Konza Prairie Reserve in Kansas (Sellers *et al.*, 1989) has provided an additional opportunity to assess this particular sensor. FIFE was another large-scale field experiment, similar to HAPEX-MOBILHY, but with a different scale (225 km^2), a single vegetative cover (tall prairie grass), and more difficult topography, i.e., not always level, which complicated use of land surface research instruments (Shuttleworth *et al.*, 1989). Surface soil moisture was successfully mapped with the PBMR in FIFE (Schmugge *et al.*, 1988; Wang *et al.*, 1989), and this quantity was also compared with a hydrologic balance model of a small watershed (Engman *et al.*, 1989).

2.2.4 Conversion of Instantaneous Measurements to Daily Values

Remote sensing techniques provide varying degrees of spatial resolution, which is the reason for investigating their use. Unfortunately, unlike traditional ground-based techniques, remote sensing techniques have poor temporal resolution (except for geo-synchronous satellites, the limitations of which were discussed at the start of the Review of Literature). Remote sensing data with field scale resolution can only be made available at periods of time ranging from once per day on an aircraft platform to once every fourteen or eighteen days on a satellite platform such as the NASA LandSat and French SPOT[4] series of Earth observing satellites. Thus, the results of an instantaneous, or one-time-of-day measurement, must be extrapolated to daily values which are of the most use in various hydrologic studies.

2.2.4.1 Relational Procedures

In relational approaches, researchers have attempted to provide a means to convert the instantaneous value of the latent heat flux measured by remote means to daily totals by relating the ratio of the two to a ratio of some other known or estimated quantity. It is generally desirable to make the known ratio relatively easy to compute based on location or ground data so that the daily total evaporative flux can be determined.

R. D. Jackson *et al.* (1983) assumed that the daily course of evaporative flux would generally follow the trend of solar radiation throughout the daylight period. They demonstrated that for cloudless sky conditions, the ratio of total daily solar radiation to a midday instantaneous value could be approximated by the relation

---

4 SPOT - Systeme Pour l'Observation de la Terre. Conceived and designed by the French Centre National d'Etudes Spatiales (CNES). SPOT-1 has a circular, near-polar, sun-synchronous orbit. The sensor payload includes two identical High Resolution Visible (HRV) imaging systems with off-nadir viewing capability, operating in either a panchromatic (10-m resolution) or color infrared (20-m resolution) mode. The nominal orbit has an altitude of 832 and inclination of 98.7°. SPOT-1 descends across the equator at 10:30hrs local solar time, with slightly later crossings in northern latitudes and slightly earlier crossings in southern latitudes. The repeat period for SPOT-1 is 26 days (Lillesand and Kiefer, 1987).

$$\frac{S_d}{S_i} = \frac{2N}{\pi \sin\left(\frac{\pi t}{N}\right)} \tag{2-24}$$

where

S_d = daily total solar irradiance, $W \cdot m^{-2}$

S_i = instantaneous solar irradiance at midday, $W \cdot m^{-2}$

N = time period between sunrise and sunset, hours

t = time period since sunrise, hours

At solar noon, the ratio in equation (2-24) is equal to $2N/\pi$. The authors also found that the daylight period N could be expressed as

$$N = a + b \sin^2\left[\frac{\pi(D+10)}{365}\right] \tag{2-25}$$

where

N = time period between sunrise and sunset, hours

D = day of year (January 1 = day 1)

a = daylight period for shortest day of year at local latitude, hours

b = amount that must be added to a to obtain the daylight period for the longest day of the year at local latitude, hours

Regression equations dependent on latitude were also provided for the constants a and b. Returning to the original assumption, that daily evaporative flux follows the course of daily solar irradiance, the authors equate the ratio developed above to daily evaporation;

$$\frac{S_d}{S_i} = \frac{(L_e E)_d}{(L_e E)_i} \tag{2-26}$$

where

S_d = daily total solar irradiance, $W \cdot m^{-2}$

S_i = instantaneous solar irradiance at midday, $W \cdot m^{-2}$

$(L_eE)_d$ = daily total latent heat flux, mm

$(L_eE)_i$ = instantaneous latent heat flux, mm

This technique provided a computationally simple means to convert instantaneous midday evaporative flux measurements to daily values.

Nieuwenhuis *et al.* (1985) proposed a modification to the approach developed by R. D. Jackson *et al.* (1983). This proposal replaced the surface-air temperature difference with the temperature difference that exists between a crop that is transpiring under actual restrictions of soil moisture conditions, and that transpiring under optimal soil moisture conditions. The net radiation term was replaced with the daily potential evapotranspiration of the crop. These adjustments resulted in the expression:

$$\frac{(L_eE)_d}{(L_eE)_d^p} = 1 - \beta^r (T_c - T_c^*)_i \qquad (2\text{-}27)$$

where

$(L_eE)_d$ = actual daily evapotranspiration, mm

$(L_eE)_d^p$ = potential daily evaporation, mm

T_c = actual crop temperature, K

T_c^* = crop temperature under optimal soil moisture conditions, K

β^r = calibration constant, K^{-1}

2.2.4.2 Simulation Models

A second approach, in addition to relational approaches discussed above, is the use of simulation models to convert instantaneous values to daily totals. This approach involves

detailed modeling of the soil-plant-water-atmosphere continuum so that, given the instantaneous value of latent heat flux determined at midday be remote means, the daily total can be determined by comparison to the model.

Soer (1980) asserted that the aid of a simulation model is "indispensable" for converting instantaneous data into daily estimates of evaporative flux. The model he developed (Soer, 1977) for this purpose, the TERGA model, is a soil-plant-water simulation model for grassland based on the transport equations for heat transfer and moisture flow in soil, plant, and atmosphere. The TERGA model has also been combined with the SAIL[5] model to form TERSAIL (Hope *et al.*, 1986), a reflectance model used for analysis of spectral indices relationships with Leaf Area Index (LAI) and canopy resistance.

Nieuwenhuis (1986) used SWATRE[6], a one-dimensional finite-difference soil-water-root uptake model applying a simple sink term and different types of boundary conditions at the bottom of the system, to relate instantaneous measurements to cumulative totals. The concept Nieuwenhuis applied was to use this sophisticated model to simulate crop evaporation for a restricted number of locations throughout a growing season, and then relate this to remote sensing data, which in turn could be used to estimate evapotranspiration for a regional area.

---

5 SAIL - Scattering from Arbitrarily Inclined Leaves, a radiative transfer model.

6 SWATRE - Soil-Water-Atmosphere Transpiration Evaporation. A one-dimensional finite difference model.

3 MATERIALS AND METHODS

The instrument systems and remote sensors used to collect data examined in this study are described in this section. The physical basis for ground-based instruments is reviewed for each system. The theory of remote sensing is contained in the Review of Literature (Section 2.2.1, The Electromagnetic Spectrum). Validation studies are cited were appropriate.

3.1 Ground Instrumentation

The ground-based monitoring in the HAPEX-MOBILHY Program involved extensive instrumentation. The Lubbon northern central site included a precise weighing lysimeter and intensive soil data collected during aircraft overflights (Dijckmeester and Katwijk, 1986). The lysimeter data would be of great interest in this study, but unfortunately but data from this instrument were deemed unrepresentative of surrounding field condltions (Cuenca *et al.*, 1988; Cuenca 1988b). This is somewhat expected because the lysimeter was in its first year of use, and new lysimeter installations generally suffer from this problem. More effective were the SAMER and the neutron probe networks. These two measurement systems provided the widest coverage during the Special Observation Period (SOP) and good agreement has been demonstrated (Cuenca and Noilhan, 1988).

3.1.1 SAMER System

The HAPEX-MOBILHY Program included twelve SAMER stations operated throughout the SOP. The twelve SAMER stations are listed in Table 3.1, along with each stations identity number, location, elevation, crop cover, and an indication whether the crop was irrigated or not. All twelve stations were operated by CNRM[1] Toulouse, France.

---

1 CRNM - Centre National de Recherches Météorlogiques, Toulouse, France.

Table 3.1 SAMER stations (Bessemoulin *et al.*, 1987; SAMER database key).

SAMER Number	Site Name	Latitude	Longitude	Altitude (meters)	Soil Type (%)			Crop	Irrigated
					Clay	Silt	Sand		
1	Lubbon 1	44°07'N	000°03'W	146	2	5	93	Oats	No
2	Casteljaloux	44°19'N	000°07'E	131	35	49	16	Maize	Yes
3	Caumont	43°41'N	000°07'W	113	17	46	37	Soybeans	No
4	Courrensan	43°49'N	000°16'E	148	-	-	-	Wheat	No
5	Lubbon 2	44°07'N	000°03'W	146	1	2	97	Maize	Yes
6	Sabres	44°05'N	000°50'W	81	3	1	96	Maize	Yes
7	Bats	43°38'N	000°26'W	144	18	51	31	Maize	No
8	Vicq	43°46'N	000°51'W	15	10	16	74	Maize	Yes
9	Tieste	43°32'N	000°02'E	145	12	61	27	Maize	Yes
10	Castelnau	43°35'N	000°03'W	239	11	66	23	Maize	No
11	Fusterouau	43°42'N	000°01'W	146	20	34	46	Maize	Yes
12	Lagrange	43°58'N	000°03'W	152	-	-	-	Maize	Yes

The SAMER system applied the surface energy balance equation (2-1) to compute latent heat flux as a residual. Net radiation was directly measured with a net radiometer, and a buried flux-meter was used to measure soil heat flux. The sensible heat flux was determined from a simplified aerodynamic method. Complete details regarding the parameters measured and the specific sensors used are provided in Table 3.2. All parameters except rainfall were averaged over a 15-minute time interval. Basic Measurements refer to parameters required for computing the actual evapotranspiration, whereas Other Measurements refer to parameters collected for related research.

The simplified aerodynamic formula applied by the SAMER system was developed by Itier and Riou (de Pescara *et al.*, 1988) of INRA[2]. Measurements of wind speed and dry bulb air temperature at two levels above the canopy were required to compute the sensible heat flux. The first step in this method is to compute the Richardson Number, R_i, to determine the thermal stability of the lower atmosphere;

2 INRA - Institut National Recherches Agronomique, France.

Table 3.2 SAMER station measurements (adapted from Goutorbe, 1988).

MEASUREMENT	INSTRUMENT AND PRECISION (If known)
BASIC MEASUREMENTS	
Net Radiation	CROUZET net radiometer ($0.3 to 50\,\mu m$)
Ground Heat Flux	Thornwaite fluxmeter
Temperature Difference	6 copper-constantan thermocouples in 2 probes 1.5-m apart
Wind Speed Difference	2 MCB anemometers, 1.5-m apart
OTHER MEASUREMENTS	
Air Temperature	Platinum wire, 0.1 °C precision
Air Humidity	SPSI capacity sensor, 5% estimated precision
Rainfall	Précis Mécanique tipping bucket rain gage
Radiation	4 SCHENCK radiometers:
	Short-wave ($0.3 to 3.0\,\mu m$), upward
	Short-wave ($0.3 to 3.0\,\mu m$), downward
	Total ($0.3 to 60\,\mu m$), upward
	Total ($0.3 to 60\,\mu m$), downward

$$R_i = \sqrt{z_1 z_2}\left(\frac{g}{T}\right)\log\left(\frac{z_2}{z_1}\right)\left(\frac{DT}{DV^2}\right) \tag{3-1}$$

where

R_i = Richardson Number, dimensionless

DT = temperature difference between two probes, $°C$

DV = wind speed difference between two probes, $m \cdot s^{-1}$

z_1 = height above reference datum of lower probe, m

z_2 = height above reference datum of upper probe, m

The sensible heat was then computed from one of four equations. Which equation was used depended upon the value of the Richardson Number computed above.

$$R_i < -1 \qquad H = ADT^{3/2} \tag{3-2a}$$

$$-1 < R_i < 0 \qquad H = H_0(1 - 16R_i)^{3/4} \tag{3-2b}$$

$$0 < R_i < 0.14 \qquad H = H_0(1 - 5R_i)^2 \tag{3-2c}$$

$$0.14 < R_i \qquad H = H_0/10 \tag{3-2d}$$

where

$$A = \frac{1.3\rho C_p\sqrt{\frac{g}{T}}}{3(z_1^{-1/3}z_2^{-1/3})^{3/2}}$$

$$H_0 = -\frac{\rho C_p k^2}{\left(\log\left(\frac{z_2}{z_1}\right)\right)^2} DT\,DV$$

k = von Karman's constant = 0.38, dimensionless

The network of SAMER stations provided a useful ground truth against which remote methods may be developed, calibrated, and tested. Consideration of the precision with which the SAMER stations measured the surface fluxes is important before data are used to calibrate and test any remote sensing techniques. Goutorbe (1988) reported on validation studies for the equipment, and identified the principal errors to be expected from SAMER data collected during the SOP. Relative uncertainty in an individual H estimate is expected to be on the order of 25 percent. This error could be reduced by using daily averages instead of 15 minute values. The most important error is for net radiation, which is underestimated on clear days for most stations by 5 to 10 percent. Taken together, the validation studies indicated that SAMER station measurements were unable to differentiate surfaces with fluxes differing by less than 15 to 20 percent.

Goutorbe (1988) noted that a good general check on the SAMER system is the computation of the local water balance using precipitation and evaporation from SAMER stations and soil moisture variation from neutron probe data. This will be discussed later in a later section on validation of SAMER data by use of a hydrologic balance model.

3.1.2 Hydrologic Balance Model Using Neutron Probe Data

Neutron probe access tubes were installed in fourteen sites, twelve of which coincided with SAMER station locations. These tubes were monitored weekly during the SOP using a

neutron probe of French design. A hydrologic balance model using neutron probe data (Cuenca, 1988a) was developed to compute profile soil moisture content and actual evaporative flux at these sites.

A neutron probe emits high velocity neutrons, which are slowed by collision with hydrogen ions of similar mass. Through a detector device, the number of slow neutrons may be counted. Since water contains hydrogen ions, the number of neutrons counted by the detector is highly correlated to the soil moisture content within in the sphere of influence of the neutron source. To quantify the proportionality between soil moisture content and neutron probe detector counts, a calibration is required. The calibration is a regression equation that relates the neutron probe count to gravimetrically determined soil moisture content;

$$\Theta_v = a\left(\frac{NPC}{STD}\right) + b \tag{3-3}$$

where

Θ_v = soil moisture content, percent

NPC = neutron probe count

STD = standard count

a, b = slope and intercept linear regression coefficients, respectively

The use of equation (3-3) allows soil moisture content to be determined for a profile in discrete depth layers. In addition to direct interest in this parameter, soil moisture serves as an input to a hydrologic balance model. Use of such a model permits independent confirmation of the long-term accuracy of the SAMER stations located at the same sites as neutron probe access tubes.

The accuracy of the hydrologic balance driven by neutron probe measured soil moisture has been questioned. In HAPEX-MOBILHY the data were collected in weekly intervals and the error in calculated actual evapotranspiration at this time step appears small. Subsequent investigation of the same hydrologic balance model (Carrijo, 1988) concluded that daily use of the model introduces an error in the evaporative flux estimate of unacceptable magnitude, i.e. greater than 1 standard error.

3.1.3 Additional Ground Data

In addition to the SAMER stations and neutron probe network discussed above, a set of intensive ground data was collected during the SOP at the central site, Lubbon. Data collection was timed to coincide with the overflights by the NASA C-130 participating in the HAPEX-MOBILHY Program. The discussion of the ground-based program is summarized below from a paper issued by the Free University, Amsterdam (Dijckmeester and Katwijk, 1986), the group which conducted the ground-based data collection. The ground-based data program consisted of

1. Surface temperature and soil moisture measured in each field at Lubbon within a three hour window of all low altitude flights, at depths 2-, 5-, and 15-cm.
2. A general description of crops recorded on each flight day.
3. Bulk density determined every two weeks at two to four field locations using a volumetric displacement procedure.
4. Soil moisture measured by gravimetric means once a week at two locations in each field.
5. Color photograph slides taken of each field approximately once a week from the third week of the SOP.
6. Biomass samples taken once a week from the third week of the SOP on.

The soil moisture measurements provided the ground data required for calibration of the PBMR. Other parts of the ground-based data program are mentioned for completeness.

3.2 Remote Sensing Instrumentation

The NASA C-130 in the HAPEX-MOBILHY configuration carried two sensors of interest in this study: the NS001 Thematic Mapper Simulator (TMS) and the Push Broom Microwave Radiometer (PMBR). Along with other sensors, these were flown in the HAPEX-MOBILHY Program following the flight lines indicated in Figure 3.1. A schematic illustrating the spatial coverage of the various sensors on board the C-130 during the SOP is shown in Figure 3.2.

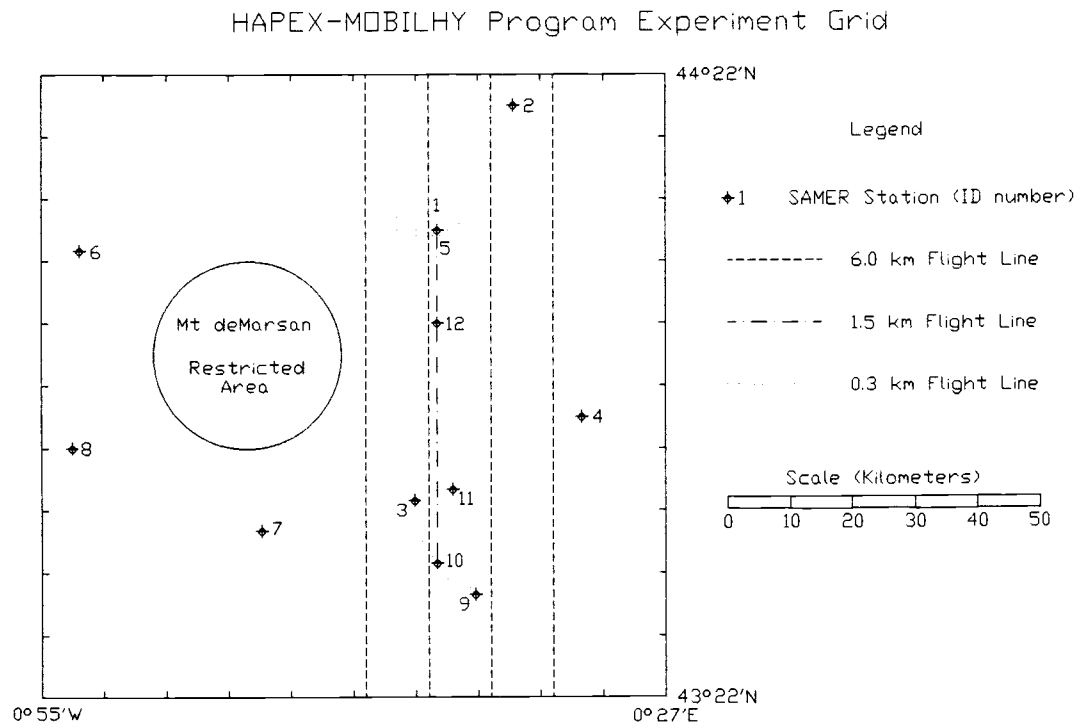

Figure 3.1 NASA C-130 flight lines in HAPEX-MOBILHY.

The TMS and the PBMR sensors are discussed below for reference. The data collected by these sensors constitute the remote sensing database available for this study.

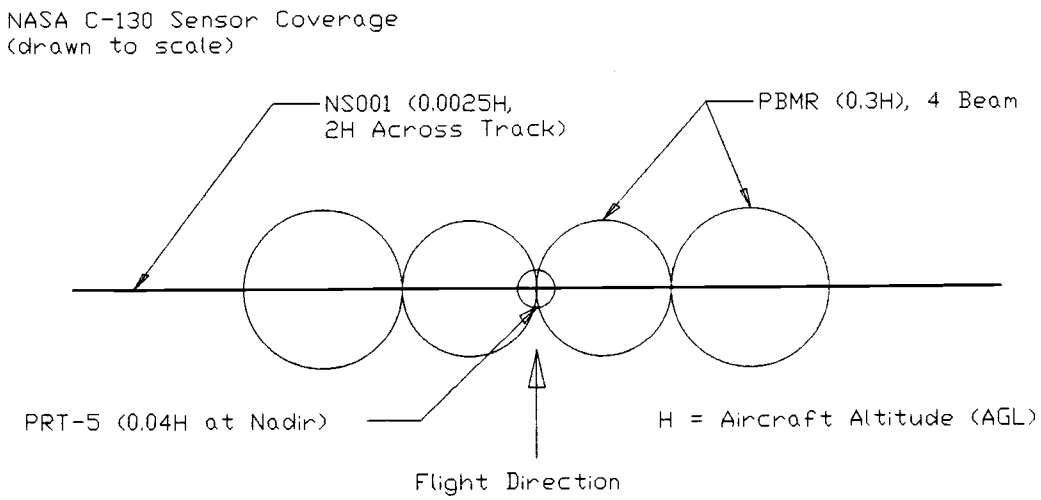

Figure 3.2 NASA C-130 sensor coverage (HAPEX-MOBILHY).

3.2.1 Thematic Mapper Simulator

The NS001 Thematic Mapper Simulator (TMS) is a multispectral scanner that operates in the visible to thermal infrared regions of the electromagnetic spectrum. The eight discrete TMS wavelength bands are given in Table 3.3. The sensor has a 2.5 mrad IFOV (instantaneous field of view). The thermal channel (band 8) was inoperable during the HAPEX-MOBILHY missions flown by NASA (Schmugge and Janssen, 1988). The NS001 was operated on all NASA C-130 flights during the SOP.

The geometry of this sensor is reviewed here to enable later computations of resolution. The resolution of the sensor is defined in picture elements, or *pixels*, which are the finest resolution at which particular scanner can discriminate between objects. Pixel size is a function of the scanners optical characteristics and of the height of the scanner when imagery is collected. The NS001 sensor scans an area 2.5×10^{-6} times the altitude of the sensor in the direction of the flight line and 2.0 times the altitude in the direction normal to the flight line. This resulted in 756 pixels in the direction normal to the flight line, which were re-sampled to 512 pixels to correct for distortion.

Table 3.3 NS001 Thematic Mapper Simulator (TMS) bands (adapted from Sabins, 1987).

BAND	WAVELENGTH, μm	CHARACTERISTICS
1	0.46 - 0.52	Visible blue - Maximum penetration of water, useful for distinguishing soil from vegetation and deciduous from coniferous plants as well as mapping forest types and cultural feature identification.
2	0.53 - 0.60	Visible green - Matches green reflectance peak of vegetation, which is useful for assessing plant vigor. Also useful for cultural feature identification.
3	0.63 - 0.70	Visible red - Matches a chlorophyll adsorption band that is important for discriminating vegetation types. Cultural feature identification also.
4	0.77 - 0.91	Reflected near infrared - Useful for determining biomass content and for mapping shorelines. Also useful for soil moisture discrimination.
5	1.13 - 1.35	Reflected near infrared -
6	1.57 - 1.71	Reflected mid infrared - Indicates moisture content of soil and vegetation. Penetrates thin clouds. Good for contrast between vegetation types and for differentiation of snow and clouds.
7	2.10 - 2.38	Mid infrared - coincides with an absorption band caused by hydroxol ions in minerals. Ratios of bands 5 and 7 are potentially useful for mapping hydrothermally altered rocks associated with mineral deposits.
8	10.9 - 12.3	Thermal infrared - Night time images are useful for thermal mapping, vegetation stress analysis, and for estimating soil moisture.

3.2.2 Push Broom Microwave Radiometer

The Push Broom Microwave Radiometer (PBMR) is a four beam microwave radiometer operating at a center frequency of 1.41-GHz (21-cm wavelength, L-band) with a 25-MHz band width and a 0.5-s integration time (Schmugge *et al.*, 1988). The relative sensitivity is 1-K and the absolute sensitivity is approximately 2-K. The antenna receives horizontally polarized radiation. The data logging equipment records brightness temperature values as a function of time.

The PBMR was operative on all 300-m and 1500-m flights of the NASA C-130 aircraft in HAPEX-MOBILHY. There were 15 flights during the SOP during which 300-m and up to 1500-m (depending on cloud base) thermal infrared and microwave data were obtained over two intensive test sites (Schmugge and Janssen, 1988). Both data and ground position maps are available for this study from twelve overflights of the Lubbon site (Northern Central Site) and

five overflights of the Castelnau site (Southern Central Site). The dates of these six flights and some additional information is presented in Table 3.4. The aircraft position as a function of time was determined using a nadir viewing video camera and drawn on IGN (Institut Géographique National) 1:25000 scale maps. The flight paths were digitized as a part of this study and stored in data files by date, site, and flight pass number to assist in ground coordinate assignment.

Table 3.4 Lubbon - Northern Central Site flight dates for PBMR data in HAPEX-MOBILHY, 1986.

Day of Year	Calender Date	300 meter Transects	1500 meter Transects
149	29 May	4, +1 Aborted	1
151	31 May	4	0
154	3 June	4, +1 Aborted	0
157	6 June	4	0
165	14 June	4, +1 Aborted	1
167	16 June	4	2
169	18 June	4	0
174	23 June	4	1
176	25 June	4	1
178	27 June	5	1
181	30 June	4	1
183	2 July	4	1

Table 3.5 Castelnau - Southern Central Site flight dates for PBMR data in HAPEX-MOBILHY, 1986.

Day of Year	Calender Date	300 meter Transects	1500 meter Transects
149	29 May	1	0
151	31 May	1	0
154	3 June	1	0
157	6 June	1	0
160	9 June	1	0

3.2.2.1 Distribution of PBMR Data to Ground Coordinates

The PBMR sensor recorded brightness temperature as a function of time. The time basis must be transformed into spatial coordinates so that the data may be analyzed and compared to other sensors and ground instruments. This Transformation is based on the flight lines digitized using the IGN maps and nadir-viewing camera carried aboard the NASA C-130 aircraft.

To perform the transformation from time to spatial coordinates requires an understanding of the geometry of the PBMR sensor. The beam pattern of the PBMR is illustrated in Figure 3.3.

Several PBMR observations are usually recorded between any two ground points marked on the IGN map, and each map point is associated with an overflight time. Ground coordinate assignment can be based on time scaling, assuming a linear flight line between known (mapped) points and constant aircraft speed. These assumptions are reasonable for the HAPEX-MOBILHY flight missions since these were the objectives of the pilots and the resulting flight lines were reasonably linear. The geometry of a flight line segment between known coordinates is depicted in Figure 3.4.

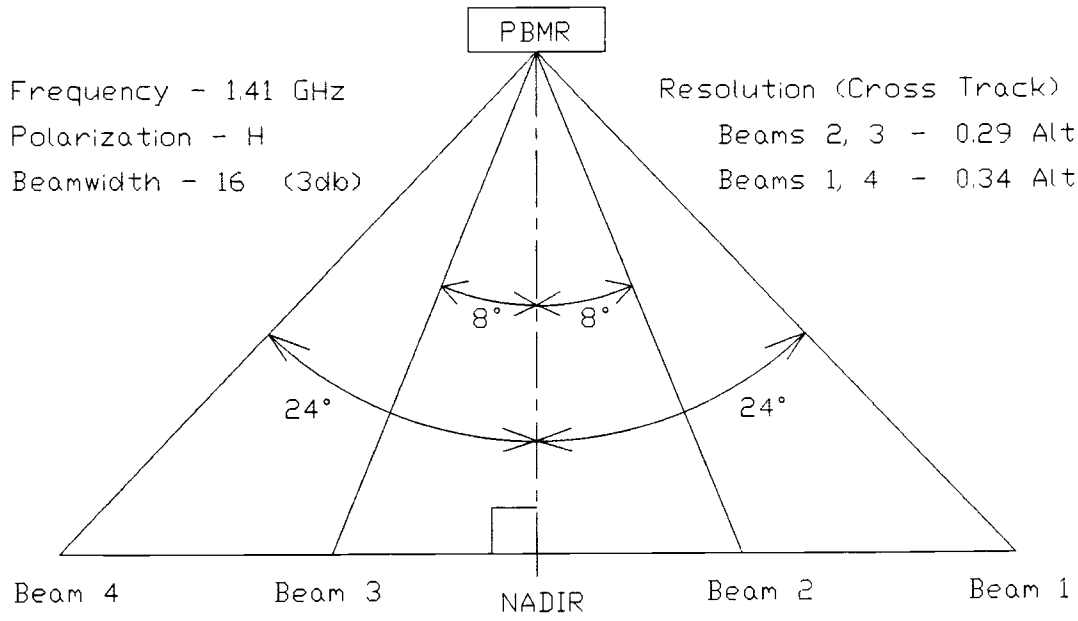

Figure 3.3 PBMR beam pattern (adapted from Schmugge *et al.*, 1988).

To assign the PBMR data to ground coordinates, the flight line segment illustrated in Figure 3.4 is examined using plane geometry to develop a set of appropriate equations. These equations are used to convert a given time to a set of Cartesian coordinates. The first step is to apply the linear, constant speed flight line assumption to scale all sensor time points along the assumed nadir line. For any sensor-recorded time, the nadir position is given in terms of the two known ground points and corresponding times immediately prior and following;

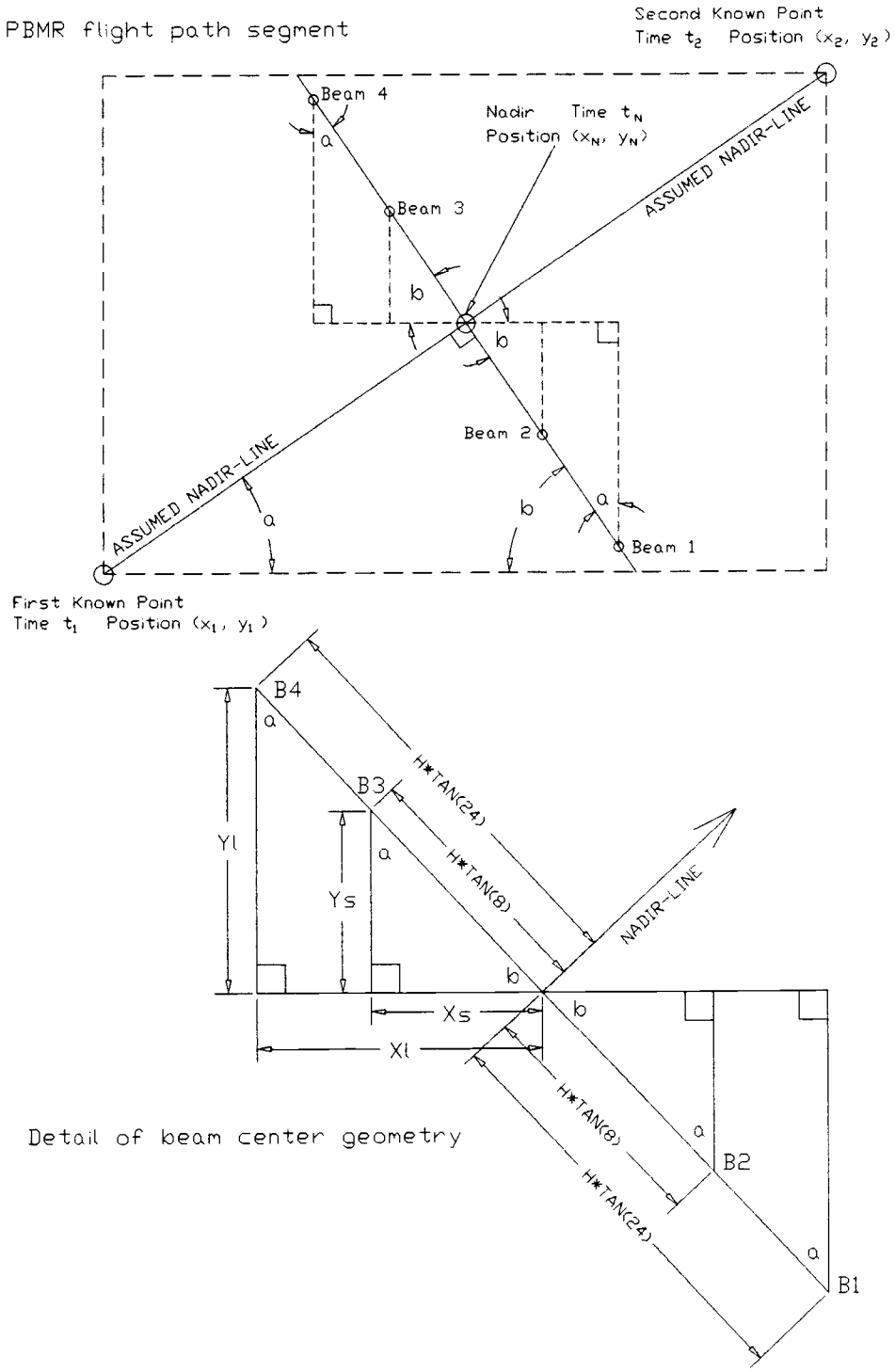

Figure 3.4 PBMR flight line segment geometry.

$$x_N = x_1 + \left(\frac{t_N - t_1}{t_2 - t_1}\right)(x_2 - x_1) \tag{3-4a}$$

$$y_N = y_1 + \left(\frac{t_N - t_1}{t_2 - t_1}\right)(y_2 - y_1) \tag{3-4b}$$

where all terms are as identified in Figure 3.4.

With the nadir position known for any sensor time, the beam center positions can be found. The lower portion of Figure 3.4 is a detail of the line perpendicular to the nadir line intersecting at the current nadir. All four PBMR beam centers occur on this line. Use of right triangles and similar triangles permits the beam center coordinates to be computed. The basic angle ($<\alpha$, *a* in Figure 3.4) is the angle between the nadir line and the x-axis, computed as

$$<\alpha = \tan^{-1}\left(\frac{y_2 - y_1}{x_2 - x_1}\right) \tag{3-5}$$

This angle is repeated in the right triangles in the detail of Figure 3.4. Using this computed angle, the beam coordinates are computed by the following equations;

$$\sin(\alpha) = \frac{x_s}{\tan(8°)H} = \frac{x_l}{\tan(24°)H} \tag{3-6a}$$

$$\cos(\alpha) = \frac{y_s}{\tan(8°)H} = \frac{y_l}{\tan(24°)H} \tag{3-6b}$$

Simple algebraic manipulation yields

$$x_s = \sin(\alpha)\tan(8°)H \tag{3-7a}$$

$$x_l = \sin(\alpha)\tan(24°)H \tag{3-7b}$$

$$y_s = \cos(\alpha)\tan(8°)H \tag{3-7c}$$

$$y_l = \cos(\alpha)\tan(24°)H \tag{3-7d}$$

8° and 24° are the angles indicated in Figure 3.3. The four distances computed in the above equations are added or subtracted from the nadir coordinates [computed previously in equation (3-4) to obtain the four sets of beam center coordinates];

$$x_{B1} = x_N + x_l \tag{3-8a}$$

$$y_{B1} = y_N - y_l \tag{3-8b}$$

$$x_{B2} = x_N + x_s \tag{3-9a}$$

$$y_{B2} = y_N - y_s \tag{3-9b}$$

$$x_{B3} = x_N - x_s \tag{3-10a}$$

$$y_{B3} = y_N + y_s \tag{3-10b}$$

$$x_{B4} = x_N - x_l \tag{3-11a}$$

$$y_{B4} = y_N + y_l \tag{3-11b}$$

The above equations apply only to a flight vector in the first quadrant of the Cartesian coordinate system. A different quadrant requires different signs on the distances added to the nadir coordinates such that beams 1 and 2 are positioned 90° and beams 3 and 4 are positioned 270° relative to the flight vector.

The system of equations developed here were incorporated into a computer program called POINT which used digitized flight line information and original PBMR data (time-basis) to create a data file with PBMR data and separate coordinates for each data point. The POINT source code listing is provided in Appendix A. POINT was designed to operate in either prompt mode (prompting the user to input appropriate file names and information) or command-line mode (where the necessary information is provided in the DOS[3] command line used to invoke the program). The command-line option allows use of batch files to process several data sets while the computer is unattended.

---

3 DOS - Disk Operating System. Operating system environment for IBM and compatible personal computers (PC's), the system used in this study. MS-DOS is a registered trademark of Microsoft Corporation. IBM and PC-DOS are registered trademarks of International Business Machines Corporation.

3.2.2.2 Development of PBMR Imagery

Once the PBMR data were assigned ground coordinates following the previous algorithm it was possible to form the data into imagery. Another algorithm was required to spatially distribute data for this process. This section outlines the algorithm developed for this study.

The data files generated by the POINT program provided brightness temperatures for each beam, the Cartesian coordinates of the center of that beam, and header information, e.g., aircraft altitude. A grid-based approach was used to create an image with this information. Image size and grid resolution were determined in advance of data processing.

The algorithm is presented here in a step-by-step format for clarity. Each operation is performed for one PBMR beam at a time.

1. Compute the radius of the view area of the beam. Use the radius to determine if any of the view area of the beam is within the desired image area. If not, repeat this step with the next beam.
2. Identify a "search box" encompassing the view area of the beam. Search box dimensions are to coincide with grid nodes.
3. For each grid node within the search box compute the euclidian distance between the grid node and the beam center. If this distance is greater than the beam radius return to step one for the next beam.
4. Assign the grid node the brightness temperature recorded for the current beam. If the grid node is observed by more than one beam, assign the average of all observations.

Use of the above algorithm resulted in brightness temperatures imagery over specified areas of interest. Notice that the portions of the image not viewed by the PBMR possessed values of zero, reflecting the lack of data. To some extent judgement is required in selecting both the image size and the grid resolution. The grid cell size should be less than the typical beam diameter, and the smaller the cell size the better the resolution of the resulting image. Conversely, too small of grid cell size will require unnecessary computations and processing time.

The program developed to incorporate this algorithm was DISTRIB. A flowchart outlining the operations of DISTRIB is shown in Figure 3.5. The source code for DISTRIB is provided in Appendix A. DISTRIB may be used in either prompt or batch file modes. In prompt mode the program queries the user for the information necessary to run. In batch mode a prompt file may be recorded in advance. The batch mode allows unattended processing of several large images.

DISTRIB uses binary file storage to attain rapid image file creation with minimal data storage requirements during processing. In binary mode, any grid node in the image is represented by a single precision real number in the image file. A value's location in the binary file corresponded to its spatial location. Binary file handling permitted any record to be read and written at random, relieving the program of the need to open and close files. To facilitate the averaging of multiple observations of a particular grid node, a "shadow file" technique was developed. A shadow file was the same size as the image file and was used to record the number of times the grid node is viewed. This value was retrieved from the shadow file each time the grid node was viewed during processing and used to properly weight each observation using the equation

$$T_B^{AVG} = \frac{n-1}{n} T_B^{NEW} + \frac{n}{n-1} T_B^{OLD} \qquad (3\text{-}12)$$

where

T_B^{AVG} = averaged brightness temperature

T_B^{NEW} = "new" brightness temperature, for current observation

T_B^{OLD} = "old" brightness temperature, previously recorded

n = number of observations, from the "shadow file"

This equation applies to any value of n, permitting the binary image file to be updated with averaged brightness temperatures for each grid node as the node is encountered in a program looping structure.

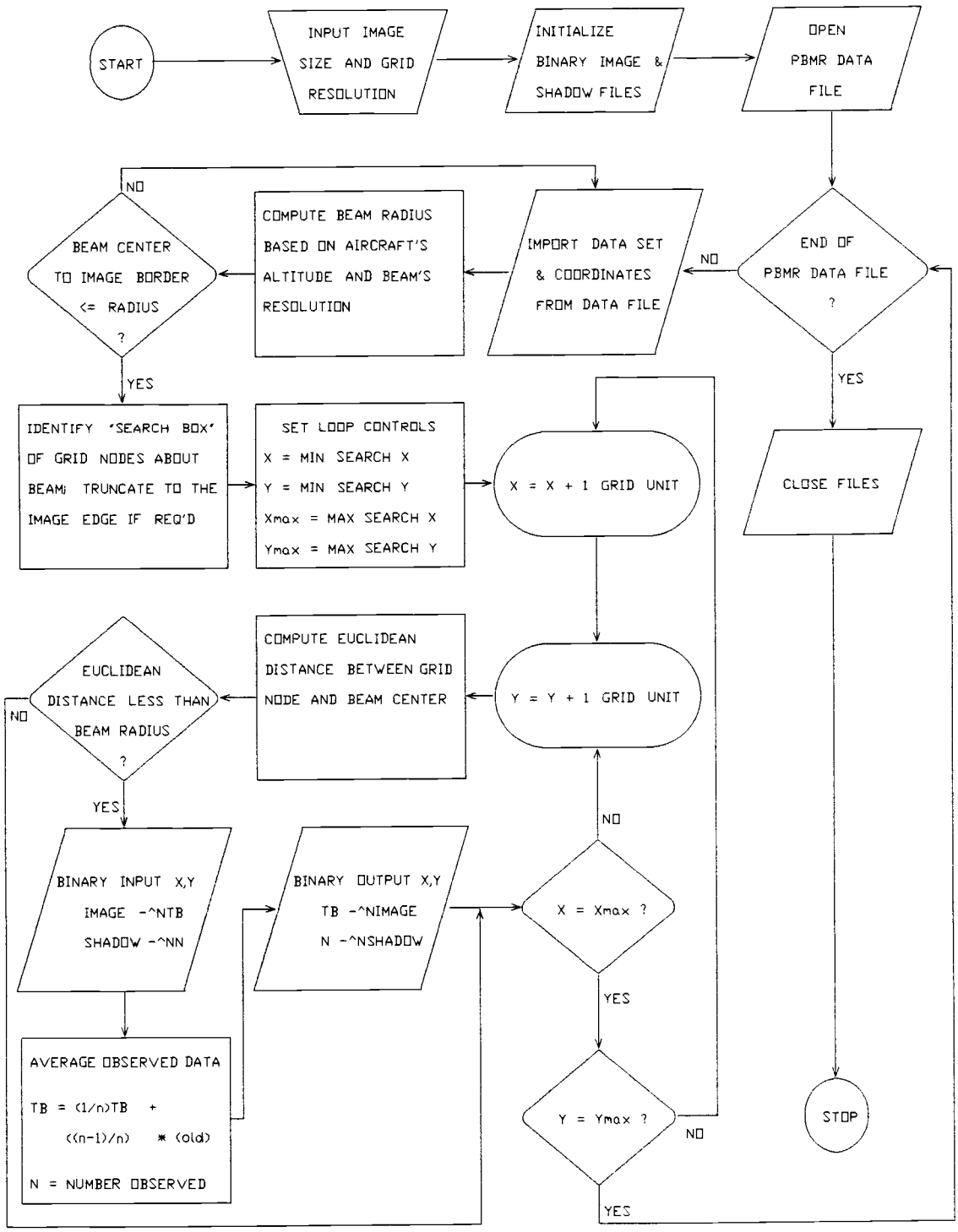

Figure 3.5 Flowchart of Program DISTRIB.

Several commercial software packages were available for image processing and analysis. For this study IDRISI Version 3.0 was selected as the basic software set to use in viewing, manipulating, and presenting imagery. A major strength of this particular package is its modular nature. IDRISI is a grid-based geographic analysis system, comprised of a variety of modules that share a common data format. This allows the addition of new modules to meet the user's specific needs if the distributed modules do not. The grid-based approach is not to be confused with a Geographic Information System (GIS), though IDRISI can serve in this capacity.

Two modules, UNPACK and MAKEMASK, were developed for processing and analysis of the PBMR data. To support construction of these modules a user's library, IDRISI.LIB, was also developed. IDRISI.LIB contains the base subroutines used by all IDRISI modules to read and create data files and to read the IDRISI environment file. UNPACK is a conversion utility required for conversion of IEEE[4] standard binary numbers (used by DISTRIB and MAKEMASK, but unintelligible to IDRISI) to ASCII[5] numbers. MAKEMASK filled a need not addressed by existing IDRISI modules for easy definition of query masks. These masks were necessary for extraction of image data representing the locations of fields where ground crews collected surface soil moisture data. The values of the pixels extracted from the image were related to the ground truth data in the calibration procedure (see Section 4.2.2, Brightness Temperature and Surface Soil Moisture). Both UNPACK and MAKEMASK were developed as IDRISI modules because of their general utility beyond the boundaries of this study. Source code is provided in Appendix A for IDRISI.LIB, UNPACK, and MAKEMASK.

---

4 Institute of Electrical and Electronics Engineers, Inc (IEEE). IEEE format numbers are used by QuickBASIC 4.5, the language in which POINT, DISTRIB, UNPACK, and MAKEMASK were written and compiled in.

5 American Standard Code for Information Interchange (ASCII), a format commonly used for alpha-numeric data storage in IBM-compatible personal computers.

4 DATA ANALYSIS AND RESULTS

This section presents the results of analysis of data collected by a variety of sensors in the HAPEX-MOBILHY Program. The analysis was aimed at meeting the objectives outlined in Section 1 concerning examination of the surface energy balance and variation in surface soil moisture.

4.1 Evaporative Fraction

The evaporative fraction (EF) was previously defined (see Section 2.1.1, Surface Energy Balance) as the ratio of latent heat flux to the sum of sensible heat flux and latent heat flux. FIFE investigators found the evaporative fraction to be a useful tool for characterization of the relative energy partition because it provided a relatively stable and direct measure of this quantity (Sellers *et al.*, 1989; Shuttleworth *et al.*, 1989). A different database, the SAMER system data collected during the HAPEX-MOBILHY SOP was used in this study. The purpose of this study was to determine if the evaporative fraction is stable during daylight periods when the surface energy balance is most significant. If this quantity is stable, then is the evaporative fraction of the midday period representative of the entire daylight period, i.e., can it be used to characterize the energy balance of the day? If the answers to these questions are affirmative, the potential for remote sensing applications is significant. The usefulness of a single parameter detected at an instantaneous midday time and used to infer the complete diurnal surface energy balance is evident.

FIFE investigators examined the behavior of the evaporative fraction for the four "golden days" of the 1987 FIFE program. For fairly ideal conditions, i.e. no clouds and a "typical" diurnal surface energy balance, the EF was relatively stable. The interest of this study was in whether this observed stability, and hence representativeness, holds true in less than ideal conditions. To determine this the SAMER database has been examined for both "clear sky" conditions and for a more complete database comprised of all dates and stations with a full daylight record amounting to 566 samples.

It is necessary to point out the reason for analyzing the daylight period only. Figure 4.1 depicts a typical surface energy balance for a nearly ideal diurnal cycle observed over the Lubbon 1 site (SAMER 01) on June 16, 1986. This station was located over a nearly mature oat field; the surface energy balance reflects this in the large proportion of energy devoted to evaporative flux. The negative sensible heat flux in late afternoon indicates the presence of advection processes. In contrast, in Figure 4.2 the sensible heat flux was of greater relative magnitude than the latent heat flux. Figure 4.2 is for the Lubbon 2 site (SAMER 05) on the same date as for Figure 4.1, but that station was located in an adjacent maize field which was immature and hence not transpiring at the high rate of the oats. Thus, surface evaporation was the dominant process over the SAMER 05 site on this date. For a land surface energy balance, the significant activity during the diurnal cycle occurs during the daylight period. Figures 4.1 and 4.2 illustrate that the significant energy transfer processes occur in the daylight period when solar radiation is available. From this it follows that if the daylight period can be adequately described, the magnitude of the various fluxes for the given day are largely known.

The EF is computed from the two turbulent flux terms between the atmosphere and the land surface (latent heat flux and sensible heat flux). At night these fluxes are relatively small in magnitude and typically undergo a sign reversal. Consequently, the EF is highly unstable or possibly undefined during at night. In this section certain aspects of the EF will be examined, but since the value is meaningless at night, the analysis was restricted to the daylight period. As noted in the preceding discussion, little information is lost from examining only daytime land surface activity. For instance, the ratio of day to night latent heat flux for Figure 4.1 is 10.8, and for Figure 4.2 this ratio is 10.6.

The EF for the dissimilar energy balances shown in Figures 4.1 and 4.2 are shown together in Figure 4.3. The lower transpiration rate of the young maize compared to the maturing oats is reflected in the evaporative fraction; the SAMER 05 evaporative fraction was consistently lower than that for SAMER 01 during the daylight period. A yet unanswered question was the relative stability of the EF during this time. To explore this, the complete SAMER database containing the information depicted in Figures 4.1, 4.2, and 4.3 was analyzed using statistical techniques. Before this, the evaporative fraction values were computed from SAMER data based on selection criteria discussed below.

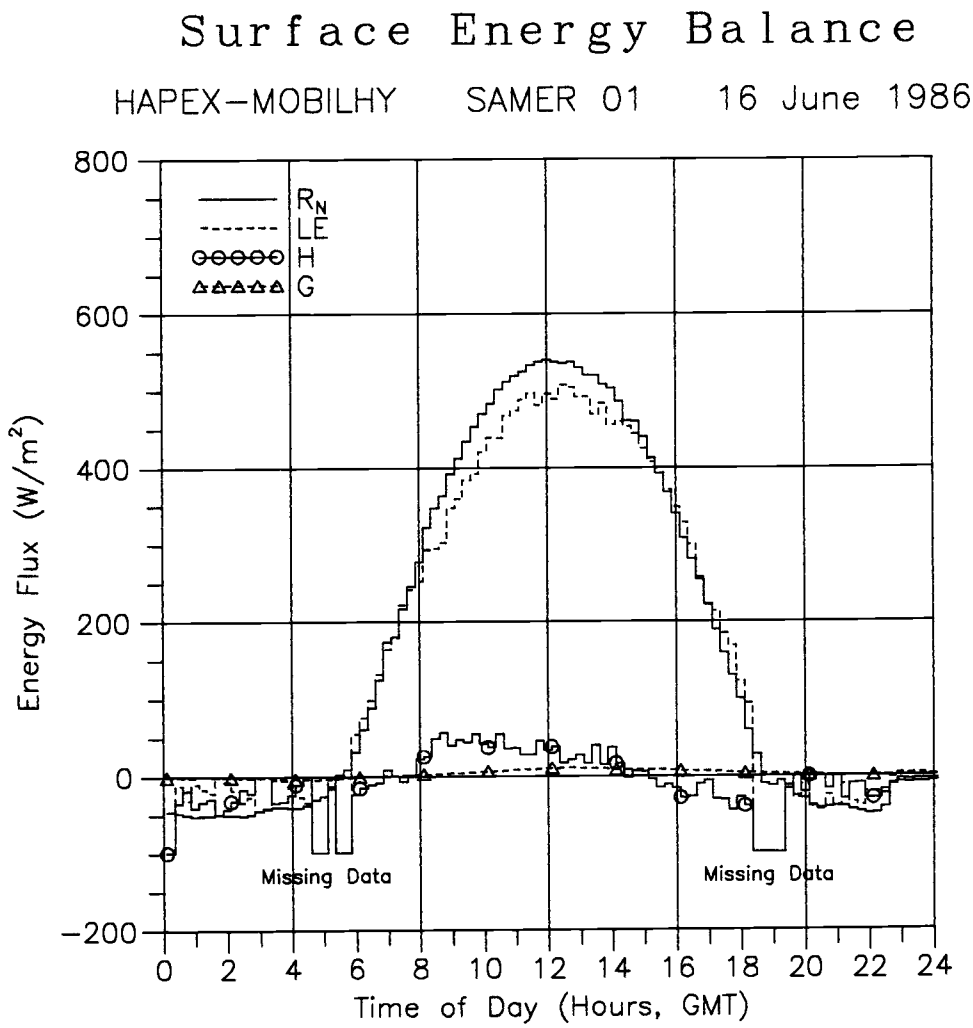

Figure 4.1 Diurnal surface energy balance for Lubbon 1 site (SAMER 01) on 16 June 1986 (86D167). This SAMER station was located over a developed oat crop with mean vegetation height of 128-cm.

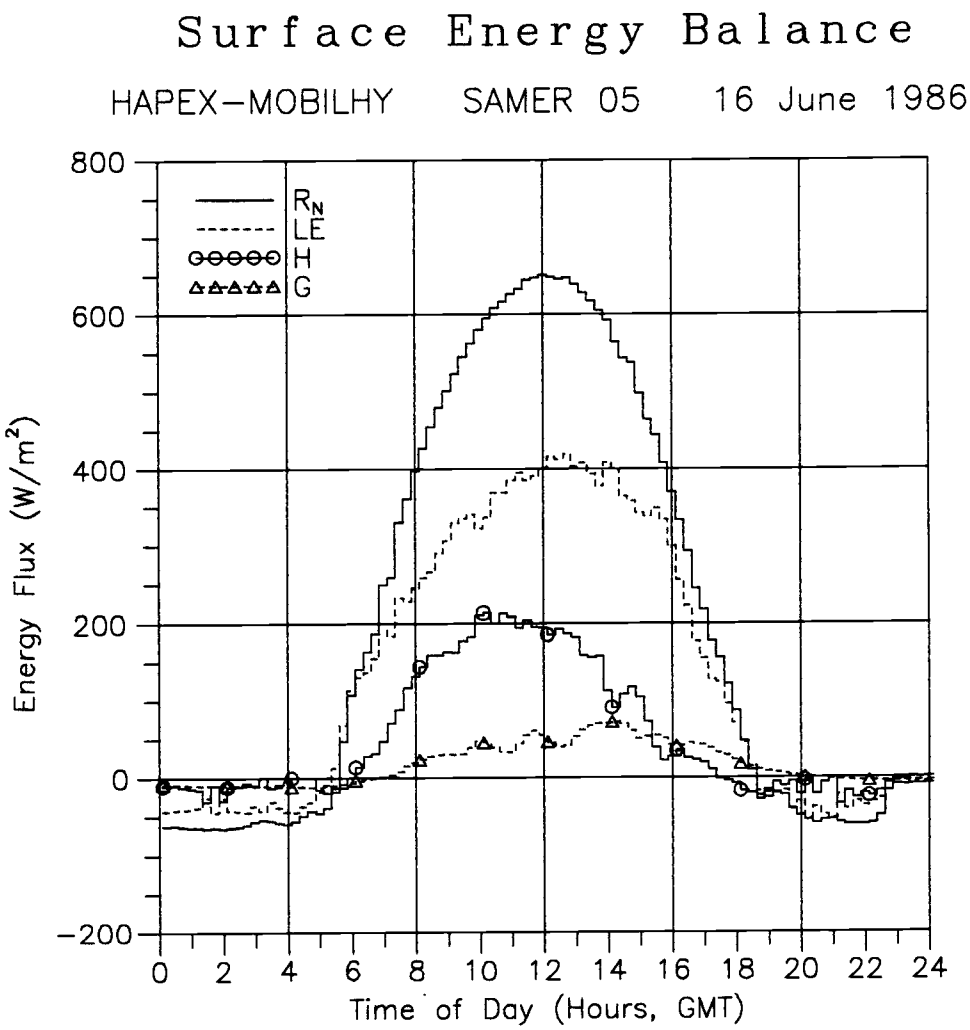

Figure 4.2 Diurnal surface energy balance for Lubbon 2 site (SAMER 05) on 16 June 1986 (86D167). This SAMER station was located over a young maize crop with mean vegetation height of 10-cm.

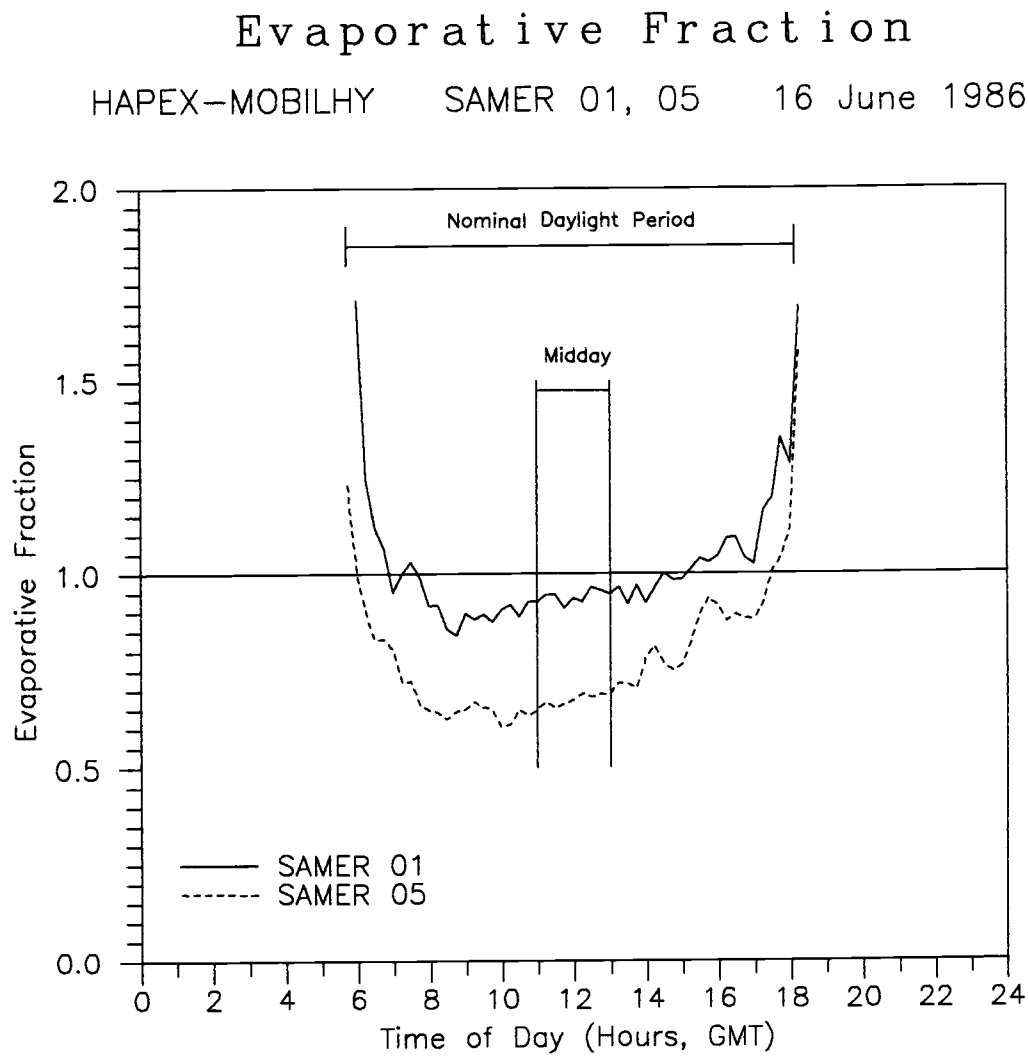

Figure 4.3 Evaporative Fraction (EF) for Lubbon 1 (SAMER 01) and Lubbon 2 (SAMER 05) on 16 June (86D167). This plot corresponds to the surface energy balances in Figures 4.1 and 4.2.

4.1.1 Computation of Evaporative Fraction

To expedite the analysis, the SAMTRAN[1] software system was used for data management. This program permitted the evaporative fraction to be computed at 15-minute intervals and downloaded along with corresponding surface energy balance data. The coding of SAMTRAN restricted the computation of the EF to those records for which both the latent and sensible heat fluxes were recorded. Since only the daylight period was of interest, the module in SAMTRAN devoted to EF computation invoked a sunrise/sunset calculation routine[2] and excluded data processing for records before local sunrise and after local sunset. The actual equations used for this purpose were;

$$t_1 = \frac{12}{\Pi}\cos^{-1}\left[\tan(\delta)\tan(\phi) + \frac{0.0145}{\cos(\delta)\cos(\phi)}\right] \tag{4-1}$$

$$t_2 = 24 - t_1$$

$$\delta = 0.41\cos\left(2\Pi\frac{N-172}{365}\right)$$

where

t_1 = sunrise time (hours)

t_2 = sunset time (hours)

---

1 SAMTRAN Version 3.6 SAMER Translation software developed by the Water Resources Engineering Team at Oregon State University for SAMER data management using IBM Personal Computers. SAMTRAN is documented separately in a User's Guide, which is available along with the software from the Water Resources Engineering Team.

2 MORECS - British Meteorological Office operation evapotranspiration system. SAMTRAN was developed in part to provide data for testing Penman-type reference evapotranspiration methods and the MORECS model which distinguishes between day and night activity. To accomplish this the time computation equations were included in SAMTRAN and this module was shared with the evaporative fraction module developed later.

ϕ = latitude (decimal degrees)

N = day of the year (Julian date; January 1 = day 1)

δ = solar declination angle (radians)

After downloading the appropriate data and the corresponding EF values, the data were inspected graphically using a program, EVAPVIEW, developed exclusively for this purpose (for a complete computer source code listing, refer to Appendix A). EVAPVIEW provides the user with two graphs to aid in accepting or rejecting EF values for further analysis. The first graph displays the surface energy balance profile, permitting the user to determine if all sensors were operative during the period of interest; if not, the EF values for that date are rejected. The second graph displays the evaporative fraction trace for the day. This graph permits the user to "trim" EF records from the start and end of the day which belong to the period of unstable nighttime activity and which cannot be considered a stable daytime value. This was generally required only for cloudy days when surface energy activity is suppressed beyond sunrise and prior to sunset, extending the effective unstable night period. A third graph displays a scatter plot of mean midday EF versus mean all-day EF for all dates already selected, so that the points position does not influence the user in acceptance or rejection of the date. This graph aids in preliminary visualization of the linear fit resulting from the data for the current station.

In accepting a date, EVAPVIEW requires the user to indicate whether the day is a "clear" date or a "rough" date. "Clear" refers to ideal or near-ideal situations associated with clear, cloud-free days, whereas "rough" indicates a departure from these conditions. This determination for a given day is largely a matter of judgement that depends on the user's experience, based on the shape of the surface flux curves depicted in EVAPVIEW's first graph. On a clear, relatively cloud-free day the curves, particularly for net radiation, take on a characteristic bell shape and are fairly smooth. Figures 4.1 and 4.2 are examples of dates designated as "clear." Conversely, any scattered cloud cover will appear as sharp depressions in the net radiation curve, while general cloudiness tends to depress the entire curve and to provide a much more "rough" appearance. Figure 4.4 depicts such an energy balance for the Fusterouau site (SAMER 11) on June 4, 1986. In the humid climate in which the

HAPEX-MOBILHY grid was located, these days tended to be more common than the "clear" conditions shown previously for the Lubbon site; the mean ratio of clear to cloudy days for the examined data was 6.5.

When a date was accepted, EVAPVIEW computed the mean midday evaporative fraction (EF_M) from all 15-minute records occurring between 1100hrs and 1300hrs, taken as the time during which most remote sensing missions are flown. The all-day evaporative fraction (EF_A) was computed from the daylight period (trimmed as necessary) exclusive of the midday period. This exclusion in computing EF_A was made to prevent auto-correlation of these statistics and maintain independence for later testing. If a date was judged to be "clear," the values computed for that date were saved to both a "clear-sky" database and a general one, while a rough date was saved only to the general database.

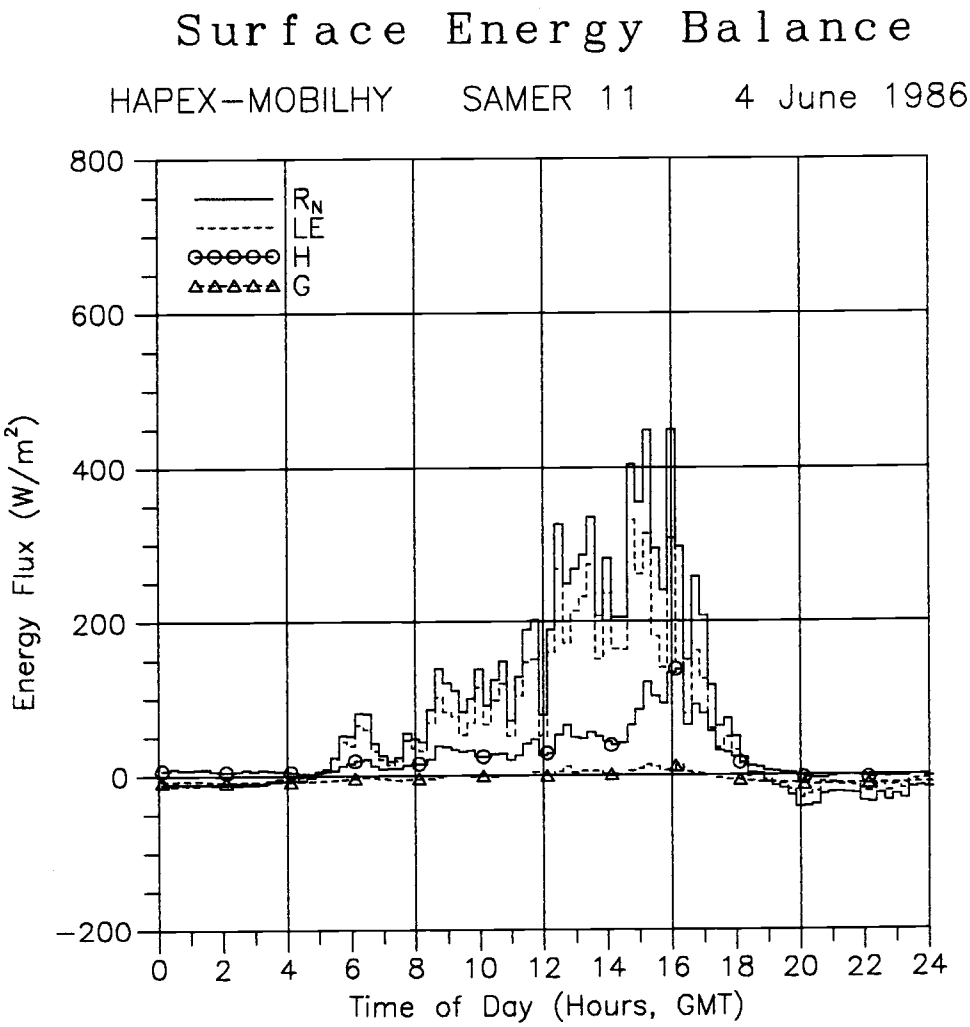

Figure 4.4 Diurnal surface energy balance for Fusterouau site (SAMER 11) on 4 June 1986 (86D155). This SAMER station was located over a young maize crop.

4.1.2 Evaporative Fraction Stability

To examine the correlation of midday evaporative fraction with the mean evaporative fraction for the full daylight period, the inspected HAPEX-MOBILHY data were plotted in a series of scatter plots. One plot was made for each station, with "clear-sky" and "rough" conditions distinguished within each plot. These plots appear in Figures 4.5 through 4.16. In each plot the best linear fit is indicated (solid line), as well as the one-to-one (x = y) line. Assuming that the midday evaporative fraction (plotted as the independent variable) is equal to the all-day value, the points should fall about the one-to-one line. In addition, Figure 4.17 depicts the scatter plot for all clear dates from all twelve SAMER stations. The strong correlation, which was observed by FIFE investigators, is apparent in this plot for near-ideal conditions, but is not apparent in the other plots for all conditions. Table 4.1 provides a summary of the linear regression parameters for each station and for the lumped database (all 12 SAMER stations) for both total and clear-sky conditions. In general, the strength of the linear relationship was stronger for clear-sky conditions at each site than for the total SOP at that site. This observation holds for the lumped data as well.

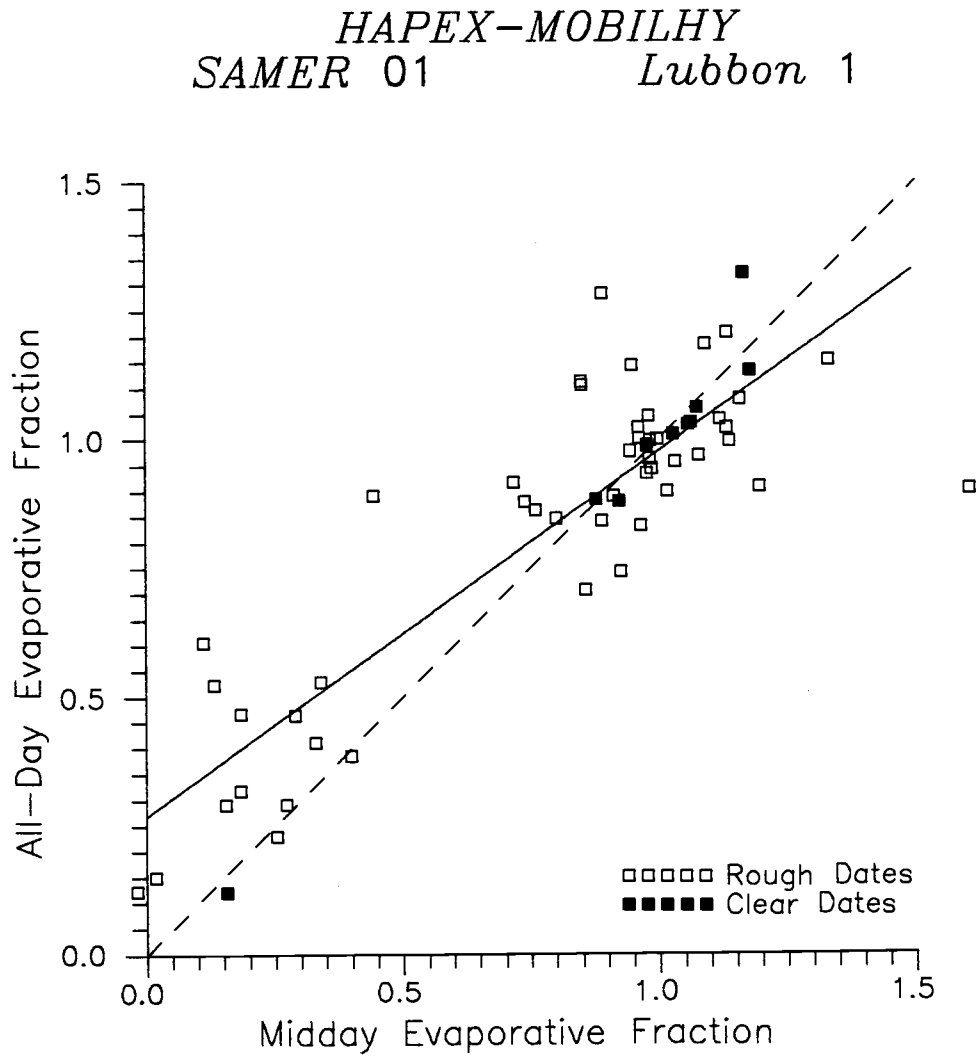

Figure 4.5 Scatter plot of midday versus all-day evaporative fraction for SAMER 01 (Lubbon 1).

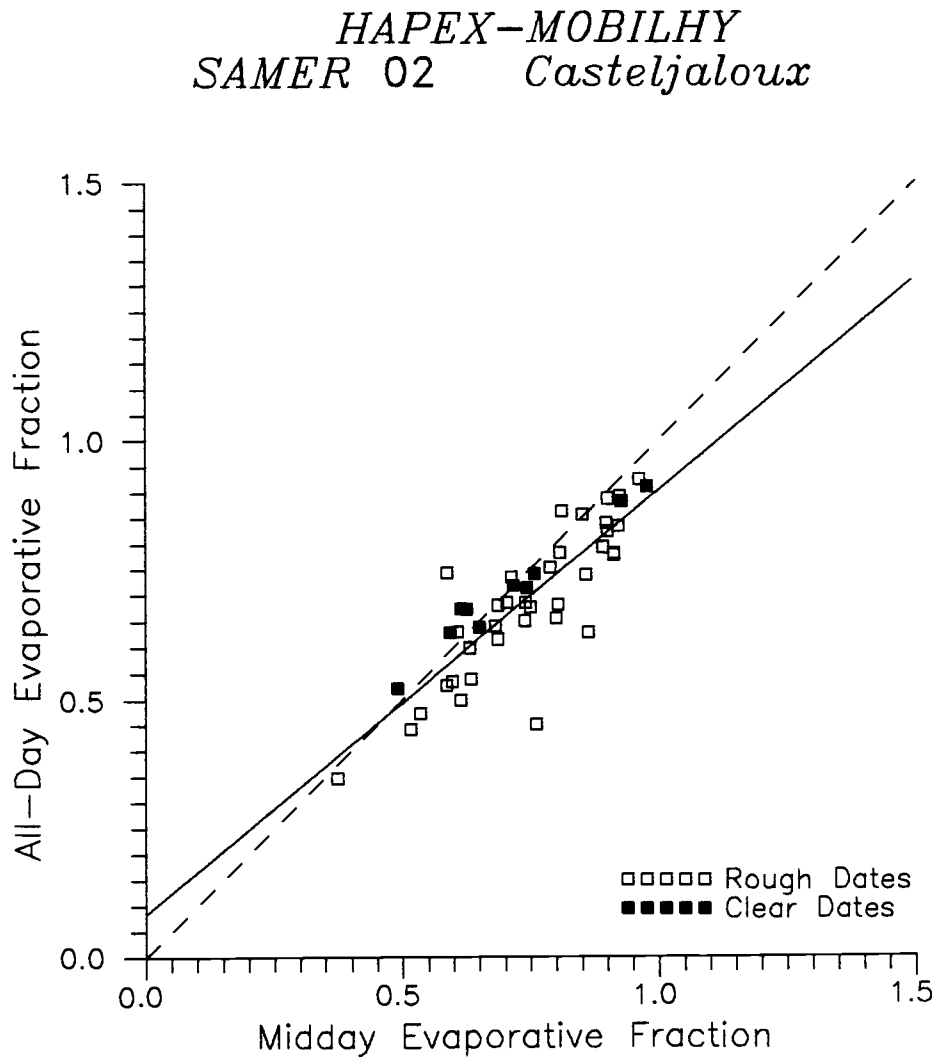

Figure 4.6 Scatter plot of midday versus all-day evaporative fraction for SAMER 02 (Casteljaloux).

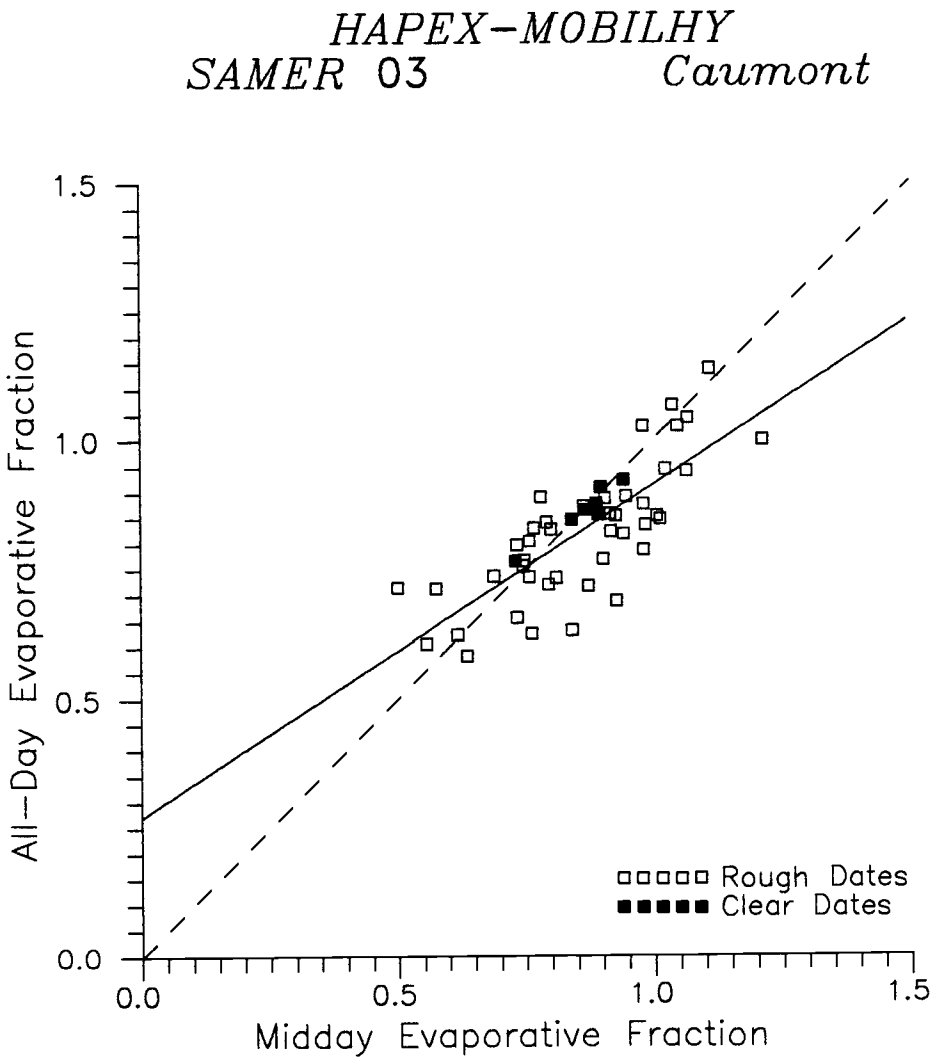

Figure 4.7 Scatter plot of midday versus all-day evaporative fraction for SAMER 03 (Caumont).

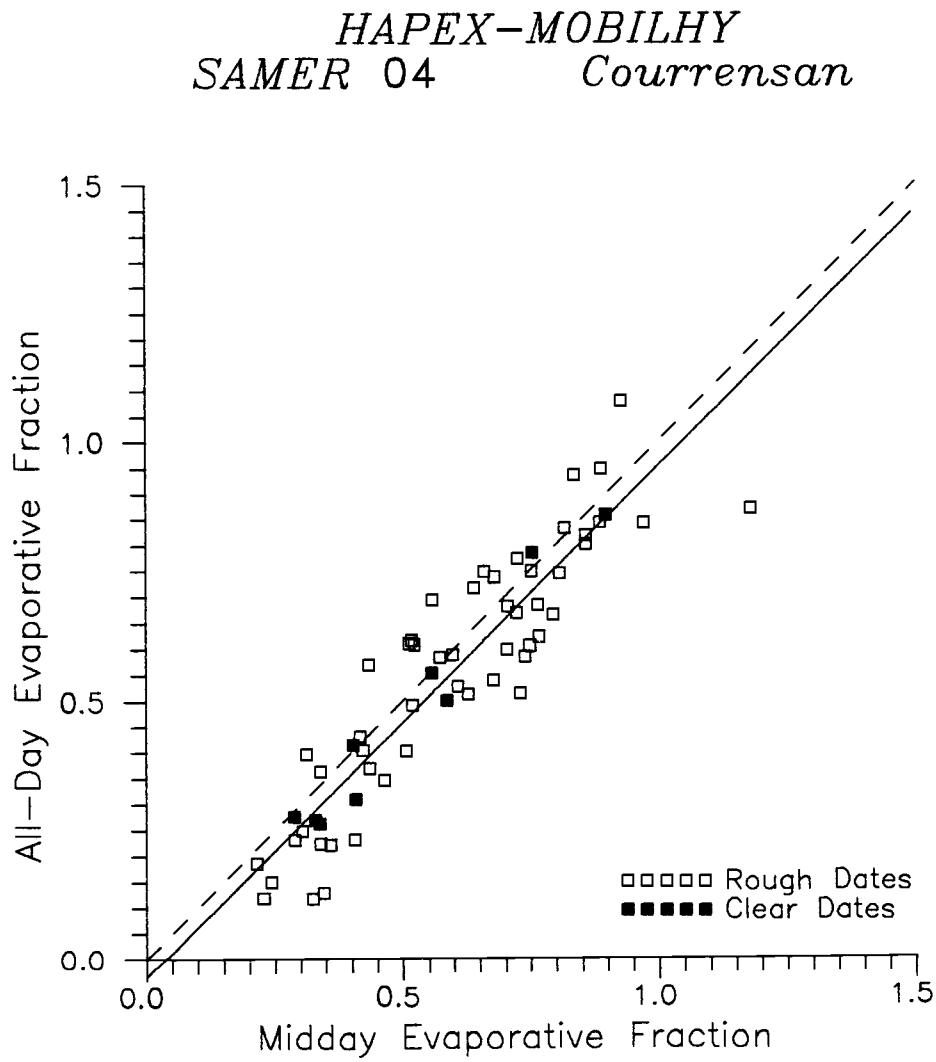

Figure 4.8 Scatter plot of midday versus all-day evaporative fraction for SAMER 04 (Courrensan).

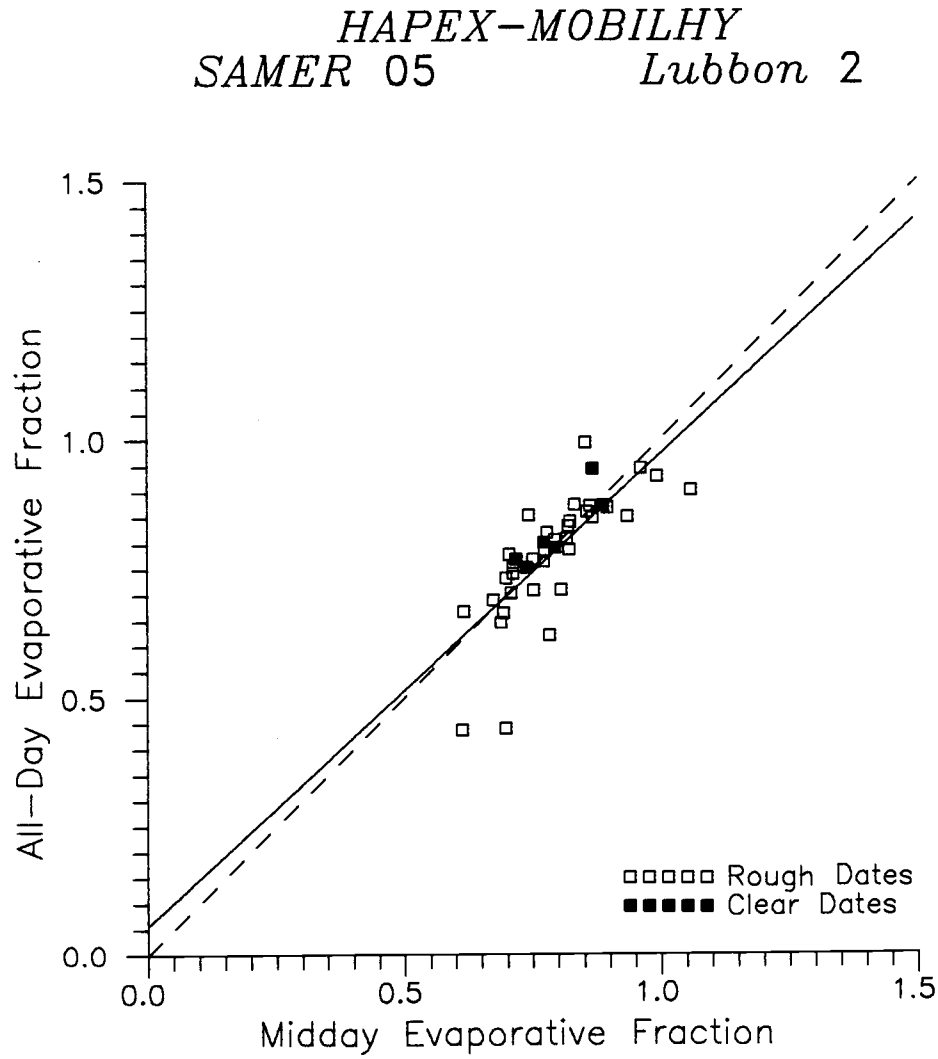

Figure 4.9 Scatter plot of midday versus all-day evaporative fraction for SAMER 05 (Lubbon 2).

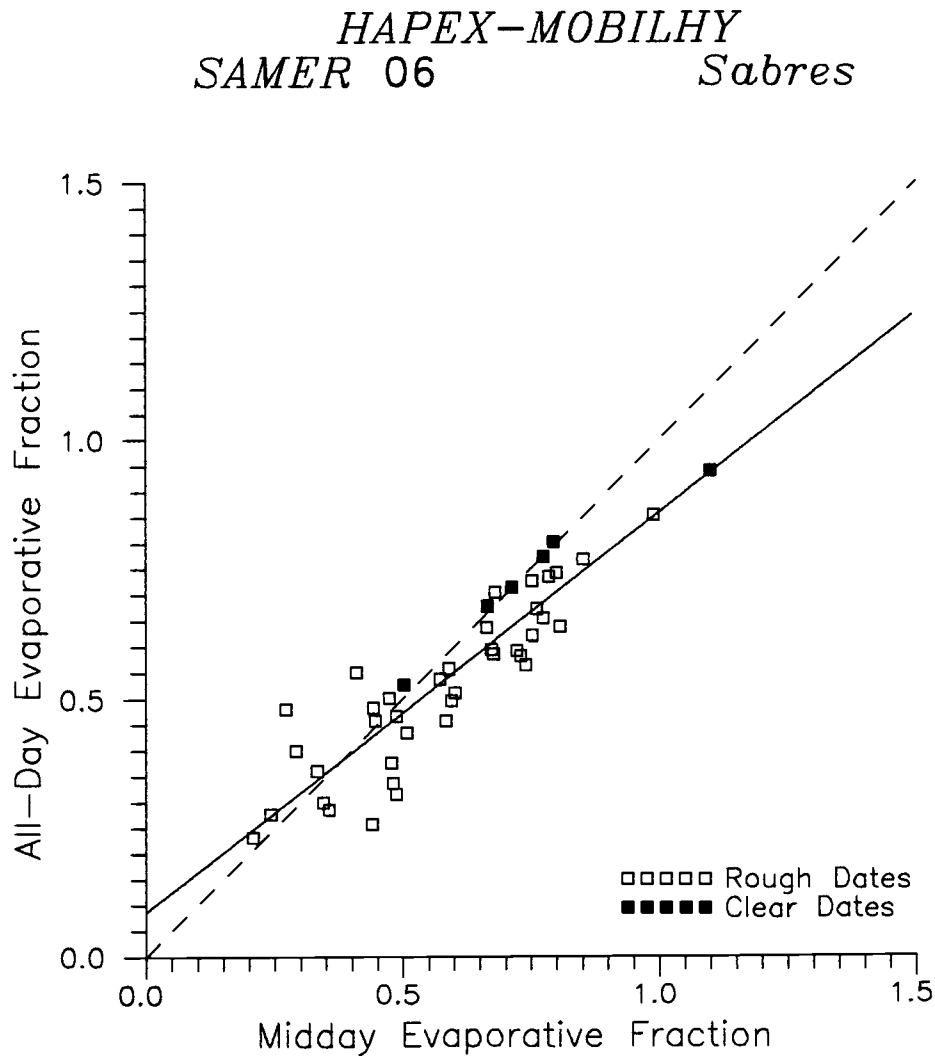

Figure 4.10 Scatter plot of midday versus all-day evaporative fraction for SAMER 06 (Sabres).

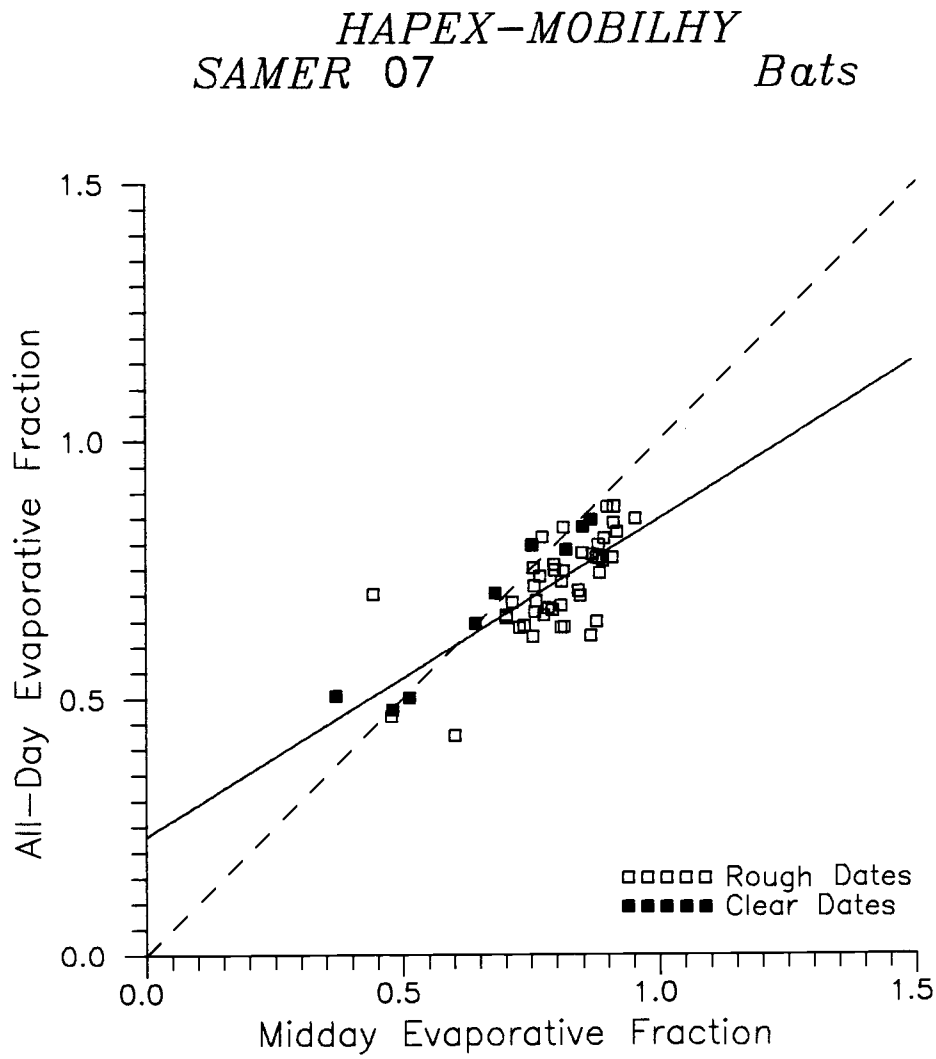

Figure 4.11 Scatter plot of midday versus all-day evaporative fraction for SAMER 07 (Bats).

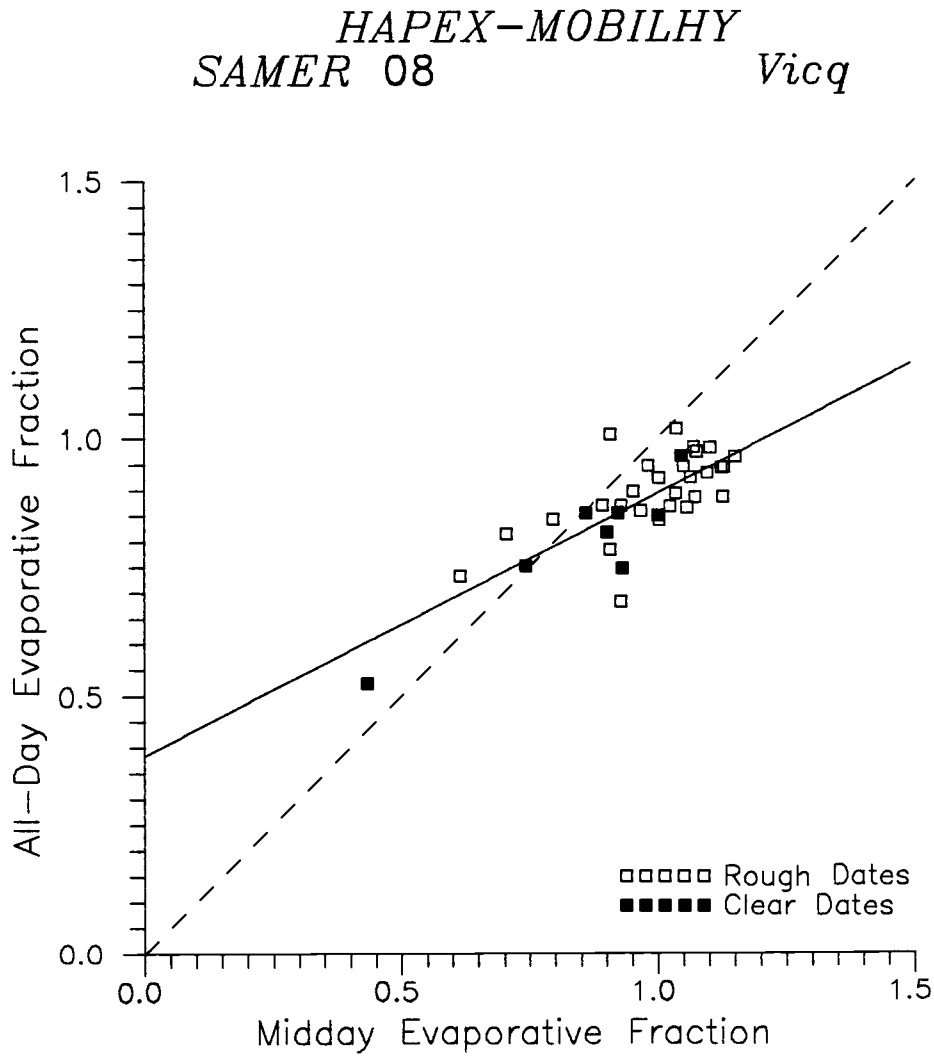

Figure 4.12 Scatter plot of midday versus all-day evaporative fraction for SAMER 08 (Vicq).

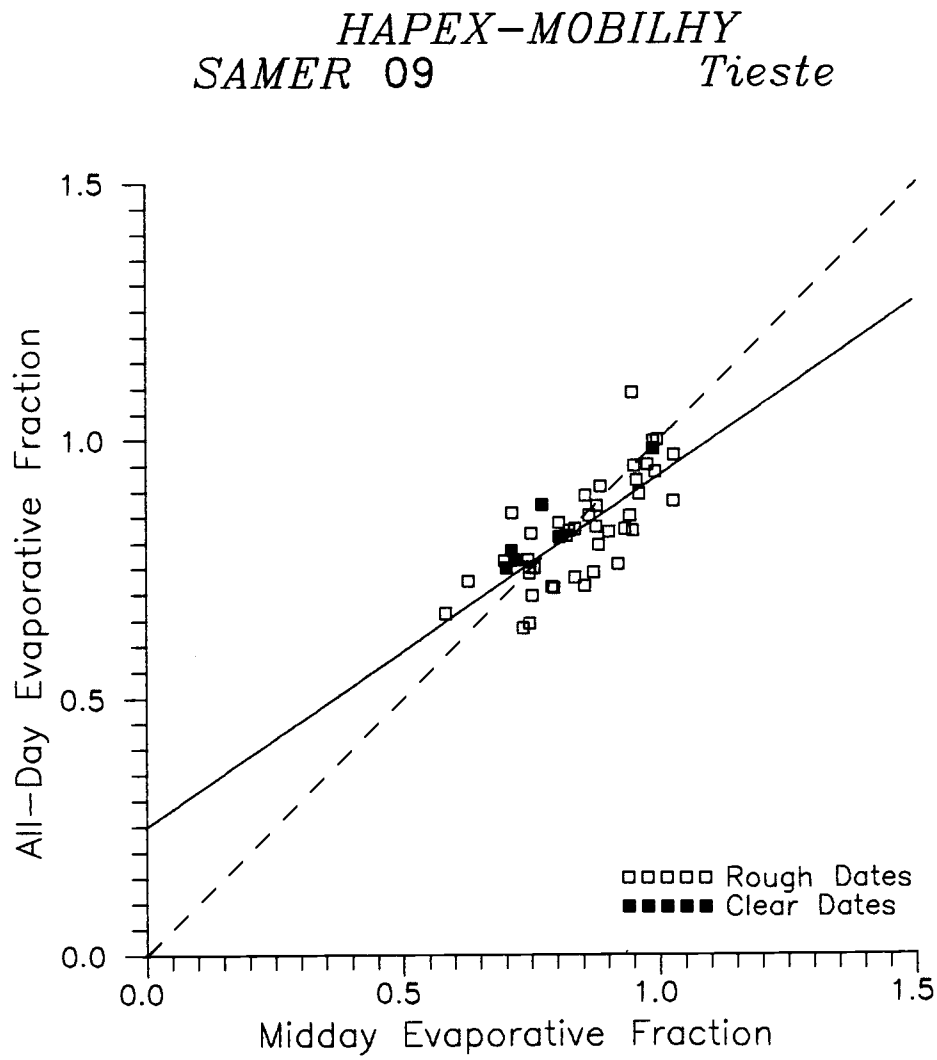

Figure 4.13 Scatter plot of midday versus all-day evaporative fraction for SAMER 09 (Tieste).

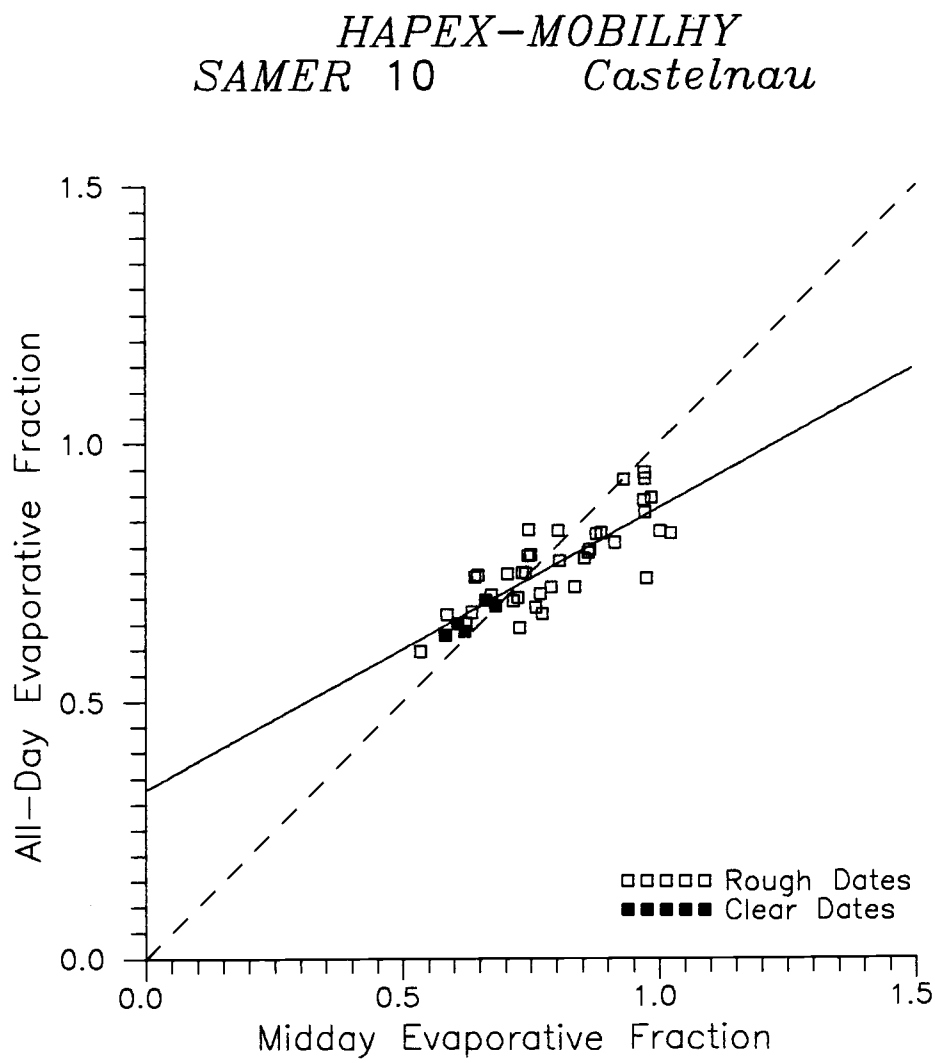

Figure 4.14 Scatter plot of midday versus all-day evaporative fraction for SAMER 10 (Castelnau).

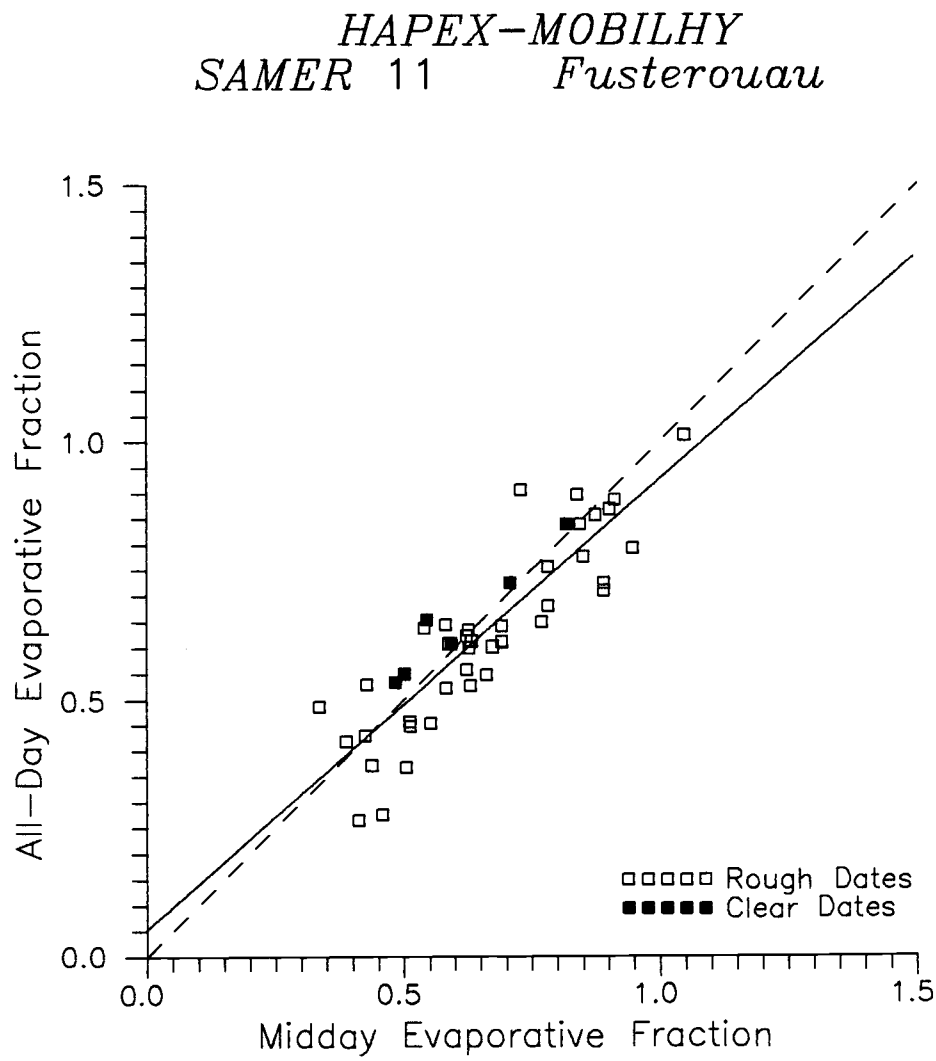

Figure 4.15 Scatter plot of midday versus all-day evaporative fraction for SAMER 11 (Fusterouau).

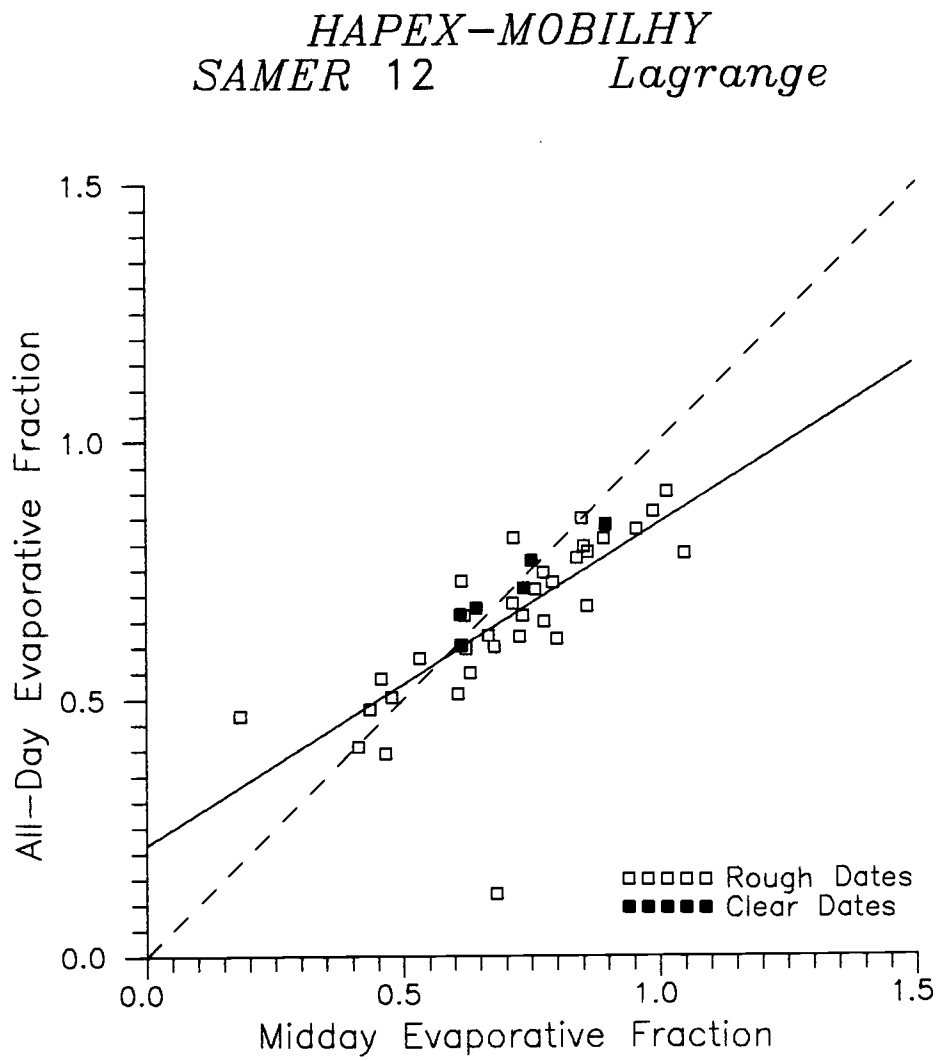

Figure 4.16 Scatter plot of midday versus all-day evaporative fraction for SAMER 12 (Lagrange).

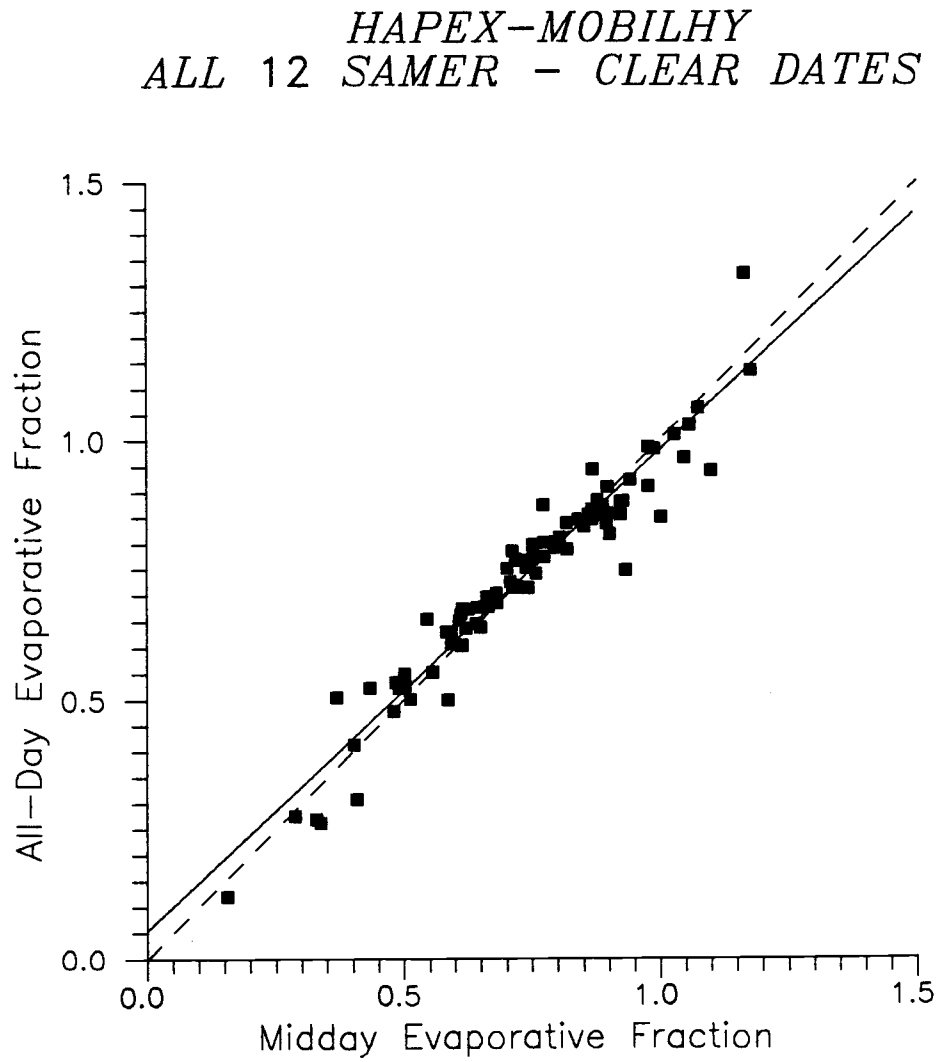

Figure 4.17 Scatter plot of midday versus all-day evaporative fraction for all twelve SAMER stations for clear-sky conditions.

Table 4.1 Summary of parameters for linear regression of midday evaporative fraction against all-day evaporative fraction.

SAMER No.	All Data				Clear Sky			
	Number of Obs.	Slope β_1	Intercept β_0	R^2	Number of Obs.	Slope β_1	Intercept β_0	R^2
01	59	0.708	0.269	0.776	9	1.06	-0.058	0.969
02	46	0.819	0.0847	0.723	10	0.758	0.173	0.969
03	51	0.641	0.272	0.599	7	0.731	0.230	0.920
04	61	0.990	-0.038	0.835	9	1.06	-0.065	0.961
05	40	0.914	0.0571	0.576	6	0.934	0.0766	0.787
06	44	0.772	0.0874	0.812	6	0.681	0.223	0.952
07	53	0.617	0.231	0.582	9	0.816	0.135	0.928
08	36	0.508	0.385	0.610	8	0.618	0.268	0.850
09	48	0.681	0.250	0.553	6	0.756	0.237	0.880
10	43	0.547	0.329	0.661	5	0.679	0.231	0.823
11	45	0.873	0.0510	0.769	6	0.853	0.133	0.930
12	40	0.625	0.217	0.530	6	0.718	0.203	0.904
ALL	566	0.805	0.113	0.762	87	0.926	0.0551	0.924

Statistical inference was required to determine if the evaporative fraction measured at midday was representative of the full daylight period. The two data parameters of interest were EF_M, the midday evaporative fraction, and EF_A, the all-day evaporative fraction (exclusive of midday values). In a sense the question was whether these statistics were equal, or expressed another way, was the difference between the two equal to zero. The parameters are by nature paired; that is, for each EF_M there is a corresponding EF_A.

From previous research it was known that the EF was stable during daylight periods for clear-sky conditions. Therefore, two data sets were prepared for the analysis. The first data set contained only clear data to confirm past research results using the HAPEX-MOBILHY database. The second database contained both clear and rough dates to examine the behavior of the EF in general, including less than ideal, conditions. Consequently, all statistical tests were repeated for each data set.

The simplest approach to making inferences about EF_M with respect to EF_A was to conduct hypothesis testing. The pairing of the data mentioned above permitted use of the paired t test. In this test the null hypothesis was constructed based on the conjecture that EF_M and EF_A were equal;

$$H_0: \ \mu_d = \mu_1 - \mu_2 = 0$$

and this was tested against the alternative hypothesis;

$$H_a: \ \mu_d \neq 0$$

which was a two-tailed test. The notation is common to statistics, but may require explanation: μ represents the true mean of a population, and the subscripts *1* and *2* represent the two statistics of interest. The subscript *d* stands for "difference." The null and alternative hypotheses are represented in notation by H_0 and H_a, respectively.

The paired t test involved an approximate normality assumption with respect to the distribution of the differences, μ_d. The relatively large sample size (on average, approximately 47 observations per station) permitted the reasonable assumption that this is the case. Examination of normal probability plots confirmed this assumption.

Because of the differing characteristics of the twelve SAMER stations (see Section 3.1.1, SAMER System) it was desirable to test the stated null hypothesis on a station-by-station basis as well as the lumped data set. If differential inferences resulted, it was possible that the occurrence of similar characteristics in groupings, such as crop cover, could help explain the results. Hence the null hypothesis was tested for the SAMER twelve stations and the sum of the twelve for both clear-sky and complete data sets. The results of these paired t tests are summarized in Table 4.2 and 4.3.

Table 4.2 Summary of paired t tests of hypothesis tests for all conditions. The null hypothesis is that the difference between the midday and daylight period evaporative fraction is zero (H_0: $\mu_d = 0$), versus the alternative that it is not (H_a: $\mu_d \neq 0$).

SAMER No.	Number of Obs.	Mean	Variance	Std. Deviation	t statistic $\alpha = 0.05$	Sig. Level	H_0 Rejected ?
01	59	-0.034	0.0341	0.1846	-1.428	0.159	No
02	46	0.050	0.0059	0.0766	4.382	6.97×10^{-5}	Yes
03	51	0.037	0.0088	0.0939	2.798	0.007	Yes
04	61	0.043	0.0094	0.0971	3.449	0.001	Yes
05	40	0.011	0.0059	0.0766	0.877	0.386	No
06	44	0.049	0.0076	0.0873	3.733	0.001	Yes
07	53	0.066	0.0070	0.0834	5.797	4.02×10^{-7}	Yes
08	36	0.089	0.0095	0.0975	5.466	4.09×10^{-6}	Yes
09	48	0.018	0.0057	0.0754	1.682	0.099	No
10	43	0.027	0.0061	0.0780	2.234	0.031	Yes
11	45	0.029	0.0073	0.0854	2.267	0.028	Yes
12	40	0.049	0.0157	0.1254	2.449	0.019	Yes
ALL	566	0.034	0.0114	0.0170	7.587	2.27×10^{-3}	Yes

Results of the paired t test, summarized in Table 4.2, gave very weak evidence for the assumption of equality between EF_M and EF_A for the complete database (p-value of 2.27×10^{-3} for all stations); on a station-by-station basis, only three SAMER stations out of twelve provide evidence of equality in these statistics. However, Table 4.3 shows that for the clear sky dates the reverse occurred; only four stations out of twelve were rejected ($\alpha = 0.05$ level test), and these with only marginally weak p-values ranging from 0.024 to 0.044. For the total of all twelve stations on clear dates the evidence is clearly in favor of the null hypothesis results (p-value of 0.934). It can be concluded that the relationship between EF_M and EF_A is one of equality for "clear" dates, but there is no evidence of this with respect to all meteorological conditions. No pattern was observed relating the strength of the statistical inferences to common site characteristics such as soil type, crop cover, or site elevation.

Table 4.3 Summary of paired t tests of hypothesis for "clear sky" conditions. The null hypothesis is that the difference between midday and the daylight evaporative fraction is equal to zero (H_0: $\mu_d = 0$), versus the alternative that it is not (H_a: $\mu_d \neq 0$).

SAMER No.	Number of Obs.	Mean	Variance	Std. Deviation	t statistic $\alpha = 0.05$	Sig. Level	H_0 Rejected ?
01	9	-0.001	0.0038	0.0618	0.045	0.965	No
02	10	-0.001	0.0017	0.0417	-0.058	0.955	No
03	7	2.277	0.0005	0.0230	0.262	0.803	No
04	9	0.037	0.0021	0.0461	2.384	0.044	Yes
05	6	-0.025	0.0011	0.0336	-1.797	0.132	No
06	6	0.018	0.0049	0.0697	0.649	0.545	No
07	9	-0.014	0.0027	0.0518	-0.781	0.458	No
08	8	0.059	0.0080	0.0893	1.858	0.106	No
09	6	-0.046	0.0016	0.0401	-2.822	0.037	Yes
10	5	-0.028	0.0003	0.0179	-3.544	0.024	Yes
11	6	-0.044	0.0013	0.0360	-2.960	0.032	Yes
12	6	-3.380	0.0016	0.0402	-0.206	0.845	No
ALL	87	-0.0005	0.0032	0.056	-0.084	0.934	No

A possible explanation for the instability of the evaporative fraction on "rough" days may be the presence of interception. When water is applied to the canopy or soil surface some portion is intercepted and directly evaporated from the surface. The interception process has concerned mesoscale meteorological modelers in parameterization of land surface processes (Mahfouf and Jacquemin, 1989), and hydrologists concerned with *effective* precipitation as distinguished from total precipitation (Linsey *et al.*, 1989). When a wetted surface is present potential for evaporation increases dramatically. Such a sudden increase, and the subsequent decrease when the wetted surface is totally evaporated, would affect the value of the evaporative fraction is a noteworthy manner. To confirm this the analysis would need to be repeated, distinguishing clear, cloudy, and rainy dates. The result may be that the stability applied to cloudy dates without precipitation events as well as clear-sky dates.

With the evaporative fraction identified as a useful characterization of a given location's surface energy balance, it is interesting to examine some aspects of its behavior. Figure 4.18 shows the time evolution of the midday evaporative fraction for Lubbon 1 (SAMER 01). Notice the high evaporative fraction for this oat field until the onset of senescence (approximately 86D175). Following maturity, indicated by the change in slope of the vegetation height curve, the evaporative fraction underwent a rapid decrease with time. This decrease represented the reduced capacity of the plant to transport vapor because of senescence. A second example of time evolution is given in Figure 4.19 for Castelnau, a maize field which did not fully mature during the during the period of observation. Note the shallow decrease in evaporative fraction values with time until approximately 86D165. This decrease is likely due to surface evaporation, considering the lack of vegetation development. With the onset of growth in the maize field the evaporative fraction begins to increase.

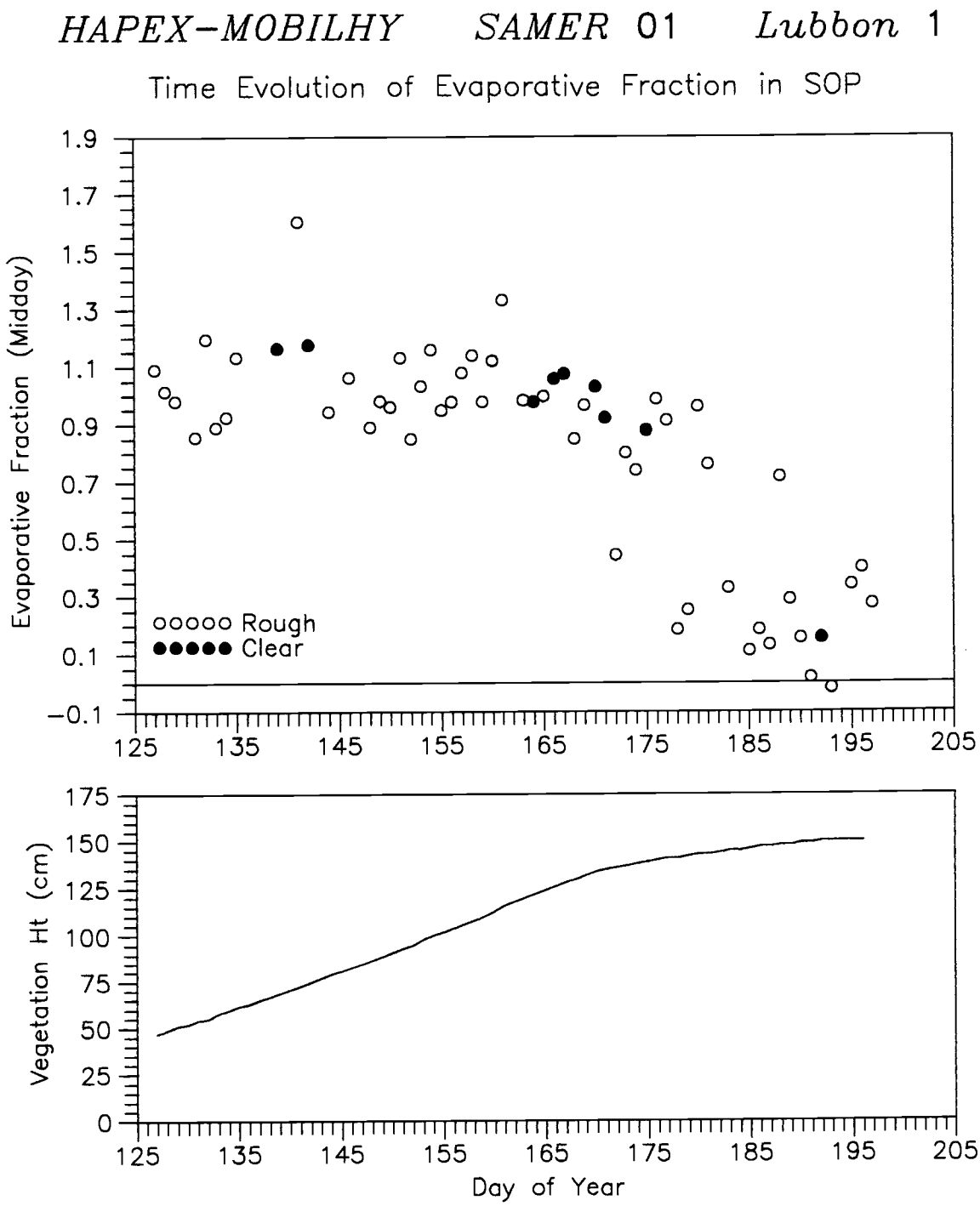

Figure 4.18 Evaporative fraction and mean vegetation height variation during the SOP for Lubbon 1 (SAMER 01) site.

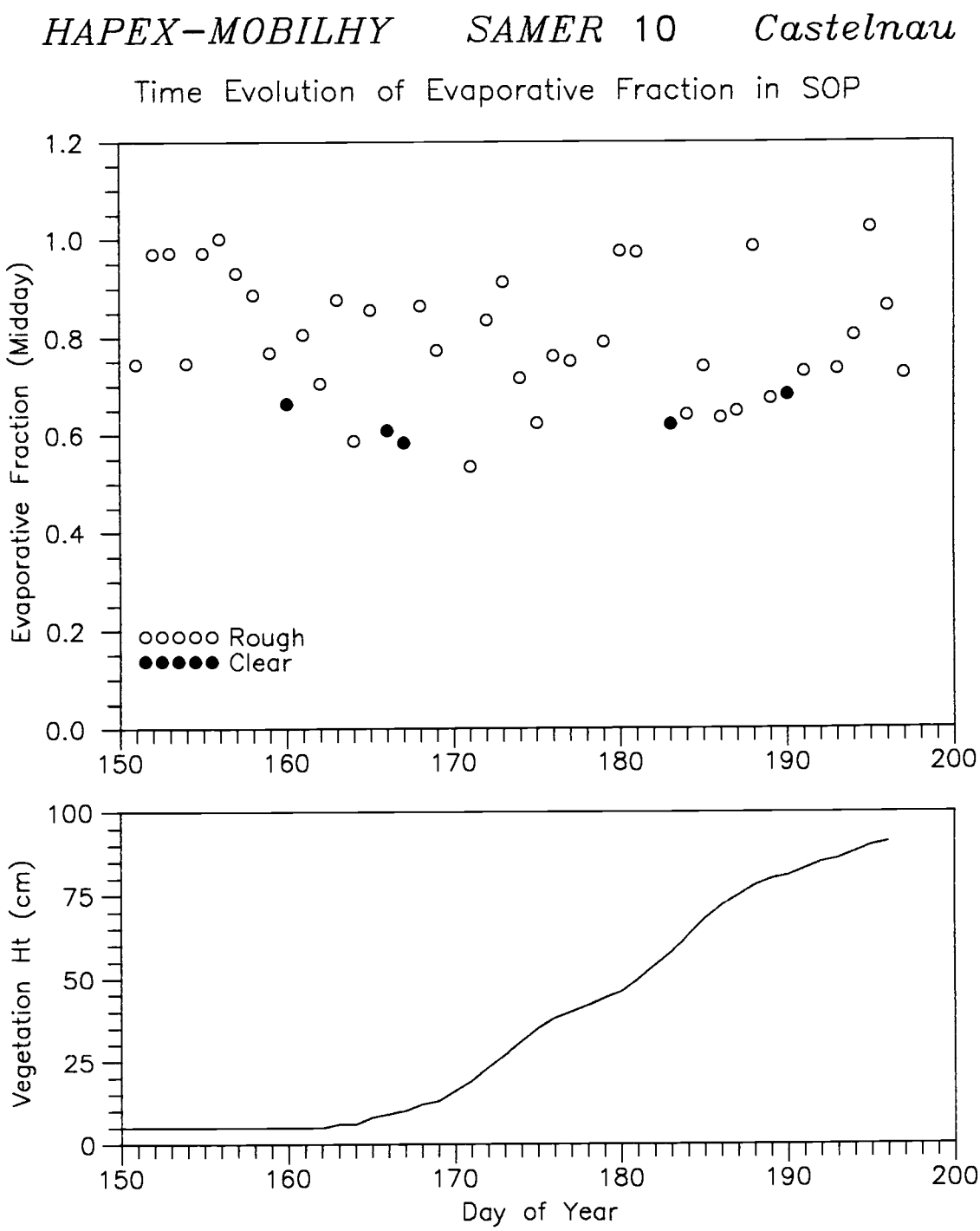

Figure 4.19 Evaporative fraction and mean vegetation height variation during the SOP for Castelnau (SAMER 10) site.

4.2 Surface Soil Moisture

The variation of surface soil moisture in the vicinity of Lubbon - Northern Central Site of the HAPEX-MOBILHY Program is examined in this section using data collected with the Push Broom Microwave Radiometer (PBMR). For a discussion of the available data refer to Section 3.2.2, Push Broom Microwave Radiometer.

4.2.1 Push Broom Microwave Radiometer Image Processing

Using computer programs developed specifically for this study (see Section 3.2.2, Push Broom Microwave Radiometer), all available days of PBMR data in the vicinity of Northern Central Site Lubbon and Southern Central Site Castelnau were processed to produce brightness temperature imagery. These images were restricted to exactly the same dimensions for each date to maintain consistency; 4000-m by 3000-m (12 km^2) for Lubbon and 2000-m by 2000-m (4 km^2) for Castelnau. A digitized map of Northern Central Site Lubbon is shown in Figure 4.20 at the imagery scale for that site. Notice from this map that the area includes all six PBMR calibrations fields (N0, N1, ... , N5) available from the HAPEX-MOBILHY Program. The imaging area in both cases were selected to include most of the area viewed by the PBMR on the 300-m flight missions.

Several brightness temperature images are presented in Figures 4.22 through 4.27. It should be noted that brightness temperature is negatively related to soil moisture, i.e., lower brightness temperature translates into higher soil moisture content. The brightness temperature is depicted in 5-K degree increments. Table 4.4 provides the legend for the color keys shown at the base of each image.

These images were selected to provide illustrative examples of the variation apparent in PBMR imagery examined in this study. Figures 4.22 though 4.24 show the Northern Central Site Lubbon vicinity on three dates spanning the SOP. The black lines represent field boundaries digitized from IGN maps (see Figure 4.20 above) and placed in the imagery through a vector rasterization process. Due to the small view area for the 300-m flights shown

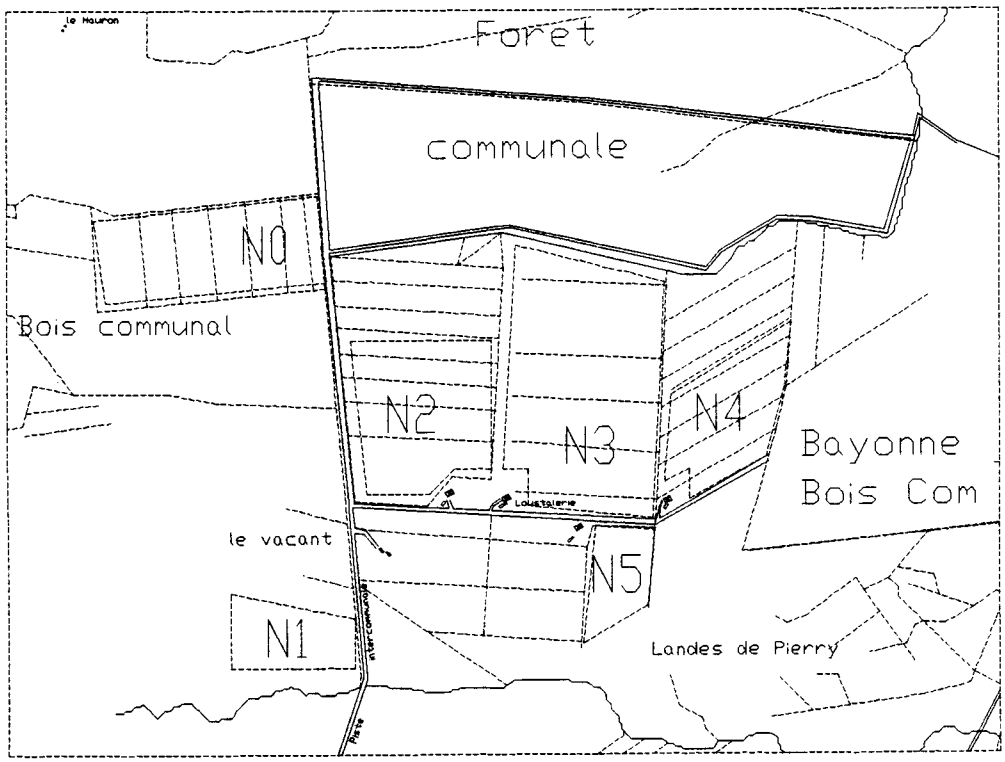

Figure 4.20 Map of Northern Central Site Lubbon vicinity. The map is drawn to coincide with the same location as the PBMR brightness temperature images shown in Figures 4.22 through 4.24. This map is taken directly from a CAD (Computer Assisted Drafting) digitalization of the Lubbon area based on an IGN topographic 1:25,000 map.

in these images, sensor coverage was only about 50 percent of the image area for Lubbon and 25 percent for Castelnau. Because flight lines did not coincide exactly, on each date different portions of the image area were mapped on different dates.

Examination of the Lubbon - Northern Central Site imagery indicated a strong response of the PBMR to both spatial and temporal soil moisture variation. The temporal aspect is evident by comparing the three images; there is a pronounced shift towards a drier surface soil moisture condition with each successive image. The spatial aspect is notable in any single image. For example, in the first image (29 May) the cultivated areas in the clearing (central image) tend to be 5 to 15-K degrees "cooler" (brightness temperature) than the surrounding forest, indicating higher surface moisture content at the beginning of the period of observation. By 16 June the clearing has become significantly drier, registering 5 to 15-K degrees "warmer" than the surrounding forest. The oat field (calibration field N2 in Figure 4.21) is also distinct

from the adjacent cereal field (N3), indicating a higher moisture content. By the time of the third image (2 July) the oat field has fully matured, and it appears as one of the driest portions of the image. The field boundaries indicated in black are distinctly reflected in brightness temperature variation in each image.

Figures 4.25 through 4.27 are images for the Castelnau - Southern Central Site vicinity on three dates. These images also illustrate the soil moisture depletion of the area imaged during the period of observation. The Castelnau area failed to provide much spatial variation, indicating more local surface soil moisture uniformity than in the Lubbon case.

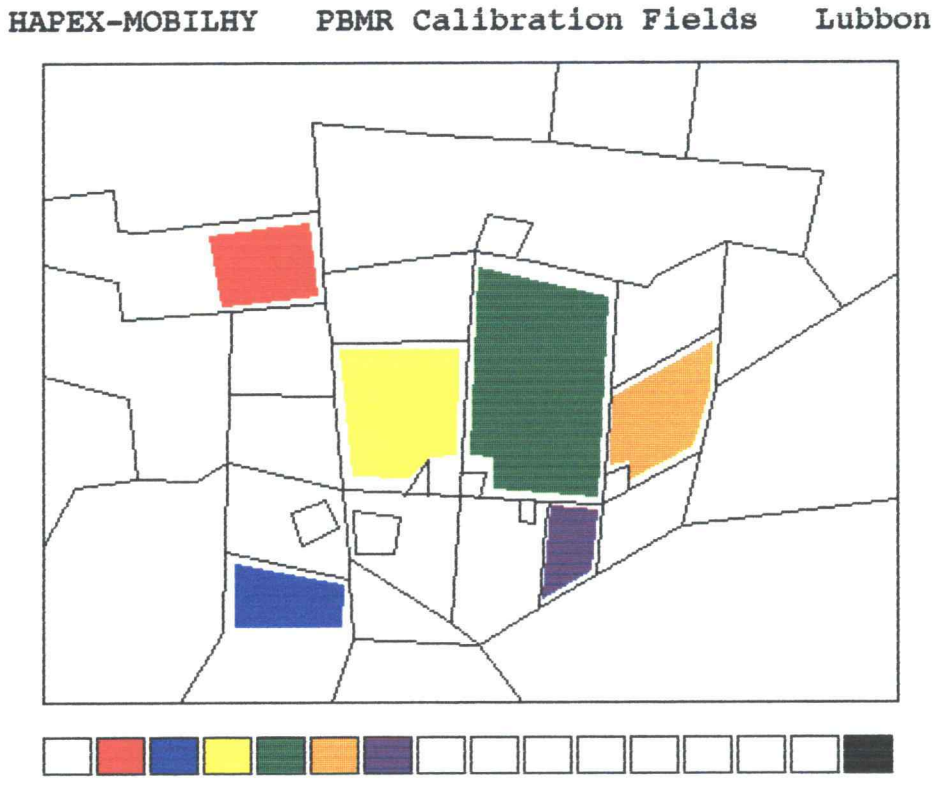

Figure 4.21 Calibration fields for Lubbon - Northern Central Site. These six fields were sampled gravimetrically as part of the ground truth mission to provide surface soil moisture data for PBMR calibration. This image was used as a "query mask" to extract brightness temperature values from each Lubbon vicinity image for use in the calibration analysis.

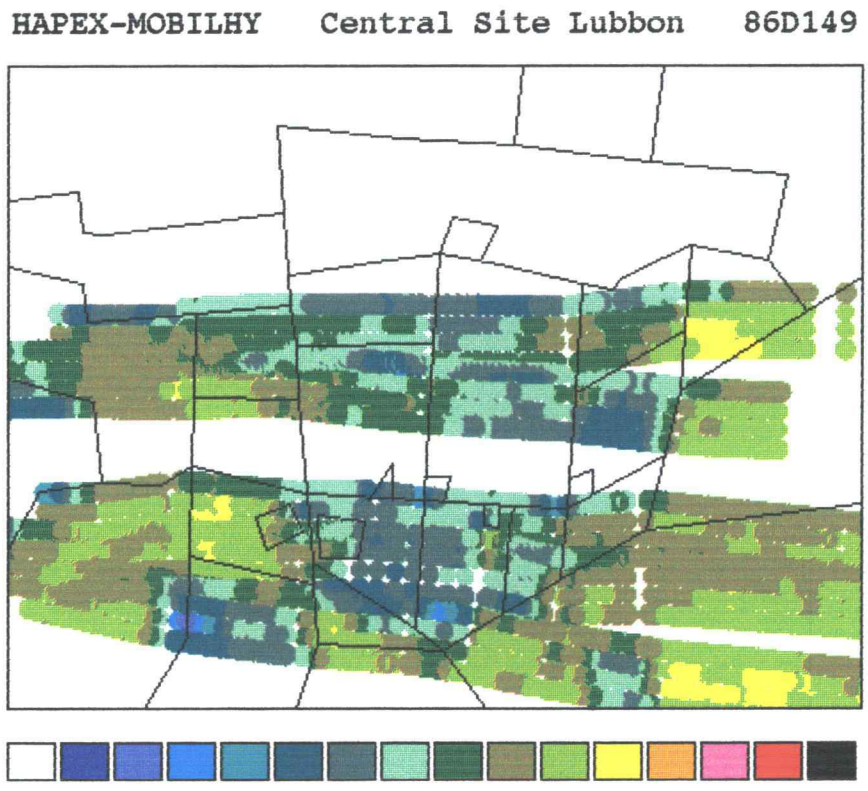

Figure 4.22 PBMR brightness temperature image for 86D149 (May 29, 1986) over Lubbon - Northern Central Site vicinity of the HAPEX-MOBILHY Program experiment grid. Sensor coverage for this image was 49.3 percent.

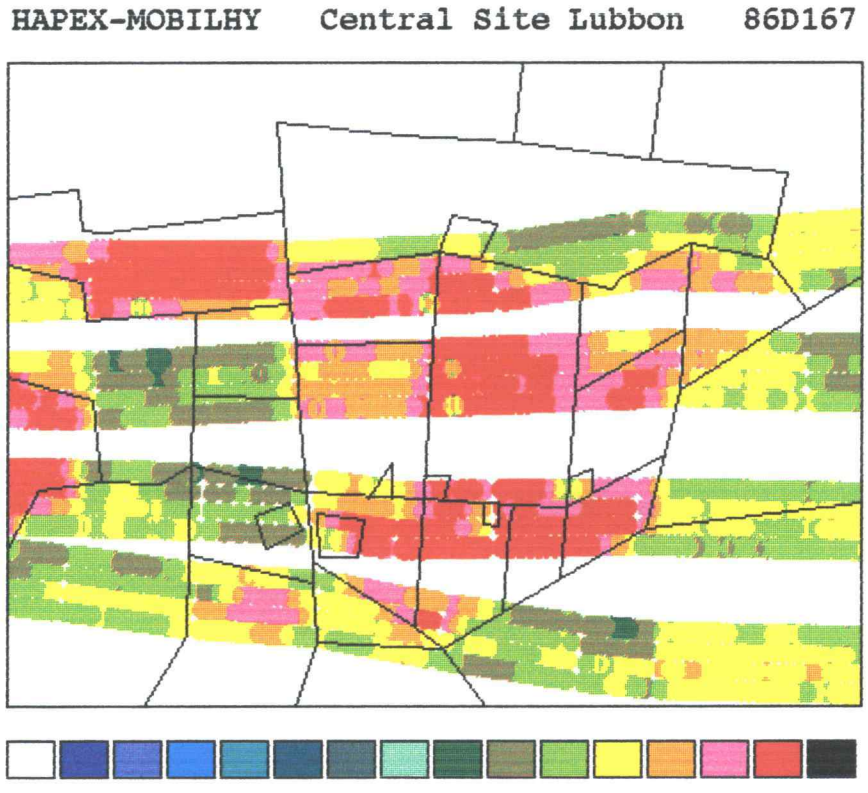

Figure 4.23 PBMR brightness temperature image for 86D167 (16 June 1986) over Lubbon - Northern Central Site vicinity of the HAPEX-MOBILHY Program experiment grid. Sensor coverage for this image was 49.8 percent.

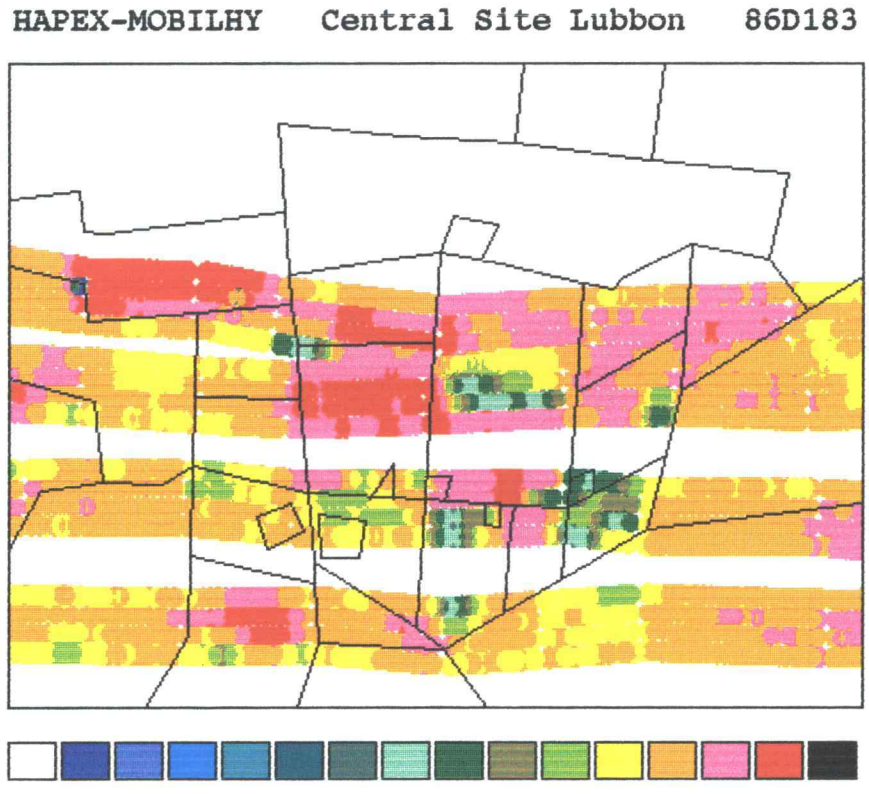

Figure 4.24 PBMR brightness temperature image for 86D183 (2 July 1986) over Lubbon - Northern Central Site vicinity of the HAPEX-MOBILHY Program experiment grid. Sensor coverage for this image was 48.9 percent.

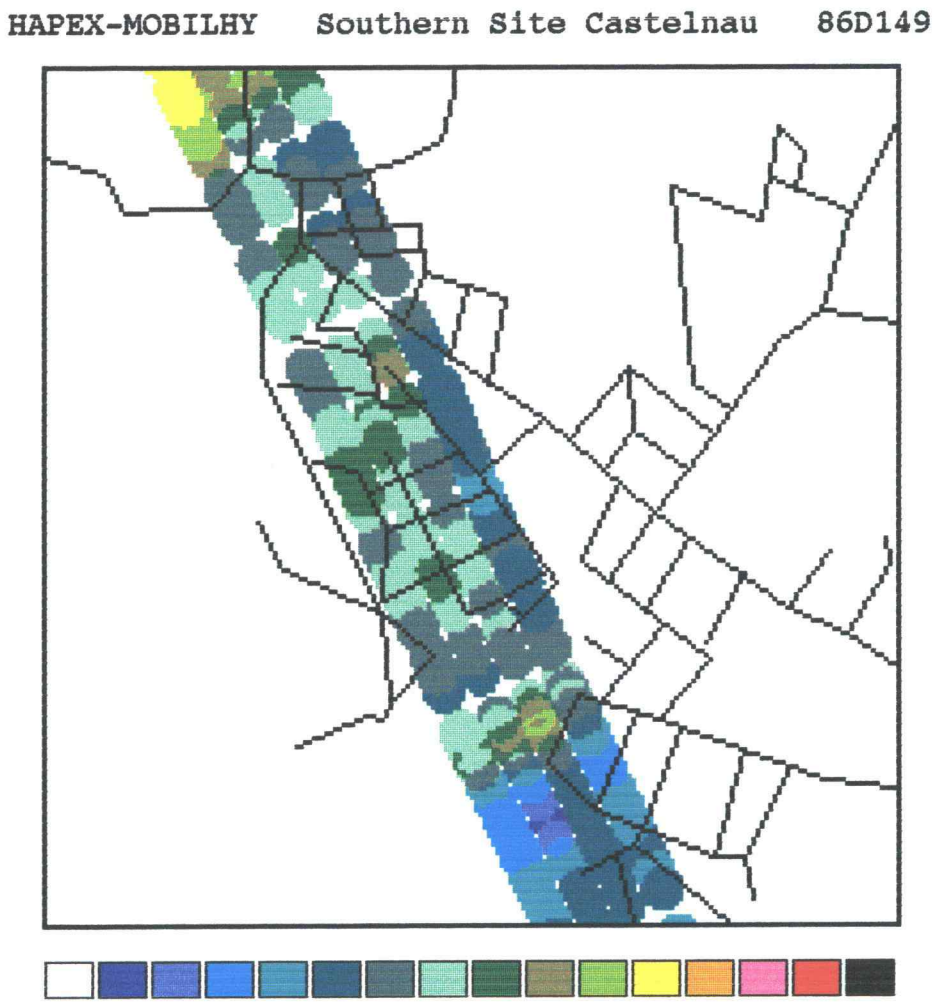

Figure 4.25 PBMR brightness temperature image for 86D149 (29 May 1986) over Castelnau - Southern Central Site vicinity of the HAPEX-MOBILHY Program experiment grid. Sensor coverage for this image was 23.3 percent.

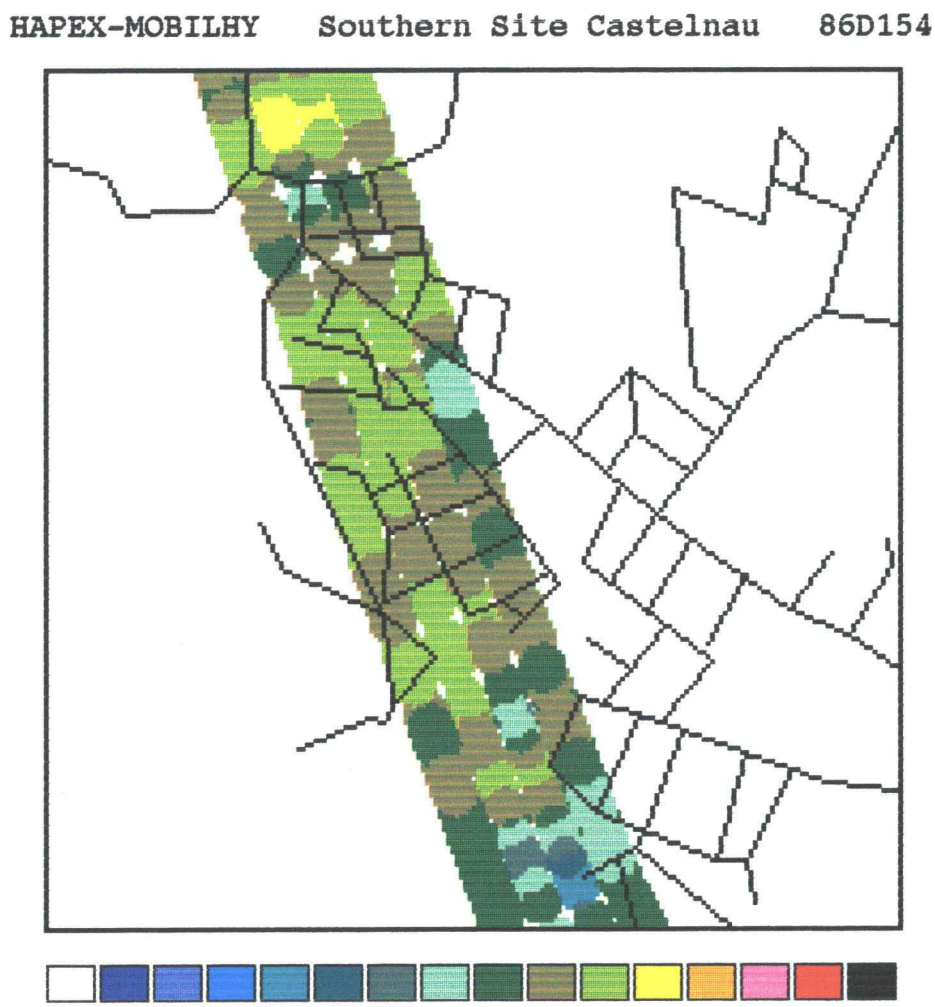

Figure 4.26 PBMR brightness temperature image for 86D154 (3 June 1986) over Castelnau - Southern Central Site vicinity of the HAPEX-MOBILHY Program experiment grid. Sensor coverage for this image was 25.1 percent.

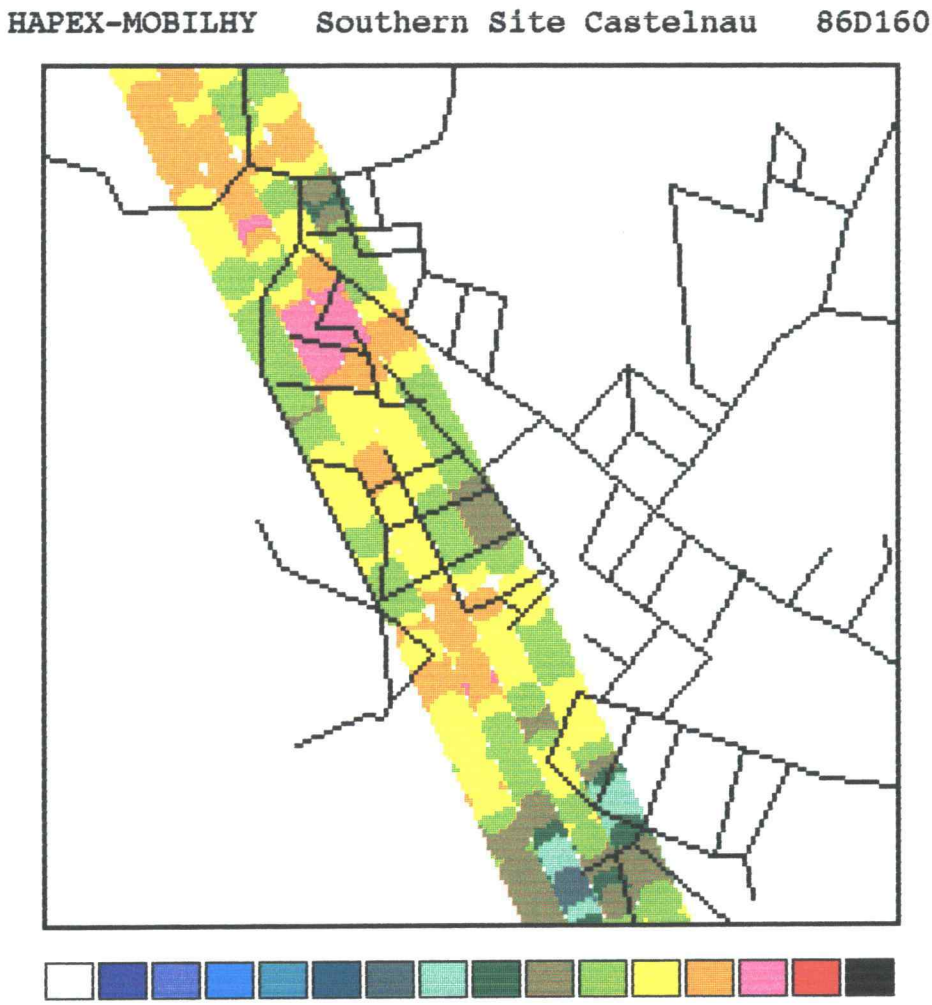

Figure 4.27 PBMR brightness temperature image for 86D160 (9 June 1986) over Castelnau - Southern Central Site vicinity of the HAPEX-MOBILHY Program experiment grid. Sensor coverage for this image was 24.5 percent.

Table 4.4 Legend for PBMR imagery color keys.

Key Number	Description
1	(Black) - Indicates digitized field boundaries
2	$T_B \leq 225$-K
3	225-K $\leq T_B \leq$ 230-K
4	230-K $\leq T_B \leq$ 235-K
5	235-K $\leq T_B \leq$ 240-K
6	240-K $\leq T_B \leq$ 245-K
7	245-K $\leq T_B \leq$ 250-K
8	250-K $\leq T_B \leq$ 255-K
9	255-K $\leq T_B \leq$ 260-K
10	260-K $\leq T_B \leq$ 265-K
11	265-K $\leq T_B \leq$ 270-K
12	270-K $\leq T_B \leq$ 275-K
13	275-K $\leq T_B \leq$ 280-K
14	280-K $\leq T_B \leq$ 285-K
15	$T_B \geq 285$-K
16	(White) No data; not in view area of PBMR.

4.2.2 Passive Microwave Measurements and Surface Soil Moisture

The theoretical relationship between surface soil moisture and passive microwave measurements was presented in the Review of Literature (see Section 2.2.3.1, Fundamentals of Microwave Remote Sensing). The correspondence of these quantities is illustrated in Figure 4.28 which contrasts emissivity computed from passive microwave and thermal infrared remote sensing data with neutron probe measurements of the surface layer of soil moisture. The negative relationship between these quantities is reflected in the opposing slopes in the

two measurements with time, while both appear to respond to indicated water application events. To quantify the relationship between surface soil moisture and remote sensing observations, linear regression techniques were employed.

The quantity most closely related to surface soil moisture is emissivity, which requires measures of brightness temperature collected in the microwave region and surface (kinetic) temperature collected in the thermal infrared region to compute. The PBMR provides the first measurement, which can be extracted from the brightness temperature imagery discussed in the previous section. Surface temperature has generally been estimated in previous use of the PBMR using the PRT-5 radiometer. This sensor provides an excellent measurement of surface temperature for a small beam centered at the nadir and serves well for nearly homogeneous land surfaces. In the disjointed land surface found in the HAPEX-MOBILHY Program grid area, with patchwork arrangements of fields and forest, use of this sensor with the PBMR was highly suspect. It was not difficult to conceive of situations in which the PRT-5 measured completely different fields than were measured by an outside PBMR beam (see Figure 3.3). This would have lead to erroneous estimates of emissivity where the error would be a function of the difference between the PRT-5 temperature and the true surface temperature for the area measured by a given PBMR beam.

To correct for the lack of spatial correspondence and obtain accurate emissivity estimates, emissivity was not computed from simultaneous PBMR and PRT-5 measurements. Instead, *field-averaged* values of each sensors observations were computed for the calibration fields available. Passive microwave data were extracted from the brightness temperature imagery for the six calibration fields. PRT-5 data were treated as line transects, with all data observed over a given calibration field averaged to estimate the mean surface temperature of that field. An example of a line transect from Lubbon is shown in Figure 4.29. Note the indicated field boundaries along the transect and the corresponding temperature transitions. The ratio of brightness temperature grid values extracted from the imagery to the mean surface temperature was the estimate of mean field emissivity, which could be regressed against gravimetric surface soil moisture measurements. This approach allowed examination of the relationship between soil moisture and emissivity. This approach is not a substitute for a completely image-based approach since it did not permit development of emissivity imagery.

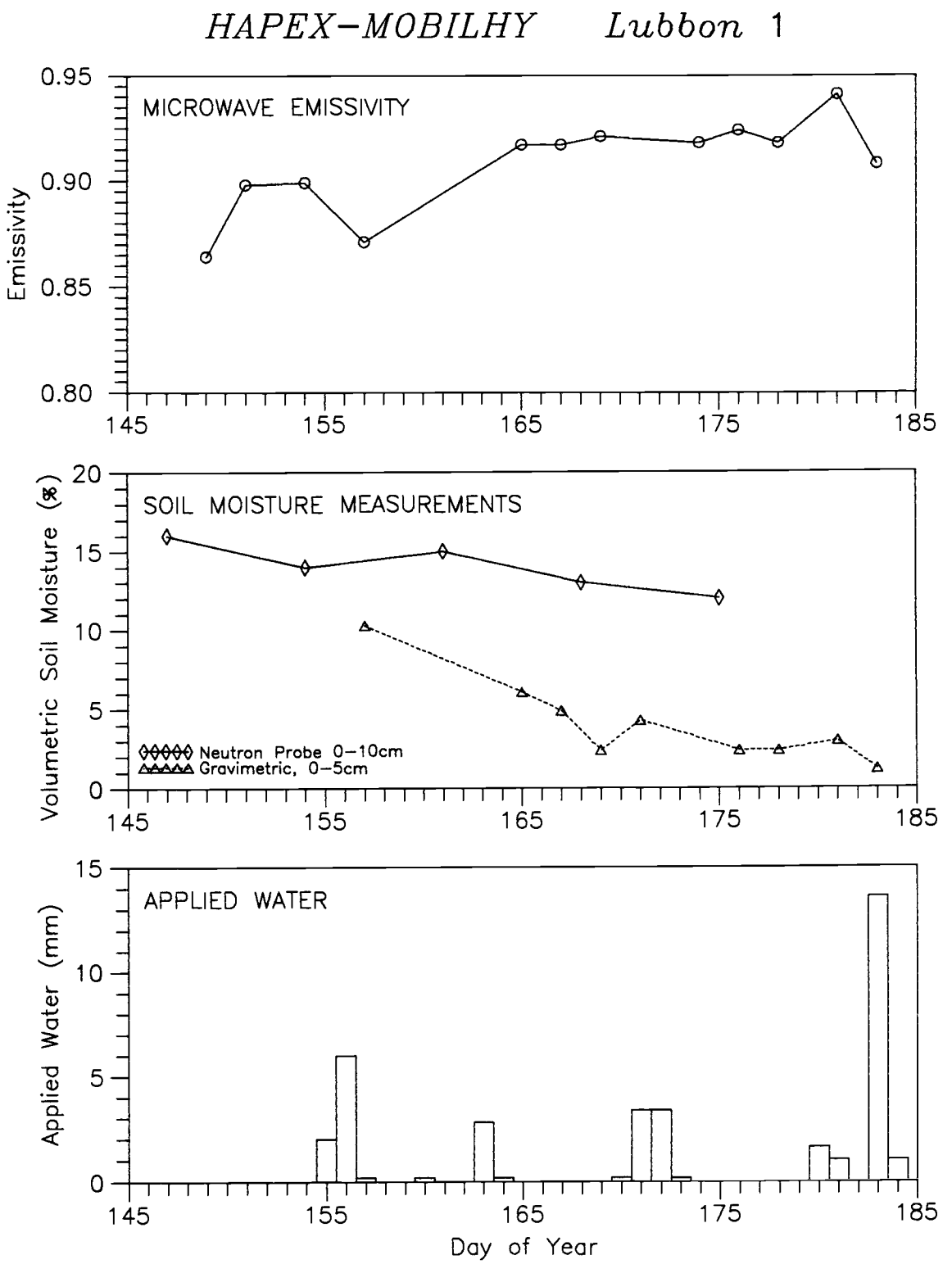

Figure 4.28 Comparison of surface soil moisture variation detected by neutron probe and by gravimetric sampling, emissivity computed from PBMR and PRT-5 data, and applied water for Lubbon 1 site during the SOP.

Neither can the relationship be applied to areas viewed the PBMR which were not viewed by the PRT-5. A more spatially distributed measure of surface temperature, such as that provided by the Thermal Infrared Multispectral Scanner (TIMS) is required to accomplish this.

The field-averaged emissivity - surface soil moisture regression is depicted in Figure 4.30. The coefficient of determination indicates a weak linear relationship (R^2 = 0.32), for reasons discussed below.

Brightness temperature is less directly correlated to water presence because it includes the effects of kinetic temperature differences. Emissivity imagery was not available for reasons already discussed, but brightness temperature imagery was. For this reason the regression analysis was repeated for brightness temperature and surface soil moisture. Brightness temperature has been compared to soil moisture in a number of previous studies, e.g. Schmugge *et al.*, 1988; Jackson and Schmugge, 1986.

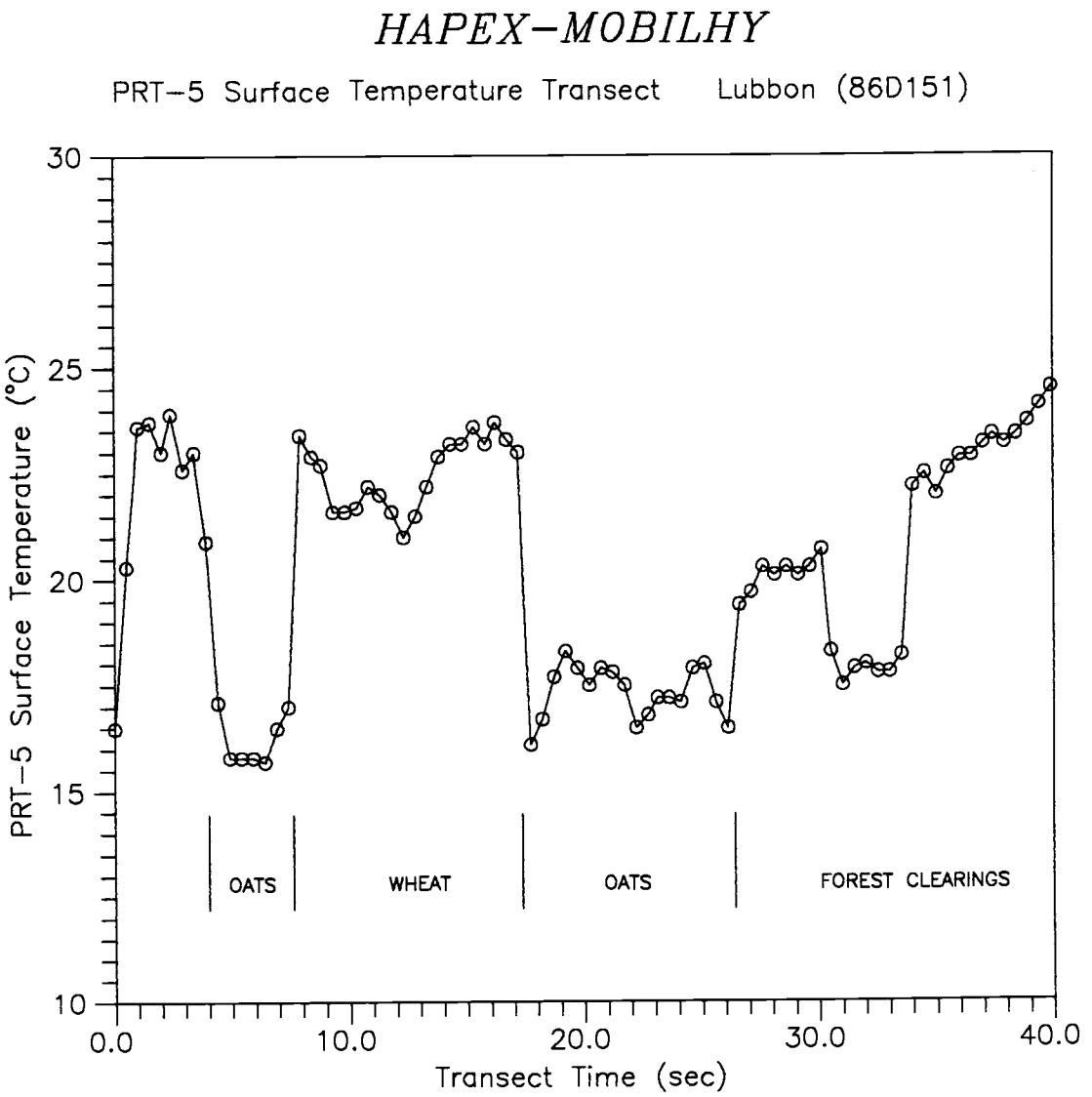

Figure 4.29 PRT-5 temperature transect over Lubbon on 3 June (86D151). Field boundaries along the transect are indicated for two oat fields, a wheat field, and forest clearings. The second oat field was the location of SAMER 01.

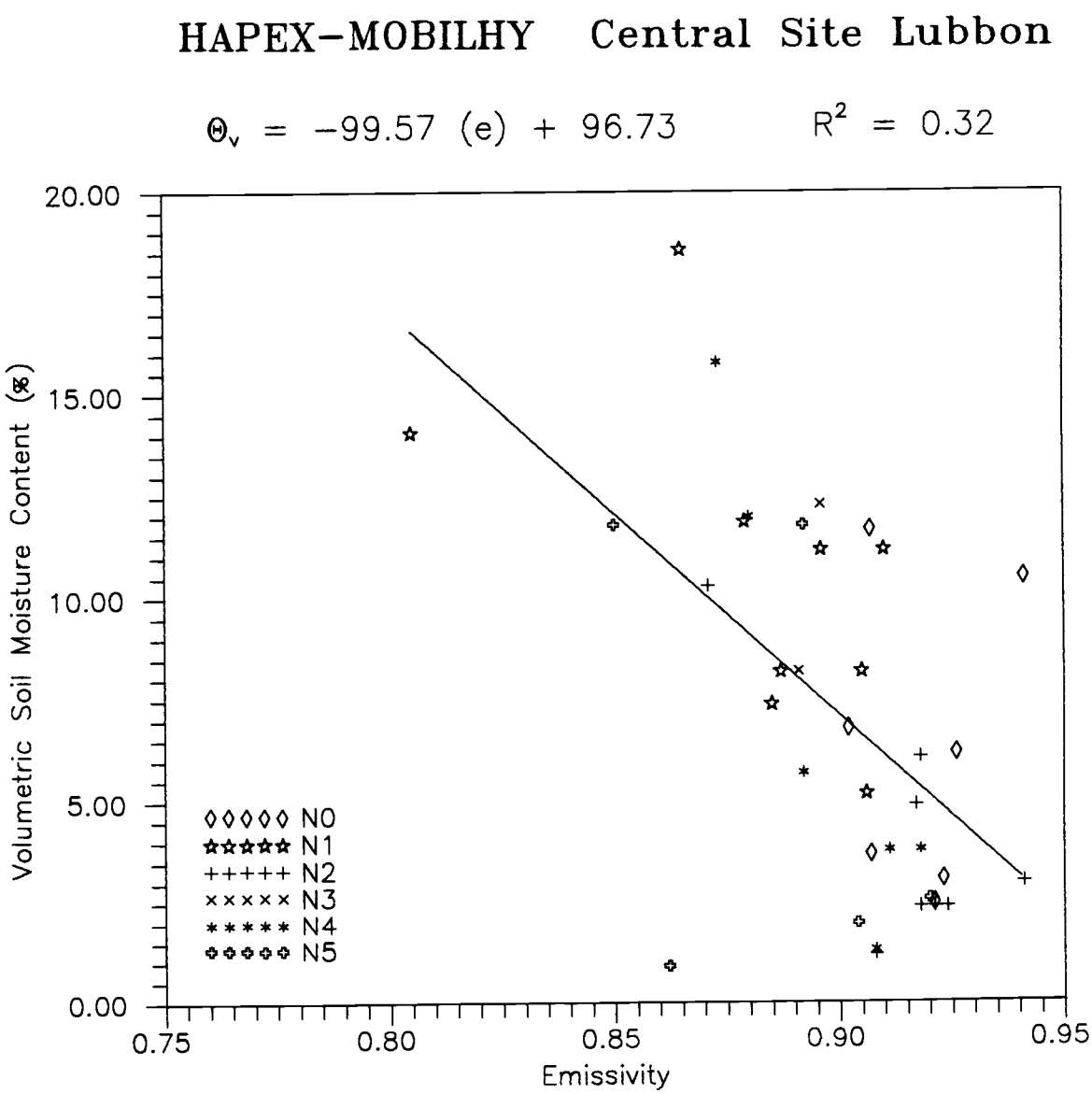

Figure 4.30 Scatter plot of field averaged emissivity values versus surface soil moisture for two sites, Lubbon 1 (SAMER 01) and Castelnau (SAMER 10).

The relationship reported by Schmugge *et al.* (1988) for the FIFE Program is depicted in Figure 4.31. This figure was altered from the scatter plot produced in the original paper (Schmugge *et al.*, 1988) so that the predictor and predicted variables (brightness temperature and surface soil moisture, respectively) are shown on the axes traditionally assigned in statistical analysis. Schmugge *et al.* (1988) originally used multiple brightness temperature measurements over a single watershed against the same soil moisture measurement. The average of brightness temperature observations has been substituted in Figure 4.31. The re-computed R^2 for this linear regression is 0.55, which compares to the value of 0.50 reported by Schmugge *et al.* (1988). The unburned watersheds were excluded by Schmugge *et al.* (1988) based on the microwave attenuation properties of these grasslands when a thatch layer had developed.

The process followed by Schmugge *et al.* (1988) was repeated for the HAPEX-MOBILHY data. The image data were extracted for the six calibration fields from the PBMR brightness temperature imagery previously generated. This was accomplished through use of the MAKEMASK program and several IDRISI modules. The resulting collection of data files containing all grid cell brightness temperature values for particular calibration fields and flight dates. The summary statistics for these fields are given in Tables 4.5a and 4.5b.

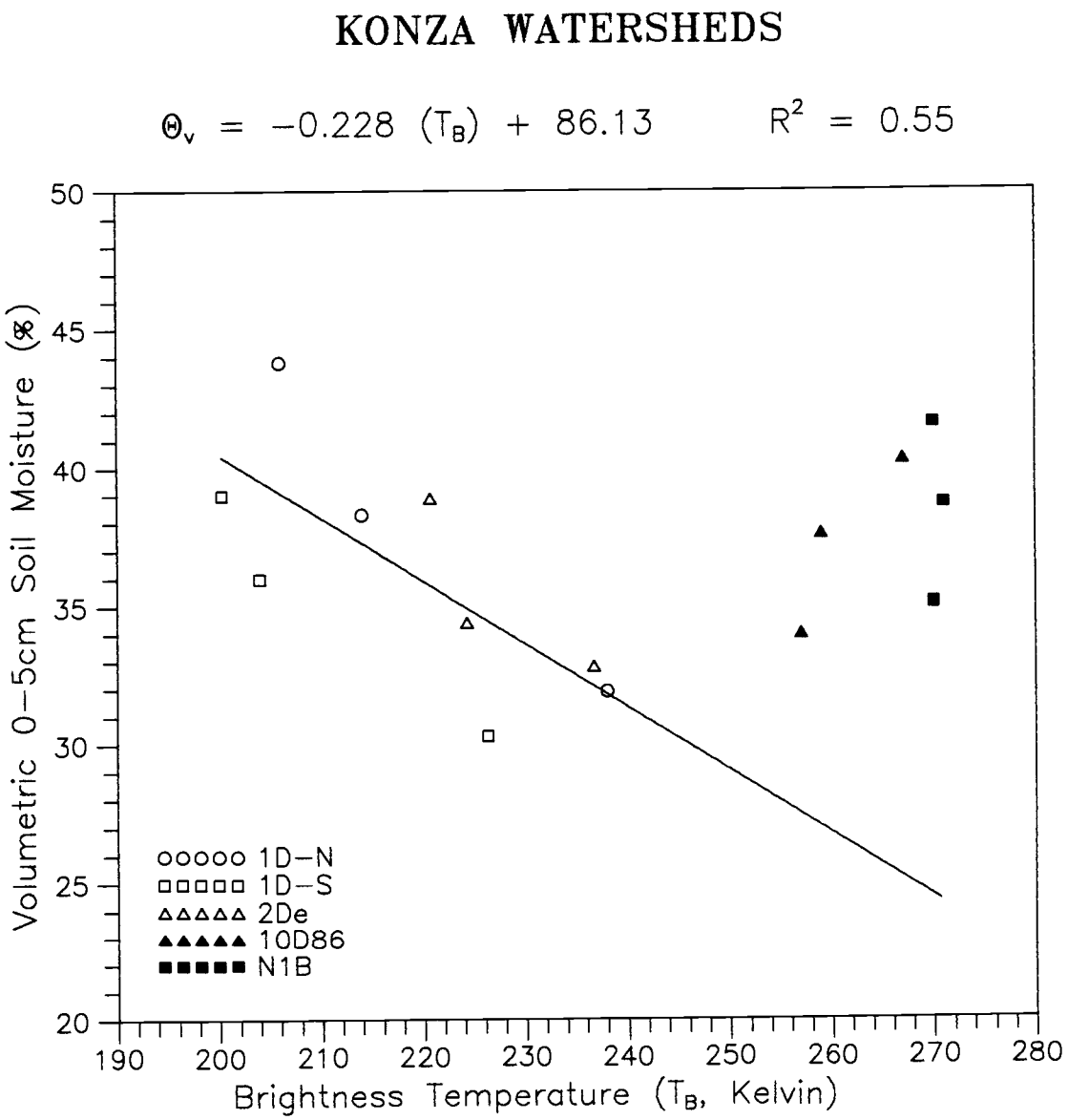

Figure 4.31 Scatter plot of PBMR measured brightness temperature versus ground observations of surface soil moisture for both burned (open symbols) and unburned (closed symbols) watersheds in the Konza Prairie National Reserve Area. Data were reported by Schmugge *et al.*, 1988 and pertain to flight missions in 1985 for the FIFE Program. The regression line is only for the burned watersheds.

Table 4.5a Summary statistics for PBMR brightness temperature observations of Northern Central Site Lubbon calibration fields.

DOY	Statistic	N0	N1	N2	N3	N4	N5
86D149	Observations	173	1245	1917	4091	1429	782
	Mean	253.38	252.42	254.39	250.97	248.34	252.30
	Maximum	255.5	269.9	266.2	262.9	267.2	263.10
	Minimum	251.5	230.9	234.2	239.0	240.6	239.00
	Variance	0.817	54.629	34.172	21.625	34.778	17.209
	Standard Dev.	0.904	7.391	5.846	4.650	5.897	4.148
86D151	Observations	1337	958	2061	3458	910	388
	Mean	275.52	257.32	260.99	264.84	252.43	266.28
	Maximum	279.7	266.1	267.4	273.2	265.5	269.35
	Minimum	263.8	231.9	251.5	252.1	243.9	261.5
	Variance	10.309	49.756	9.897	14.241	39.640	3.574
	Standard Dev.	3.211	7.054	3.146	3.774	6.296	1.891
86D154	Observations	396	846	1988	3738	1319	672
	Mean	272.10	259.56	263.65	267.23	257.16	267.75
	Maximum	278.0	270.3	273.5	274.9	267.8	274.7
	Minimum	265.8	239.7	250.8	252.0	247.4	252.9
	Variance	5.442	46.679	22.569	12.993	38.190	9.941
	Standard Dev.	2.333	6.832	4.751	3.605	6.180	3.153
86D157	Observations	1529	1175	1884	3974	1088	536
	Mean	258.91	235.10	253.04	249.10	242.38	248.95
	Maximum	264.2	257.4	257.9	259.1	261.0	259
	Minimum	253.2	216.0	245.4	237.3	230.0	242
	Variance	8.656	56.729	9.149	11.619	75.761	22.473
	Standard Dev.	2.942	7.532	3.025	3.409	8.704	4.741
86D165	Observations	906	1211	2639	4674	1365	410
	Mean	279.75	267.59	268.80	278.03	274.68	278.92
	Maximum	285.2	276.3	280.8	284.8	279.6	281.4
	Minimum	268.6	246.7	258.2	265.4	263.6	271
	Variance	17.848	32.893	14.769	6.721	7.799	1.267
	Standard Dev.	4.225	5.735	3.843	2.593	2.793	1.126
86D167	Observations	1323	1255	1793	3336	801	474
	Mean	287.75	276.70	277.66	285.68	283.25	287.93
	Maximum	291.2	284.8	285.3	289.1	287.2	290
	Minimum	274.9	261.8	268.6	260.7	271.4	268
	Variance	11.680	32.022	9.180	10.451	9.290	3.850
	Standard Dev.	3.418	5.659	3.030	3.233	3.048	1.962

With the statistics given in Tables 4.5a and 4.5b and frequency histograms for each case (not presented in this paper), each calibration field was individually inspected before inclusion in the regression analyses. The resulting regression for the HAPEX-MOBILHY data is shown in Figure 4.32. Each field is identified by a unique symbol in the figure to aid in analysis. Note the range of soil moisture observed in the HAPEX-MOBILHY data collection; from approximately 20 percent (volumetric basis) to nearly zero. This dry condition is in sharp contrast to the FIFE data previously shown, which ranges from 20 percent to 50 percent (mass basis).

Table 4.5b Summary statistics for PBMR brightness temperature observations of Northern Central Site Lubbon calibration fields.

DOY	Statistic	N0	N1	N2	N3	N4	N5
86D169	Observations	1496	1249	1988	3282	1194	630
	Mean	282.31	275.94	272.26	283.31	280.39	280.86
	Maximum	290.2	285.4	279.6	288.3	287.4	287.1
	Minimum	224.3	252.4	251.2	265.9	270.5	268.4
	Variance	48.484	46.802	41.528	7.065	8.636	13.670
	Standard Dev.	6.963	6.841	6.444	2.658	2.939	3.697
86D174	Observations	1544	1257	1711	3425	898	426
	Mean	283.81	278.52	274.43	279.21	281.10	277.76
	Maximum	289.2	284.2	282.5	288.6	285.5	283.45
	Minimum	269.8	264.0	253.6	249.2	268.1	259.3
	Variance	22.073	17.431	14.817	84.474	10.810	41.428
	Standard Dev.	4.698	4.175	3.849	9.191	3.288	6.436
86D176	Observations	1495	906	1924	3022	1004	423
	Mean	289.09	283.22	280.20	283.86	284.56	270.46
	Maximum	293.4	290.3	296.6	290.4	289.3	287.8
	Minimum	276.6	272.6	175.5	245.9	257.4	240.5
	Variance	12.802	24.051	98.262	46.332	9.186	195.776
	Standard Dev.	3.578	4.904	9.913	6.807	3.031	13.992
86D178	Observations	1523	1216	2007	3545	1183	557
	Mean	286.12	282.60	279.50	279.02	275.75	275.76
	Maximum	293.2	290.4	286.9	289.0	287.6	285.4
	Minimum	256.3	271.5	252.0	222.0	259.3	266.3
	Variance	37.613	19.491	81.647	115.244	66.808	26.605
	Standard Dev.	6.133	4.415	9.036	10.735	8.174	5.158
86D181	Observations	1461	564	2298	3663	1329	335
	Mean	277.49	260.12	275.65	266.93	258.86	263.42
	Maximum	283.1	273.4	284.5	278.0	276.1	268.5
	Minimum	259.4	253.9	258.8	242.1	242.3	252.1
	Variance	19.721	19.797	23.546	73.506	57.052	14.161
	Standard Dev.	4.441	4.449	4.852	8.574	7.553	3.763
86D183	Observations	748	1039	2297	4537	1166	375
	Mean	286.51	282.07	283.67	276.04	275.80	279.50
	Maximum	292.2	289.6	289.4	288.2	283.1	284.6
	Minimum	263.1	274.0	252.6	250.2	254.6	261.2
	Variance	21.348	16.048	22.972	89.027	56.612	27.192
	Standard Dev.	4.620	4.006	4.793	9.435	7.524	5.215

In neither case does the coefficient of determination (R^2) indicate an exceptional fit. The limited range of observed emissivity values, and consequently the limited soil moisture range, would tend to indicate that the poor linear fit may be due to examining a limited range for which the expected relationship is defined. When the range of any predictor variable (X) is narrow, the variation in the predicted variable (Y) ignoring X is not much greater than the variation in Y given X. In these cases summary statistics such as R^2 can be misleading (Weisberg, 1985), i.e., a low R^2 does not necessarily mean that a linear relationship is not an appropriate description.

The least-squares linear regression equations describing surface soil moisture as functions of brightness temperature and emissivity are

$$\Theta_v = -0.250(T_B) + 75.44 \quad (4\text{-}2a)$$

$$\Theta_v = -89.71(e) + 87.40 \quad (4\text{-}2b)$$

where

Θ_v = soil moisture (volumetric basis), percent

T_B = PBMR measured brightness temperature, K

e = emissivity

To gain perspective on the effect of the narrow range of soil moisture the FIFE PBMR data and the HAPEX PBMR were combined. Since the FIFE data tend to the moist end of the spectrum, while HAPEX-MOBILHY data were exceptionally dry, the range of the combined data set was quite large. Combining the burned watershed data from the FIFE Program with the data developed in this study lead to the plot shown in Figure 4.33. The coefficient of determination for the combined data set was 0.89. Although it would be very satisfying to apply such a statistically significant linear fit, physical reservations with respect to the highly different soil types in the two programs argue against this. The regression was performed to stress that a sufficiently large soil moisture range is required in order to adequately define the relationship between passive microwave measurements and surface soil moisture.

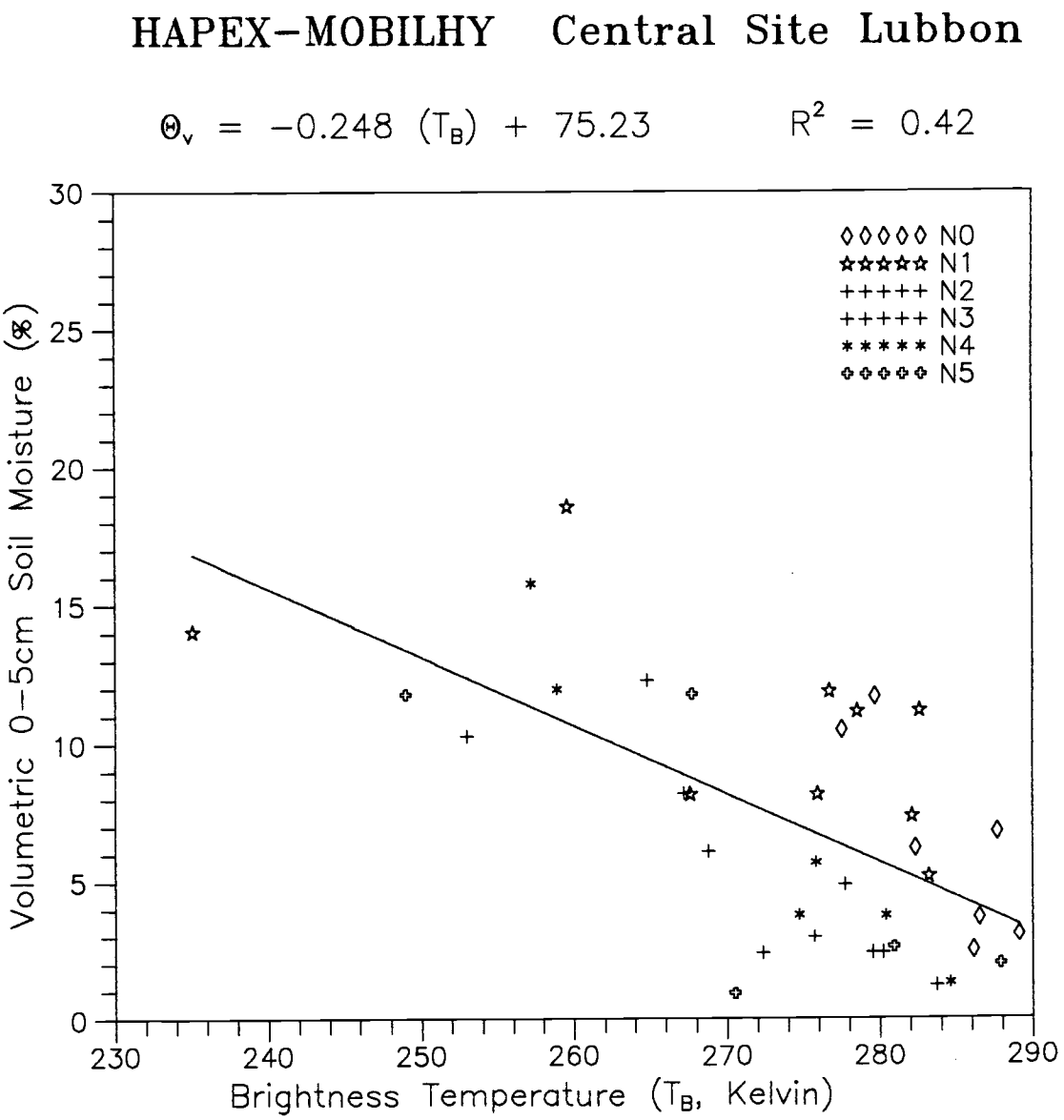

Figure 4.32 Scatter plot of PBMR measured brightness temperature versus ground observations of surface soil moisture for the HAPEX-MOBILHY Program in the vicinity of Lubbon - Northern Central Site.

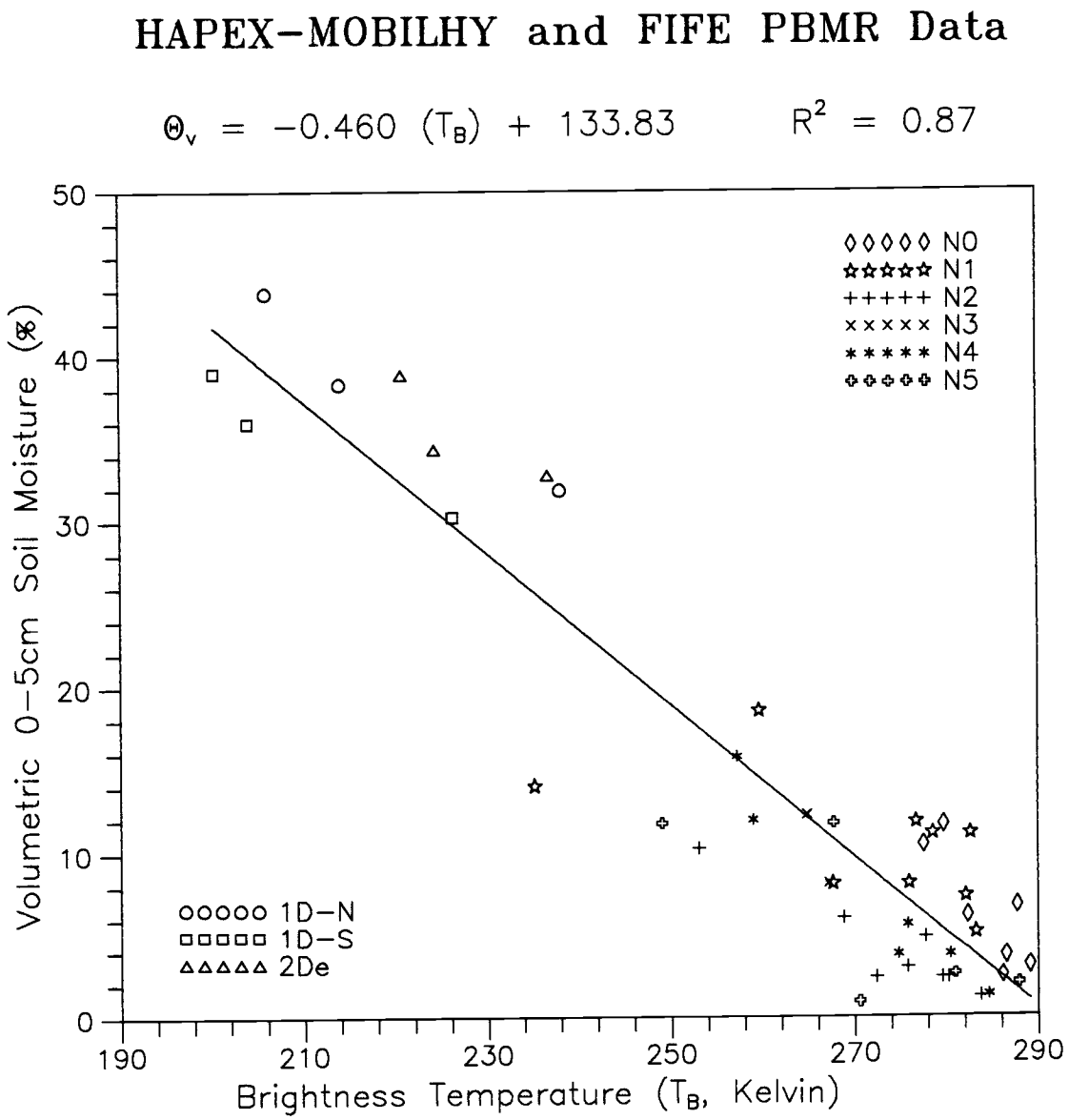

Figure 4.33 Combined scatter plot of PBMR measured brightness temperature versus ground observations of surface soil moisture. Data were taken from the burned watersheds of FIFE (as reported by Schmugge *et al.*, 1988) and the HAPEX-MOBILHY data.

Because the fit for HAPEX-MOBILHY PBMR data was so poor, no effort was undertaken to convert passive microwave observations into surface soil moisture units. The explanation for this inadequate description of the relationship is important to future research in passive microwave and is worth considering. Two factors contributed in large part to the uncertainty observed. The first factor was the narrow range of soil moisture observed, as noted above. The second factor was the inadequacy of the ground truth data. Only four samples were collected from each calibration field in the vicinity of Northern Central Site Lubbon on each overflight date. These four samples were expected to represent the mean surface soil moisture of the field sampled. Unfortunately the high degree of variation in the values of these samples indicates that four samples was an insufficient number for this purpose. The resulting scatter is explained in part by this.

4.3 Relationships Between Evaporative Fraction and Soil Moisture

The final objective of this research was to examine the relationship, if any, between surface soil moisture and the evaporative fraction for several sites. A statistically significant relationship would indicate the potential advantage of using microwave detection of surface soil moisture coupled with measurement of land surface fluxes.

The original objective called for comparison of remotely sensed surface soil moisture with the evaporative fraction. The poor linear fit resulting from the regression between surface soil moisture and emissivity, or even brightness temperature, dictated that soil moisture values computed using this linear conversion not be used in such an analysis. The inherent uncertainty would only further cloud the results of the additional analysis. It was noted in the previous section that the brightness temperature imagery provided an exceptional description of expected soil moisture variation between fields, while ground truth values suffered from large scatter and small sample sizes. Assuming that the scatter was largely a function of inadequate ground truth sampling, the remotely sensed values remain acceptable indicators of surface soil moisture. Instead of examining *surface soil moisture* computed from a regression equation, the *emissivity* was used directly in the comparison.

The field-averaged emissivity values were paired with midday evaporative fraction values for corresponding dates to examine the possibility of a relationship. These scatter plot for these variables is shown in Figure 4.34. The scatter was so significant that no attempt was made to fit a regression line to the data. The only conclusion possible in this case was that the surface soil moisture was not linked in any fundamental way to the partitioning of surface energy in these observations, and that activity in the surface layer is independent of activity in the root zone to a large extent.

The surface energy balance is always in one of two regimes: energy-limited or water-limited. In the energy-limited case, water is plentiful and maximum latent heat flux occurs for the given energy and system efficiency. In the water-limited case, latent heat flux is reduced from this optimum as a function of the water availability, with a corresponding increase in sensible heat flux. The lack of a discernable relationship was true only for the soil depth observed by the L-band radiometer (4 to 5-cm). Thus, for the vegetated surfaces examined the energy balance was influenced by water availability in a deeper zone than was detectable with an L-band microwave radiometer. The relationship between soil moisture and energy partition must then have involved the root zone at depth and must have been only weakly linked to surface soil moisture. To confirm this hypothesis, total root zone soil moisture was compared with the evaporative fraction.

Neutron probe measurements of soil moisture for the complete root zone during the SOP were collected and used to compute the relative water content (RWC), defined as

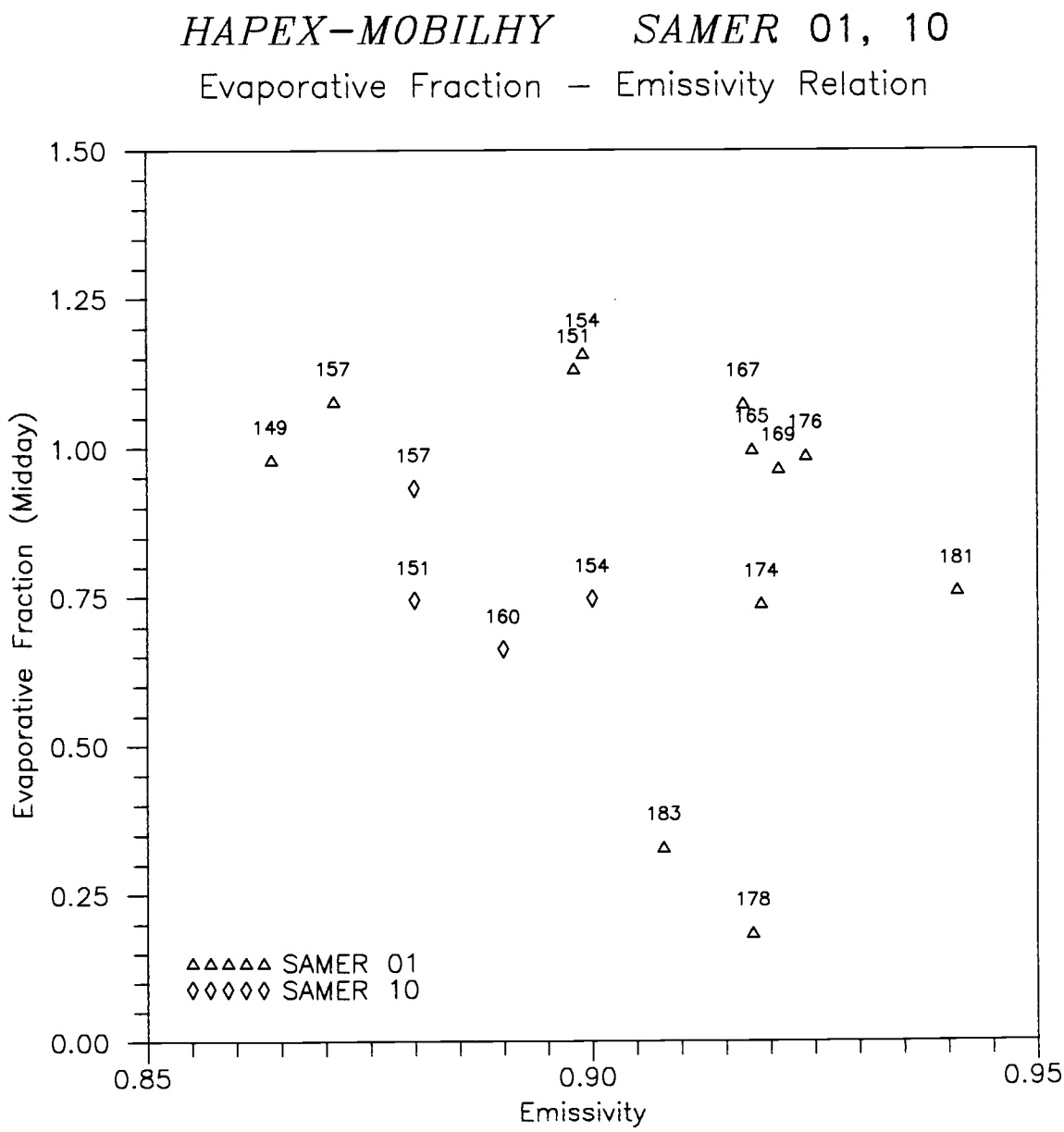

Figure 4.34 Scatter plot of midday evaporative fraction versus field-averaged emissivity for the Lubbon 1 and Castelnau sites. No regression was attempted for lack of a discernable relationship.

$$RWC = \frac{\Theta_E - \Theta_E^{MIN}}{\Theta_E^{MAX} - \Theta_E^{MIN}} \quad (4\text{-}3)$$

where

Θ_E = soil moisture at the time of interest for the root zone, equivalent depth (mm)

Θ_E^{MAX} = maximum observed soil moisture, equivalent depth (mm)

Θ_E^{MIN} = minimum observed soil moisture, equivalent depth (mm)

The use of relative water content permitted direct comparison between soil profiles of differing water holding capacities.

The computed relative water content values from the SOP were paired with evaporative fraction values from the corresponding dates as was done in the emissivity analysis and the results plotted in Figure 4.35. In examining Figure 4.35, recall that evaporative fraction values greater than one imply negative sensitive heat flux, typically caused by advection. Post-senescence dates were excluded from this analysis because the soil moisture at depth is not available to the system and hence are not valid for this comparison. A weak linear relationship was present (R^2 = 0.40) for this comparison. Based on these results, it appears that the evaporative flux over vegetated surfaces is more closely correlated with the complete soil moisture profile rather than with the surface soil moisture content monitored by passive microwave remote sensing.

Based on these results it appears that passive microwave remote sensing can not provide for detection of a state variable, moisture, in vegetated land surfaces for use in evaporative flux measurement or modelling. Nor is surface soil moisture to the depth monitored by L-band microwave radiometers significantly related to soil moisture at depth in such environments.

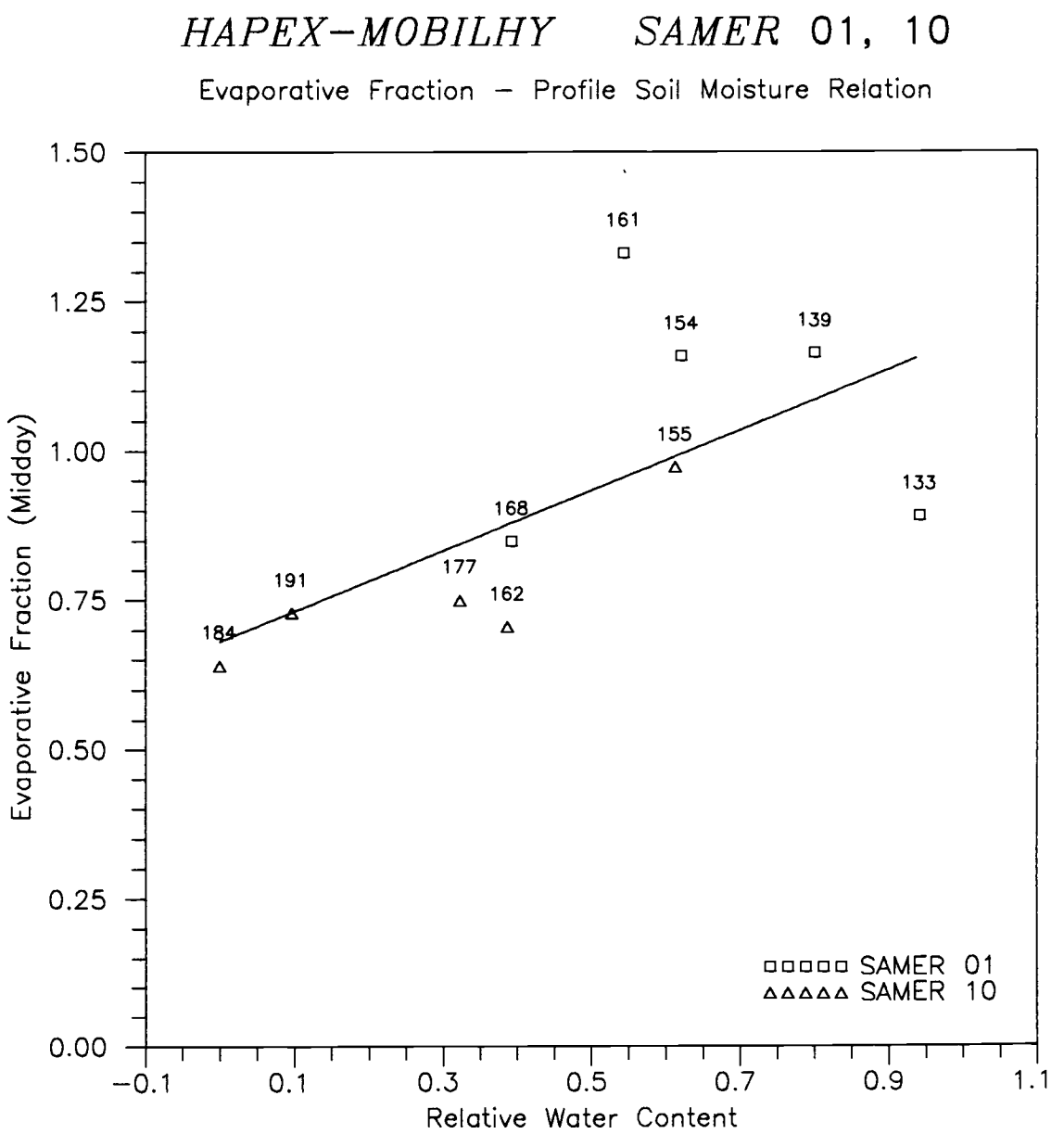

Figure 4.35 Scatter plot of midday evaporative fraction versus relative water content computed from neutron probe data for the root zone at the Lubbon 1 site. The coefficient of determination for the indicated regression line is 0.40.

5 CONCLUSIONS AND RECOMMENDATIONS

Analysis of the evaporative fraction resulted in confirmation of previous research of land surface energy balance relationships using the HAPEX-MOBILHY database. The evaporative fraction is a stable quantity describing the energy partition at the surface of the Earth in daylight periods on clear days, and its value at midday is representative of the daylight average. This implies that if the evaporative fraction could be estimated at midday by remote sensing techniques, it could be used to convert instantaneous land surface energy measurements made at midday to daily values. For "rough" dates however, this representativeness is not valid. Thus instantaneous measurements on days with intermittent cloudiness may not be scaled with the same degree of confidence as for clear days using this technique. The potential cause of the instability on rough dates may be the increase in evaporation potential during and following water application to the surface due to interception. Ensuing research will be devoted to clarifying this. The result may be that the stability extends to rough days without precipitation.

The results of the passive microwave mapping of surface soil moisture were mixed. The PBMR detected both spatial and temporal variation in surface microwave emissions, with a surprising degree of definition corresponding to field boundaries. Attempting to relate these data to surface soil moisture resulted in a poor description of the theoretical linear fit: $R^2 = 0.43$ for regression against brightness temperature and $R^2 = 0.32$ for regression against emissivity. Therefore, no effort was made to convert the microwave observations into surface soil moisture values.

The scatter observed in the microwave - soil moisture relationship was largely due to two factors: an inadequate range of observed surface soil moisture in calibration fields and an insufficient ground truth data set. Recommendations for addressing these factors in future passive microwave research are in order.

In addressing the limited (dry) range of observed surface soil moisture, one of two options (or both) are available. If the limited (dry) range is expected in an experiment conducted during the annual soil moisture depletion period, one aircraft mission could be flown earlier in the season, together with a ground truth mission, to obtain a "wet" data set. This

solution sounds simple and reasonable, but may involve prohibitive costs in aircraft operation or problems with aircraft priority and availability. A second approach involves making use of an irrigated field in the experiment. The field should be thoroughly irrigated to field capacity one day prior to a flight mission. This would not interfere with normal aircraft operations, and would provide the required "wet" data set. The only complication to this may be the difficulty usually encountered by researchers working on private farms where land owners do not wish to operate the land to meet a research schedule. The only solution possible for the limited soil moisture range if it is located in the wet end of the curve is to fly a mission later in the soil moisture depletion period.

The second factor, an inadequate ground truth data set, can be addressed though better sampling techniques. Limitations on the ground truth effort will always involve limited time and human resources; time because the data must be collected close to the overflight time, and human resources because limited samples may be collected by research personnel in a given time. The point is made that adequate sampling of a few fields is preferable to the limited sampling of many fields. Ideal sampling would involve a large number of samples, e.g., more than 30, evenly distributed over the sampled field, all collected at the overflight time. Due to the destructive nature of gravimetric sampling techniques, it may be undesirable to sample in this manner. The neutron scattering technique (Cuenca, 1988) could be used to obtain the required measurements without this difficulty. The limitations to use of neutron scattering are the depth range of the surface layer observed (typically 10-cm, or twice the effective depth viewed by an L-band microwave radiometer; see Figure 4.28), and dependence on the calibration of the neutron probe.

An example of how these measurements could be collected is found in a research plot near Corvallis, Oregon operated by the Oregon State University Water Resources Engineering Team. On this 1.85-Ha (4.6 acre) irrigated grass plot, a network of neutron probe access tubes is distributed across the site in a configuration designed to sample the field for application to remote sensing observations. Five access tubes are installed to monitor the complete root zone at the center of the field. Ten "surface" tubes are distributed across two line transects in the field to a depth of 30-cm to monitor the surface layer. The neutron scattering technique permits replicated, non-destructive sampling of soil moisture in a rapid manner for this plot.

Use of this kind of moisture controlled (through irrigation), intensely measured field site in a large scale experiment for PBMR calibration would be ideal, solving many of the problems encountered in the HAPEX-MOBILHY analysis.

Additional research is suggested based on the results of this study and on related topics not evaluated here. These topics include examination of the variation of evaporative fraction relations with vegetation cover, improving spatial resolution of emissivity mapping over disjointed land surfaces, and *in situ* testing of an instrumented land surface field site for use with passive microwave remote sensing.

The relationship between the evaporative fraction and vegetation cover could be quantified though use of the Normalized Difference Vegetation Index (NDVI). The HAPEX-MOBILHY database provides an opportunity to investigate this index. The evaporative fraction database for HAPEX-MOBILHY is available along with the computer processing code developed for this study. The NDVI is computed from Bands 3 (red) and 4 (near infrared) of the NS001 Thematic Mapper Simulator (TMS). An example NDVI image is shown in Figure 5.1 for Lubbon - Northern Central Site on 16 June 1986 (86D167). The high resolution of this sensor and the strong response of the NDVI imagery in this example indicate promise for this research topic in relating a known remote sensing indice to a single parameter quantifying the partition of energy flux. The Perpendicular Vegetation Index (PVI) discussed by Theis *et al.* (1988) may be a better means of quantifying the effect of vegetation on the microwave signal. This index should also be included in future research.

Development of emissivity imaging techniques is recommended due to the frustration encountered in processing PBMR imagery for disjointed land surfaces in the HAPEX-MOBILHY Program. The problem lies in the use of the PRT-5 thermal infrared radiometer to provide surface temperatures for emissivity calculation (refer to equation (2-22a) for this details of this computation). The PRT-5 is a nadir-viewing radiometer of very small viewing area compared to the PBMR 4-beam radiometer. Figure 3.2 illustrated the relative coverage of these two sensors among others carried aboard the NASA C-130 for participation in HAPEX-MOBILHY. In a near-homogeneous environment (where relative uniformity exists in surface soil moisture and vegetation cover; e.g., the FIFE project area), the use of the PRT-5 provides no complications since the surface temperatures that the sensor detects are representative of the larger viewing area of the PBMR. However, in an environment such as HAPEX-MOBILHY, the PRT-5 could

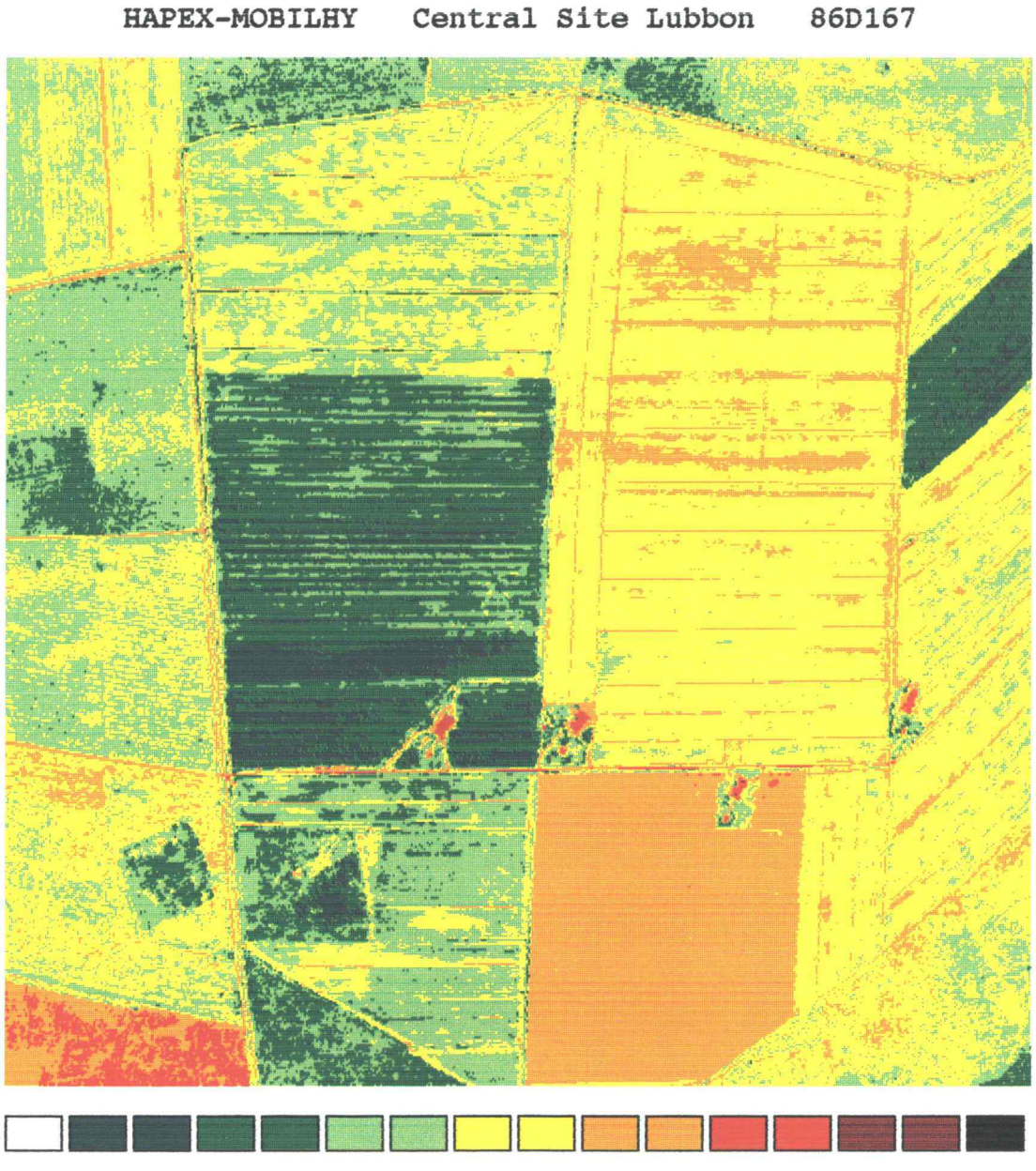

Figure 5.1 Normalized Difference Vegetation Index (NDVI) image for Northern Central Site Lubbon on 86D167 (16 June 1986). This image was obtained using NS001 Bands 3 (red) and 4 (near infrared).

conceivably be detecting surface temperatures at a certain flight time for one field while the outside PBMR beam(s) are measuring a different field out of the PRT-5 view area. This in turn would lead to severe errors in computing emissivity as a function of the difference in the PRT-5 measured surface temperature and the true field temperature in each PBMR beams view area. The cause of this error was in the uniformity assumption implied in the use of PRT-5 data. This was handled in this study by careful, independent selection of PBMR and PRT-5 data for distinct fields so as to provide a mean brightness temperature and a mean surface (kinetic) temperature for each field. The resulting emissivity computed represented an estimate of the mean for that field. This corrected for the spatial disparity in this analysis, but this approach is a short-term remedy rather than a final solution. The need to incorporate thermal infrared observations with spatial extent for use with microwave observations in computing areal emissivity requires inclusion of data collected by a sensor such as the TIMS. Techniques should be developed and applied to demonstrate the strength of using spatially distributed measurements of both measurements. This would allow for an image-based approach to surface soil moisture mapping.

The *in situ* monitoring of an intensive land surface field site is suggested to test the results of this study and the recommendations made. With future large-scale experiments such as HAPEX-Spain, HAPEX-Sahel, and SIFE (Second ISLSCP Field Experiment) in the planning stages, some of these questions need to be answered and remote sensing / ground truth collection techniques tested. This is best done in advance, using available intensive research sites. An excellent opportunity is available in the upcoming OTTER[1] Program to be conducted in 1990-1991. The Water Resources Engineering Team's ETIP[2] is already an integral part of the OTTER Program, providing the most intensive field measurements of the surface energy balance available in Oregon. NASA's participation in OTTER will include overflights by the C-130 research aircraft, which could be equipped with the PBMR to address these questions.

---

1 OTTER - Oregon Terrestrial Transect Ecological Research Program.

2 ETIP - Evapotranspiration Investigation Plot. An intensive land surface field measurement site equipped with micro-meteorological, soil moisture, surface energy balance, and surface radiation balance instrumentation. Located 15-km north of Corvallis, Oregon on a 1.85-ha irrigated grass field maintained in reference conditions.

Flight requests are being prepared to include the ETIP in the flight plan of the Oregon Transect, so this opportunity would require relatively little additional effort to answer several important questions and test the techniques discussed.

These three recommendations for additional research merit careful consideration. Because of the timely nature of the research opportunities and the need to maintain momentum and the continuity of knowledge of involved personnel, these efforts should be undertaken soon.

6 BIBLIOGRAPHY

Andre, J. P., *et al.*, Evaporation over land-surfaces: first results from HAPEX-MOBILHY special observing period, *Annales Geophysicae, 6(5)*, 477-492, 1988.

Andre, J. P., J. P. Goutorbe, T. Schmugge, and A. Perrier, HAPEX-MOBILHY: results from a large-scale field experiment, in *Remote Sensing and Large-Scale Global Processes, Proceedings of the IAHS Third Int. Assembly, Baltimore, MD, May 1989*, IAHS Publ. 186, pp. 13-20, edited by A. Rango, 1989.

Ayra, S. P., *Introduction to Micrometeorology*, Academic Press, San Diego, California, 1988.

Balek, J., J. Cermak, J. Kucera, A. Prax, and M. Palous, Regional transpiration assessment by remote sensing, in *Hydrologic Applications of Space Technology, Proceedings of the Cocoa Beach Workshop, Florida, August 1985*, IAHS Publ. 160, pp. 141-148, edited by A. I. Johnson, 1986.

Bausch, W. C., and C. M. U. Neale, Crop coefficients derived from reflected canopy radiation: a concept, *Trans. ASAE, 30(3)*, 703-709, 1987.

Ben-Asher, J., A. D. Matthias, and A. W. Warrick, Assessment of evaporation from bare soil by infrared thermometry, *Soil Sci. Soc. of America J., 47(2)*, 185-191, 1983.

Bernard, R., J. V. Soares, and D. Vidal-Madjar, Differential bare field drainage properties from airborne microwave observations, *Water Resour. Res. 22(6)*, 869-875, 1986.

Bernard, R., M. Vauclin, and D. Vidal-Madjar, Possible use of active microwave remote sensing data for prediction of regional evaporation by numerical simulation of soil water movement in the unsaturated zone, *Water Resour. Res., 17(6)*, 1603-1610, 1981.

Bessemoulin, P., G. Desroziers, M. Payen, and C. Tarrieu, *Atlas des donnees SAMER* (in French), EERM / CNRM, 1987.

Brady, Nyle C., *The Nature and Properties of Soils*, Macmillian Publishing Company, New York, New York, 1984.

Brutsaert, W., *Evaporation Into The Atmosphere*, D. Reidel, Hingham, Massachussetts, 1982.

Camillo, P. J., R. J. Gurney, and T. J. Schmugge, A soil and atmosphere boundary layer model for evapotranspiration and soil moisture studies, *Water Resour. Res. 19(2)*, 371-380, 1983.

Camillo, P., Modeling the HAPEX flux data - a preliminary assessment, to appear in *Proceedings of Workshop on Land Surface Processes, Banyuls, France, October 10-21, 1988*, edited by T. J. Schmugge, 1989.

Carrijo, O. A., Analysis of a hydrologic balance model and Penman-Montieth evapotranspiration estimating methods, Ph.D. thesis, Oregon State Univ., Corvallis, Oregon, 1988.

Caselles, V., and J. Delegido, A simple model to estimate the daily value of the regional maximum evapotranspiration from satellite temperature and albedo images, *Int. J. Remote Sens., 8(8)*, 1151-1162, 1987.

Choudhury, B. J., S. B. Idso, and R. J. Reginato, Analysis of a resistance-energy balance method for estimating daily evaporation from wheat plots using one-time-of-day infrared temperature observations, *Remote Sens. Environ., 19(3)*, 253-268, 1986.

Cuenca, R. H., Hydrologic balance model using neutron probe data, *ASCE J. Irrigation and Drainage Engr., 114(4)*, 644-663, 1988.

Cuenca, R. H., *Irrigation System Design: An Engineering Approach*, Prentice-Hall, Englewood Cliffs, New Jersey, 1988.

Cuenca, R. H., Measurement systems in the HAPEX-MOBILHY regional evapotranspiration experiment, *ASCE J. Irrigation and Drainage Engr.*, 1988.

Cuenca, R. H., and J. Noilhan, Use of soil moisture measurements in hydrologic balance studies, to appear in *Proceedings of Workshop on Land Surface Processes, Banyuls, France, October 10-21, 1988*, edited by T. J. Schmugge, 1989.

Cuenca, R. H., W. E. Nichols, O. A. Carrijo, and J. Noilhan, Comparison of ground-based evapotranspiration measurement systems in the HAPEX-MOBILHY regional experiment, *EOS Trans., AGU, 69(16)*, 351, 1988.

de Marsily, G., *Quantitative Hydrogeology: Groundwater Hydrology for Engineers*, Academic Press, Orlando, Florida, 1986.

de Pescara, C., M. Painine, and C. Garrigues, Theory and operation of French energy balance, Bowen ratio, and micro-meteorology instrumentation, in *Proceedings of the ASCE Conference on Planning Now for Irrigation and Drainage in the 21st Century, Lincoln, Nebraska, July 18-21, 1988*, 1988.

Devore, J., and R. Peck, *Statistics: The Exploration and Analysis of Data*, West Publishing Company, St. Paul, Minnesota, 1986.

Dijckmeester, P., and V. van Katwijk, Report on groundtruth collection as part of the HAPEX-MOBILHY Project: northern test site Lubbon, Free University, Amsterdam, The Netherlands, 1986.

Dugas, W. A., and M. L. Heuer, Relationships between measured and satellite-estimated solar irradiance in Texas, *J. Climate and Appl. Meteorol., 24*, 751-757, 1985.

Eagleson, P. S., The emergence of global-scale hydrology, *Water Resour. Res., 22(9)*, 65-145, 1986.

Engman, E. T., G. Angus, and W. P. Kustas, Relationships between the hydrologic balance of a small watershed and remotely sensed soil moisture, in *Remote Sensing and Large-Scale Global Processes, Proceedings of the IAHS Third Int. Assembly, Baltimore, MD, May 1989*, IAHS Publ. 186, pp. 75-84, edited by A. Rango, 1989.

Foster, J. L., D. K. Hall, and A. T. C. Chang, Remote sensing of snow, *EOS Trans., AGU, August 11*, 1987.

Gash, J. H. C., Analytical framework for extrapolating evaporation measurements by remote sensing surface temperature, *Int. J. Remote Sens., 8(8)*, 1245-1249, 1987.

Goutorbe, J. P., Surface energy balance in the HAPEX-MOBILHY experiment, to appear in *Proceedings of Workshop on Land Surface Processes, Banyuls, France, October 10-21, 1988*, edited by T. J. Schmugge, 1989.

Goutorbe, J. P., J. Noilhan, C. Valancogne, and R. H. Cuenca, Soil moisture variations during HAPEX-MOBILHY, *Annales Geophysicae, 7(4)*, 415-426, 1989.

Greegor, D. H., Jr, and J. Norwine, Global habitability and remote sensing: the role of meteorological satellite data, *Sci. Total Environ., 55*, 187-196, 1986.

Gupta, P. L., and P. S. N. Sastry, Estimating evapotranspiration from midday canopy temperature, *Irrigation Sci., 7(4)*, 237-243, 1986.

Gurney, R. J., and P. J. Camillo, Modelling daily evapotranspiration using remotely sensed data, *J. Hydrol., 69*, 305-324, 1984.

Hatfield, J. L., Evapotranspiration obtained from remote sensing methods, in *Advances in Irrigation, Vol. 2*, pp. 395-416, edited by D. Hillel, Academic Press, New York, New York, 1983.

Hatfield, J. L., Research priorities in ET: evolving methods, *Trans. ASAE, 31(2)*, 490-495, 1988.

Hatfield, J. L., A. Perrier, and R. D. Jackson, Estimations of evapotranspiration at one time-of-day using remotely sensed surface temperatures, *Agric. Water Management, 7*, 341-350, 1983.

Hope, A. S., D. E. Petzold, S. N. Goward, and R. M. Raggan, Simulated relationships between spectral reflectance, thermal emissions, and evapotranspiration of a soybean canopy, *Water Resour. Bulletin, 22(6)*, 1011-1019, 1986.

Hord, R. M., *Remote Sensing Methods and Applications*, John Wiley & Sons, Inc., New York, New York, 1986.

Jackson, R. D., Evaluating evapotranspiration at local and regional scales, *Proceedings IEEE, 73(6)*, 1086-1096, 1985.

Jackson, R. D., Estimating areal evapotranspiration by combining remote and ground-based data, in *Remote Sensing Applications For Consumptive Use (Evapotranspiration)*, AWRA Monograph Series No. 6, edited by A. I. Johnson and A. Rango, 1986.

Jackson, R. D., J. L. Hatfield, R. J. Reginato, S. B. Idso, and P. J. Pinter, Jr., Estimation of daily evapotranspiration from one time-of-day measurements, *Agric. Water Management, 7*, 351-362, 1983.

Jackson, R. D., P. J. Pinter Jr., and R. J. Reginato, Net radiation calculated from remote multispectral and ground station meteorological data, *Agric. Meteorol., 35*, 1342-1354, 1985.

Jackson, R. D., S. Moran, L. W. Gay, and L. H. Raymond, Evaluating evaporation from field crops using airborne radiometry and ground-based data, *Irrigation Sci., 8(2)*, 81-90, 1987.

Jackson, T. J., and P. O'Neill, Salinity effects on the microwave emission of soils, *IEEE Trans. Geosci. and Remote Sens., GE-25(2)*, 214-220, 1987.

Jackson, T. J., and T. J. Schmugge, Passive microwave remote sensing of soil moisture, in *Advances in Hydroscience, 14*, pp. 123-159, Academic Press, Washington, D.C., 1986.

Jackson, T. J., J. Shuie, P. O'Neill, M. Owe, V. Delnore, and R. W. Lawerence, Assessment of preplanting soil moisture using airborne microwave sensors, in *Hydrologic Applications of Space Technology, Proceedings of the Cocoa Beach Workshop, Florida, 1985*, IAHS Publ. 160, 111-118, edited by A. I. Johnson, 1986.

Klassen, W., and W. Van Der Berg, Evapotranspiration derived from satellite observed surface temperatures, *J. Climate And Appl. Meteorol., 24*, 412-424, 1985.

Krul, L., Some results of microwave remote sensing research in The Netherlands with a view to land applications in the 1990s, *Int. J. Remote Sens., 9*, 1553-1563, 1988.

Lillesand, T. M., and R. W. Kiefer, *Remote Sensing and Image Interpretation*, John Wiley and Sons, New York, New York, 1987.

Linsley, R. K., Jr., M. A. Kohler, and J. L. H. Paulhus, *Hydrology For Engineers*, McGraw-Hill, New York, New York, 1982.

Mahfouf, J. F., and B. Jacquemin, A study of rainfall interception using a land surface parameterization for mesoscale meteorological models, to appear in *J. Appl. Meteorol.*, 1989.

Musick, H. B., and R. E. Pelletier, Response to soil moisture of spectral indexes derived from bidirectional reflectance in Thematic Mapper wavebands, *Remote Sens. Environ., 25*, 167-184, 1988.

NASA Earth Sciences and Applications Division, *Plan for FY 1988-1989-1990*, National Aeronautics and Space Administration, Washington, D. C., 1988.

Nieuwenhuis, G. J. A., Integration of remote sensing with a soil water balance simulation model (SWATRE), in *Hydrologic Applications of Space Technology, Proceedings of the Cocoa Beach Workshop, Florida, August 1985*, IAHS Publ. 160, pp. 119-128, edited by A. I. Johnson, 1986.

Nieuwenhuis, G. J. A., E. H. Smidt, and H. A. M. Thunnissen, Estimation of regional evapotranspiration of arable crops from thermal infrared images, *Int. J. Remote Sens., 6(8)*, 1319-1334, 1985.

Penman, H. L., Natural evaporation from open water, bare soil, and grass, *Proceedings of the Royal Society, London, Ser. A 193*: 120-146, 1948.

Perry, E., and T. N. Carlson, Comparison of active microwave soil water content with infrared surface temperatures and surface moisture availability, *Water Resour. Res., 24(10)*, 1818-1824, 1988.

Peterson, D. L., M. A. Spanner, S. W. Running, and K. B. Teuber, Relationship of Thematic Mapper Simulator data to leaf area index of temperate coniferous forests, *Remote Sens. Environ, 22*, 323-341, 1987.

Pierce, L. L., and R. G. Congalton, A methodology for mapping forest latent heat flux densities using remote sensing, *Remote Sens. Environ., 24*, 405-418, 1988.

Prevot, L., R. Bernard, O. Taconet, D. Vidal-Madjar, and J. L. Thony, Evaporation from a bare soil evaluated using a soil water transfer model and remotely sensed surface soil moisture data, *Water Resour. Res., 20(2)*, 311-316, 1984.

Raffy, M., and F. Becker, A stable iterative procedure to obtain soil surface parameters and fluxes from satellite data, *IEEE Trans. Geosci. and Remote Sens., GE-24(3)*, 327-333, 1986.

Reginato, R. J., R. D. Jackson, and P. J. Pinter, Jr., Evapotranspiration calculated from remote multispectal and ground station meteorological data, *Remote Sens. Environ., 18*, 75-89, 1985.

Riou, C., B. Itier, and B. Seguin, The influence of surface roughness on the simplified relationship between daily evaporation and surface temperature, *Int. J. Remote Sens., 9*, 1529-1533, 1988.

Running, Steven W., Estimating forest evapotranspiration by coupling satellite data with ecosystem simulation, to appear in *Proceedings of Workshop on Land Surface Processes, Banyuls, France, October 1988*, edited by T. J. Schmugge, 1989.

Sabins, Floyd F., Jr., *Remote Sensing: Images and Interpretation*, W. H. Freeman and Company, New York, New York, 1987.

Sadeghi, A. M., H. D. Scott, W. P. Waite, and G. Asrar, Estimating soil water evaporation using radar measurements, *IEEE Trans. Geosci. and Remote Sens., 26(4)*, 490-493, 1988.

Schmugge, T. J., Remote sensing observations for the monitoring of land surface fluxes and water budgets, to appear in *Proceedings of Workshop on Land Surface Processes, Banyuls, France, October 10-21, 1988*, edited by T. J. Schmugge, 1989.

Schmugge, T. J., J. R. Wang, and G. Asrar, Results from the Push Broom Microwave Radiometer flights over the Konza Prairie in 1985, *IEEE Trans. Geosci. and Remote Sens., 26(5)*, 1988.

Schmugge, T., and L. Janssen, Aircraft remote sensing in HAPEX, in *Proceedings 4th International Colloquim of Spectral Signatures of Objects in Remote Sensing, Aussois, France, January 18-22, 1988*, pp. 463-467 (ESA SP-287), 1988.

Seguin, B., and B. Itier, Using midday surface temperature to estimate daily evaporation from satellite thermal IR data, *Int. J. Remote Sens., 4*, 371-383, 1983.

Sellers, P. J., et al., First ISLSCP Field Experiment: experiment execution and preliminary analyses, in *Remote Sensing and Large-Scale Global Processes, Proceedings of the IAHS Third Int. Assembly, Baltimore, MD, May 1989*, IAHS Publ. 186, pp. 49-58, edited by A. Rango, 1989.

Serafini, Y. V., Estimation of the evapotranspiration using surface and satellite data, *Int. J. Remote Sens., 8(10)*, 1547-1562, 1987.

Shuttleworth, W. J., R. J. Gurney, A. Y. Hsu, and J. P. Ormsby, FIFE: the variation in energy partition at surface flux sites, in *Remote Sensing and Large-Scale Global Processes, Proceedings of the IAHS Third Int. Assembly, Baltimore, MD, May 1989*, IAHS Publ. 186, pp. 67-74, edited by A. Rango, 1989.

Soares, J. V., R. Bernard, O. Taconet, D. Vidal-Madjar, and A. Weill, Estimation of bare soil evaporation from airborne measurements, *J. Hydrol., 99*, 281-296, 1988.

Soer, G. J. R., Estimation of regional evapotranspiration and soil moisture conditions using remotely sensed crop surface temperatures, *Remote Sens. Environ., 9*, 27-45, 1980.

Theis, S. W., and A. J. Blanchard, The effect of measurement error and confusion from vegetation on passive microwave estimates of soil moisture, *Int. J. Remote Sens., 9(2)*, 333-340, 1988.

Tipler, Paul A., *Physics*, Worth Publishers, New York, New York, 1982.

Tsang, L., J. A. Kong, and R. T. Shin, *Theory of Microwave Remote Sensing*, John Wiley and Sons, New York, New York, 1985.

van de Griend, A. A., and J. H. van Boxel, Water and surface energy balance model with a multilayer canopy representation for remote sensing purposes, *Water Resour. Res., 25(5)*, 949-971, 1989.

van de Griend, A. A., P. J. Camillo, and R. J. Gurney, Discrimination of soil physical parameters, thermal inertia, and soil moisture from diurnal surface temperature fluctuations, *Water Resour. Res., 21(7)*, 997-1009, 1985.

Wang, J. R., J. C. Shuie, T. J. Schmugge, and E. T. Engman, Mapping surface soil moisture with L-band radiometric measurements, *Remote Sens. Environ., 27*, 305-312, 1989.

Weisberg, S., *Applied Linear Regression*, John Wiley and Sons, New York, New York, 1985.

Welty, J. R., C. E. Wicks, and R. E. Wilson, *Fundamentals of Momentum, Heat, and Mass Transfer*, John Wiley & Sons, New York, New York, 1984.

APPENDICES

Appendix A Computer Source Code Listings

Several computer programs were developed for this study to facilitate data and image processing. The source codes for the following programs are presented in this appendix:

POINT.BAS	Cartesian coordinate assignment program for PBMR data. Requires digitized flight line information and PBMR data files.
DISTRIB.BAS	PBMR image forming program. Distributes data to grid-based image. Requires output files from **POINT**.
UNPACK.BAS	Conversion utility to translate binary image files created by DISTRIB into ASCII data files for use in other software packages, e.g. IDRISI.
MAKEMASK.BAS	Utility for creation of query masks used in calibration analysis.
IDRISI.LIB	Library of routines common to several of the programs listed in this appendix.
EVAPVIEW	Graphics-based data inspection program for evaporative flux analysis with SAMER database. Requires VGA. Must be used in conjunction with the SAMTRAN software system.

Some programs mentioned in the text of this report are not listed here. This occurs when the code in question was developed for general purposes and has seperate documentation. For example, SAMTRAN is a software system for SAMER database management developed to assist in a wide variety of research endeavors. A User's Guide exists for this program, hence replication of the code in this report is not necessary.

```
'
'  POINT.BAS
'                                        Last Modified: 18 Sep 1989 (WEN)
'
'  Program to compute the ground coordinates of Push Broom Microwave
'  Radiometer (PBMR) data collected by the NASA C-130.
'
'  POINT was written and compiled in Microsoft QuickBASIC 4.5 using IBM
'  PS/2 computers (Models 30-286, 50, and 70).
'
'  Developed by : William E. Nichols, 1989
'  Organization : Water Resources Engineering Team
'                 Oregon State University, Corvallis, Oregon
'  Project :      USDA-ARS Cooperative Research Project
'

'---Initialize program environment.
DECLARE FUNCTION Time10sec& (timeNumber)
REM $INCLUDE: 'IDRISI.ICL'                    '---IDRISI User's Library
DEFINT I-N
CONST Pi = 3.141592654#
CONST Inner.Angle# = (8 * (Pi / 180))         '---Angle of PBMR Beams 2,3
CONST Outer.Angle# = (24 * (Pi / 180))        '---Angle of PBMR Beams 1,4
DIM kTime&(200), xCoor(200), yCoor(200)

'---Obtain operating information.
cTot$ = COMMAND$
FOR j = 1 TO LEN(cTot$)
    c$ = MID$(cTot$, j, 1)
    IF c$ <> " " THEN FileName$ = FileName$ + c$
NEXT j
CALL Read.ENV.File

'---If prompt line does not contain necessary information, then prompt
'   the user to provide it.
IF FileName$ = "" THEN

    '---Display ID banner.
    CALL Read.ENV.File
    CLS : COLOR Banner.Color: BOX 1, 80, 1, 3, 2: COLOR Dialog.Color
    LOCATE 2, 3: PRINT "POINT : PBMR Ground Coordinate Register Program                v.3.00"
    VIEW PRINT 5 TO 23

    '---Inform user of file requirement.
    PRINT "Enter the base filename for input and output operations.  POINT assumes that"
    PRINT "there are two files for input; one with a .DAT extension containing the PBMR"
    PRINT "data with original time relations and the PRT-5 data, the other with a .TRK"
    PRINT "extension containing the digitized flight line time-coordinate pairs.  POINT"
    PRINT "will create a third file with the same name and a .REG extension containing"
```

```
    PRINT "the PBMR data registered to ground coordinates."
    PRINT
    PRINT "Enter the base filename, including drive and path"; TAB(55); ": ";
    INPUT "", FileName$

ELSEIF FileName$ = "?" THEN

    '---Initialize user interface.
    CALL Read.ENV.File
    CLS : COLOR Banner.Color: BOX 1, 80, 1, 3, 2: COLOR Dialog.Color
    LOCATE 2, 3: PRINT "IDRISI : PBMR Ground Coordinate Register Program                v.3.00"
    VIEW PRINT 5 TO 23

    '---Information on POINT
    COLOR Banner.Color: BOX 5, 76, 5, 8, 1
    LOCATE 6, 11: PRINT "          Developed by  William E. Nichols, 1989          "
    LOCATE 7, 11: PRINT "Water Resources Engineering Team  /  Oregon State University"
    LOCATE 10, 1: COLOR Dialog.Color
    PRINT "POINT registers PBMR data to ground coordinates as a preliminary to image "
    PRINT "formation.  POINT requires two information sources: The original PBMR time-"
    PRINT "registered data and a set of known ground coordinate - time pairs.  The known"
    PRINT "points are generally obtained by digitizing the flight path maps made using"
    PRINT "the aircraft's nadir camera.  POINT assumes the following file extensions:"
    PRINT
    PRINT "   .DAT extension = PBMR original data"
    PRINT "   .TRK extension = Flight path known coordinates / time data"
    PRINT "   .REG extension = POINT output; PBMR data registered to ground coordinates."
    PRINT
    PRINT "POINT may be used in either prompt or command line style.  For prompt, type"
    PRINT "POINT and press ENTER ^Q↵.  For command line, type POINT followed by a space"
    PRINT "and the base file name to process."
    END

END IF

'---Add the required extensions to the filename for each I/O file.
File1$ = FileName$ + ".DAT"
File2$ = FileName$ + ".TRK"
File3$ = FileName$ + ".REG"

'---Working notice.
COLOR Message.Color: PRINT : PRINT "Working ... ";

'---Import ground coordinates and associated overpass times.
OPEN File2$ FOR INPUT AS #2
INPUT #2, Day.Of.Year%, Description$, Pass.Number%
WHILE NOT EOF(2)
    I = I + 1
```

```
        INPUT #2, timeNumber, xCoor(I), yCoor(I)
        kTime&(I) = Time10sec&(timeNumber)
    WEND: Number.Known.Points = I: CLOSE #2

    '---Open orignal data file and read header line.
    OPEN File1$ FOR INPUT AS #1
    INPUT #1, Day.Of.Year%, Description$, Pass.Number%, Altitude, Unknown.Variable%

    '---Open output file and record header line.
    OPEN File3$ FOR OUTPUT AS #3
    WRITE #3, Day.Of.Year%, Description$, Pass.Number%, Altitude, Unknown.Variable%

    '---Move through flight pass.  PBMR time (from input file 1) is used to
    '   scale distances between known ground coordinates and overpass times
    '   (from digitized flight paths, in input file 2).  Beam centers are
    '   computed using geometrical characteristics of PBMR sensor and the
    '   aircraft's flight altitude (provided by data file).
    '
    FOR I = 1 TO (Number.Known.Points - 1)
        '---Compute ordinate distances between known flight coordinates.
        xDist = xCoor(I + 1) - xCoor(I)
        yDist = yCoor(I + 1) - yCoor(I)
        '---Compute angle of the (assumed) linear nadir-line segment.
        IF xDist <> 0 THEN Nadir.Angle! = ABS(ATN(yDist / xDist))
NextSensorPoint:
        '---Input line of sensor data.
        IF EOF(1) THEN EXIT FOR
        INPUT #1, timeNumber, Tb1, Tb2, Tb3, Tb4, PRT5
        sTime& = Time10sec&(timeNumber)
        '---Check if nadir is inside current flight path segment.
        IF sTime& < kTime&(1) THEN GOTO NextSensorPoint
        IF sTime& > kTime&(I + 1) THEN GOTO NextKnown
        IF sTime& > kTime&(Number.Known.Points) THEN EXIT FOR
        '---Compute fraction of time into this flight path segment.
        timeFrac = (sTime& - kTime&(I)) / (kTime&(I + 1) - kTime&(I))
        '---Estimate current sensor nadir coordinates.
        x.Nadir = xCoor(I) + (timeFrac * xDist)
        y.Nadir = yCoor(I) + (timeFrac * yDist)
        '---Compute coordinates of the four PBMR beam centers.
        IF xDist = 0 THEN             '---North-South axis flight path
            xB1 = x.Nadir + SGN(yDist) * TAN(Outer.Angle!) * Altitude
            xB2 = x.Nadir + SGN(yDist) * TAN(Inner.Angle!) * Altitude
            xB3 = x.Nadir - SGN(yDist) * TAN(Inner.Angle!) * Altitude
            xB4 = x.Nadir - SGN(yDist) * TAN(Outer.Angle!) * Altitude
            yB1 = y.Nadir: yB2 = y.Nadir: yB3 = y.Nadir: yB4 = y.Nadir
        ELSEIF yDist = 0 THEN         '---East-West axis flight path
            xB1 = x.Nadir: xB2 = x.Nadir: xB3 = x.Nadir: xB4 = x.Nadir
            yB1 = y.Nadir - SGN(xDist) * TAN(Outer.Angle!) * Altitude
            yB2 = y.Nadir - SGN(xDist) * TAN(Inner.Angle!) * Altitude
            yB3 = y.Nadir + SGN(xDist) * TAN(Inner.Angle!) * Altitude
```

```
            yB4 = y.Nadir + SGN(xDist) * TAN(Outer.Angle#) * Altitude
        ELSE                            '---Any non-axis flight path
            xB1 = x.Nadir + SGN(yDist) * SIN(Nadir.Angle#) * TAN(Outer.Angle#) * Altitude
            xB2 = x.Nadir + SGN(yDist) * SIN(Nadir.Angle#) * TAN(Inner.Angle#) * Altitude
            xB3 = x.Nadir - SGN(yDist) * SIN(Nadir.Angle#) * TAN(Inner.Angle#) * Altitude
            xB4 = x.Nadir - SGN(yDist) * SIN(Nadir.Angle#) * TAN(Outer.Angle#) * Altitude
            yB1 = y.Nadir - SGN(xDist) * COS(Nadir.Angle#) * TAN(Outer.Angle#) * Altitude
            yB2 = y.Nadir - SGN(xDist) * COS(Nadir.Angle#) * TAN(Inner.Angle#) * Altitude
            yB3 = y.Nadir + SGN(xDist) * COS(Nadir.Angle#) * TAN(Inner.Angle#) * Altitude
            yB4 = y.Nadir + SGN(xDist) * COS(Nadir.Angle#) * TAN(Outer.Angle#) * Altitude
        END IF
        '---Record the PBMR data with corresponding ground coordinates.
        PRINT #3, USING "#####.# #####.# ###.# "; xB1; yB1; Tb1;
        PRINT #3, USING "#####.# #####.# ###.# "; xB2; yB2; Tb2;
        PRINT #3, USING "#####.# #####.# ###.# "; xB3; yB3; Tb3;
        PRINT #3, USING "#####.# #####.# ###.# "; xB4; yB4; Tb4;
        PRINT #3, USING "#####.# #####.# ###.# "; x.Nadir; y.Nadir; PRT5
        GOTO NextSensorPoint
NextKnown:
    NEXT I: CLOSE #1: CLOSE #3

    '---End of program.
    IF LEN(cTot$) > 2 THEN
        LOCATE , 1: PRINT SPACE$(40): COLOR Message.Color
        LOCATE 21, 1: PRINT "Finished- PBMR ground coordinates recorded for ";
        PRINT Description$; " Pass"; Pass.Number%; "."
    END IF
    PRINT : END




FUNCTION Time10sec& (timeNumber)

'   ------------------------------------------------------------
'      Function to convert coded time numbers to units of 1/10 seconds
'   ------------------------------------------------------------

    '---retain decimal portion of time number seperately.
    tenths! = timeNumber - INT(timeNumber)

    '---Convert truncated time number to a string variable.
    timeString$ = RIGHT$((SPACE$(6) + STR$(INT(timeNumber))), 6)

    '---Convert time units to tenths of seconds elapsed since midnight.
    hour! = VAL(MID$(timeString$, 1, 2))
```

```
    minute! = VAL(MID$(timeString$, 3, 2))
    second! = VAL(MID$(timeString$, 5, 4))
    Time10sec& = 10 * ((hour! * 60 * 60) + (minute! * 60) + (second!) + tenths!)

END FUNCTION
```

```
'
'  DISTRIB.BAS
'                                        Last Modified: 26 Sep 1989 (WEN)
'
'  Program to distribute Push Broom Microwave Radiometer (PBMR) for use
'  an binary image file for use in IDRISI.  Input data file must have
'  already been processed using POINT.EXE to assign ground coordinates.
'
'  Version 2:  Updated to include capability to create emissivity images
'              using the PRT-5 as a surface temperature estimate, OR to
'              create PRT-5 imagery (chiefly for data extraction).
'
'  DISTRIB was written and compiled in Microsoft QuickBASIC 4.5 using
'  IBM PS/2 computers (Models 30-286, 50, and 70).  DISTRIB requires
'  VGA graphics to display flight information during processing.
'
'  Developed by : William E. Nichols, 1989
'  Organization : Water Resources Engineering Team
'                 Oregon State University, Corvallis, Oregon
'  Project :      USDA-ARS Cooperative Research Project
'

'---Declare DISTRIB subprograms.
DECLARE SUB BuildImage (J AS INTEGER, FileNum AS INTEGER, Value.Now AS SINGLE)
DECLARE SUB Explain ()
DECLARE SUB InitializeFile (FileNum AS INTEGER, Out.File$, Tmp.File$)
DECLARE SUB InitializeGraf ()

'---Declare globally visible variables.
COMMON SHARED /Global/ Alt AS SINGLE, Grd AS INTEGER
COMMON SHARED /Global/ xBeam() AS SINGLE, yBeam() AS SINGLE
COMMON SHARED /Global/ xMin AS LONG, yMin AS LONG
COMMON SHARED /Global/ xMax AS LONG, yMax AS LONG
COMMON SHARED /Global/ xSize AS LONG, ySize AS LONG

'---Include IDRISI User's Library declarations.
REM $INCLUDE: 'IDRISI.ICL'                    '---IDRISI User's Library

'---Define default integers & program constants.
DEFINT I-N                                    '---Integer defaults
CONST Pi = 3.141592654#                       '---Pi constant

'---Dimension array variables.
DIM Filename$(5)                              '---Data file names
DIM Temp(5)                                   '---Beam data values
DIM xBeam(5) AS SINGLE, yBeam(5) AS SINGLE    '---Beam coordinates

'---Read in the IDRISI environment file.
CALL Read.ENV.File
```

```
'---Check whether DISTRIB will be used in prompt or batch mode;
'---(if in batch mode then the batch file will be identified).
c$ = COMMAND$
FOR J = 1 TO LEN(c$)
    IF MID$(c$, J, 1) <> " " THEN
        BatchFile$ = BatchFile$ + MID$(c$, J, 1)
    END IF
NEXT J

IF BatchFile$ = "" THEN

    '---Initialize user interface.
    CLS : COLOR Banner.Color: BOX 1, 80, 1, 3, 2: COLOR Dialog.Color
    LOCATE 2, 3: PRINT "IDRISI : Distribute PBMR data to binary image file                v.3.00"
    VIEW PRINT 5 TO 24

    '---Enter options for processing.
    PRINT "DISTRIB will image PMBR or PRT-5 data from specified files.  Choose below"
    PRINT "whether brightness temperature, emissivity, or thermal IR images (or any"
    PRINT "combination of these) are desired.  Note that the emissivity values are"
    PRINT "computed using PRT-5 surface temperatures to represent all view areas."
    PRINT : PRINT : PRINT "Imaging Options:"
    PRINT : PRINT "   Create Brightness Temperature Image?"; TAB(55); ": ";
    INPUT "", resp$: IF UCASE$(resp$) = "Y" THEN T.Flag% = 1
    PRINT : PRINT "   Create Emissivity Image?"; TAB(55); ": ";
    INPUT "", resp$: IF UCASE$(resp$) = "Y" THEN E.Flag% = 1

    '---Enter I/O file names.
    CLS 2
    PRINT "Enter the number of POINT data files you intend to use"; TAB(60); ": ";
    INPUT "", NumFiles
    PRINT
    PRINT "Enter drive and path data files are stored in"; TAB(60); ": ";
    INPUT "", Path$
    PRINT : PRINT : PRINT
    PRINT "Enter file names below.  DO NOT INCLUDE extensions (.REG assumed)"
    PRINT
    FOR I = 1 TO NumFiles
        PRINT USING "    Data file name #: "; I;
        INPUT "", Filename$(I)
        Filename$(I) = Path$ + Filename$(I) + ".REG"
    NEXT I: PRINT
    PRINT "Drive and directory to store output in"; TAB(60); ": ";
    INPUT "", OutPath$: PRINT
    IF T.Flag% = 1 THEN
        PRINT "Enter file name for brightness temperature image"; TAB(60); ": ";
        INPUT "", OutFile1$
    END IF
    IF E.Flag% = 1 THEN
```

```
        PRINT "Enter file name for emissivity image"; TAB(60); ": ";
        INPUT "", OutFile2$
    END IF

    '---Solicit desired dimensions of image, and desired grid resolution.
    CLS 2
    PRINT "Enter binary image file specifications;"
    LOCATE 7, 3:  PRINT "x-coordinate of lower left image corner (meters)"; TAB(55); ": "
    LOCATE 8, 3:  PRINT "y-coordinate of lower left image corner (meters)"; TAB(55); ": "
    LOCATE 10, 3: PRINT "x-coordinate of upper right image corner (meters)"; TAB(55); ": "
    LOCATE 11, 3: PRINT "y coordinate of upper right image corner (meters)"; TAB(55); ": "
    LOCATE 13, 3: PRINT "Grid cell size (meters)"; TAB(55); ": "
    LOCATE 7, 57: INPUT "", xMin: LOCATE 8, 57: INPUT "", yMin
    LOCATE 10, 57: INPUT "", xMax: LOCATE 11, 57: INPUT "", yMax
    LOCATE 13, 57: INPUT "", Grd

ELSEIF BatchFile$ = "?" THEN

    CALL Explain

ELSE

    '---Input information from batch file IF it was identified in the
    '---DOS command line when DISTRIB was invoked.
    OPEN BatchFile$ FOR INPUT AS #1
    INPUT #1, T.Flag%, E.Flag%
    INPUT #1, NumFiles, Path$
    FOR I = 1 TO NumFiles
        INPUT #1, Filename$(I)
        Filename$(I) = Path$ + Filename$(I) + ".REG"
    NEXT I
    INPUT #1, OutPath$, OutFile1$, OutFile2$, OutFile3$
    INPUT #1, xMin, yMin, xMax, yMax, Grd
    CLOSE #1

END IF

'---Determine image dimensions in grid units.
xSize = (xMax - xMin + Grd) / Grd        '---No. grid units in x-direction
ySize = (yMax - yMin + Grd) / Grd        '---No. grid units in y-direction

'---Echo information to user and wait until user is ready to proceed.
IF BatchFile$ = "" THEN
    LOCATE 15, 1: PRINT "Data will now be distributed to a binary image file(s).  A graphical display"
    LOCATE 16, 1: PRINT "will indicate the coordinate axes and the beam locations as they are being"
    LOCATE 17, 1: PRINT "processed.  The image area will appear as a white rectangle on the display."
    LOCATE 19, 1: PRINT "PBMR image will contain"; xSize; "pixels in the horizontal plane and"; ySize; "pixels"
    LOCATE 20, 1: PRINT "in the vertical plane.  Each pixel will be"; Grd; "meters on a side."
```

```
    COLOR Message.Color
    LOCATE 23, 1: PRINT "Press any key to start...": WHILE INKEY$ = "": WEND
END IF

'---Initialize graphical display for data processing.
CALL InitializeGraf

'---Initialize all required binary image and shadow files.
OutFile1$ = OutPath$ + OutFile1$            '---Brightness Temperature
OutFile2$ = OutPath$ + OutFile2$            '---Emissivity
OutFile3$ = OutPath$ + OutFile3$            '---PRT-5 Temperature
TmpFile1$ = OutPath$ + "SHADOW_T.TMP"       '---Brightness Temperature
TmpFile2$ = OutPath$ + "SHADOW_E.TMP"       '---Emissivity
TmpFile3$ = OutPath$ + "SHADOW_P.TMP"       '---PRT-5 Temperature
COLOR 12: LOCATE 28, 1: PRINT "Initializing Binary Files...": COLOR 7
IF T.Flag% = 1 THEN CALL InitializeFile(2, OutFile1$, TmpFile1$)
IF E.Flag% = 1 THEN CALL InitializeFile(4, OutFile2$, TmpFile2$)
LOCATE 28, 1: PRINT SPACE$(80): COLOR 2
LOCATE 28, 1: PRINT "Current Nadir:   x =          y =       "

'---Record binary image file(s).
FOR I = 1 TO NumFiles

    '---Open input file & import header information.
    OPEN Filename$(I) FOR INPUT AS #1
    INPUT #1, dayOfYear%, description$, passNo%, Alt, unknown%
    COLOR 7: LOCATE 1, 14: PRINT USING "###"; dayOfYear%
    LOCATE 1, 25: PRINT USING "####.#m"; Alt
    LOCATE 1, 41: PRINT USING "#"; passNo%
    LOCATE 1, 51: PRINT description$: COLOR 7

    '---Process data.
    WHILE NOT EOF(1)

        '---Import PBMR / PRT-5 data (Array subscripts 1-4 are PBMR
        '---data, and subscript 5 is the corresponding PRT-5 data.
        FOR J = 1 TO 5
            INPUT #1, xBeam(J), yBeam(J), Temp(J)
        NEXT J

        '---Report current aircraft position on graphics screen
        '---(PRT-5 beam center is the nadir).
        LOCATE 28, 22: PRINT USING "#####.#"; xBeam(5)
        LOCATE 28, 36: PRINT USING "#####.#"; yBeam(5)

        '---Call subroutine to build requested imagery;
        '---Brightness temperature imagery option.
        IF T.Flag% = 1 THEN
            FOR J = 1 TO 4
                CALL BuildImage(J, 2, Temp(J))
```

```
            NEXT J
        END IF
        '---IF emissivity image requested, compute emissivities for
        '---4 PBMR beams using the PRT-5 as an estimate for the area
        '---surface temperature and pass this value to the subroutine.
        '---Note that PRT-5 Temp is in 'C and must be converted to 'K.
        IF E.Flag% = 1 THEN
            FOR J = 1 TO 4
                IF Temp(5) <> 0 THEN
                    e = (Temp(J) / (Temp(5) + 273.15))
                ELSE
                    e = 0
                END IF
                CALL BuildImage(J, 4, e)
            NEXT J
        END IF

    WEND: CLOSE #1

NEXT I


'---Close files, clean up, restore screen, end program.
CLOSE
IF T.Flag% = 1 THEN KILL TmpFile1$
IF E.Flag% = 1 THEN KILL TmpFile2$
IF BatchFile$ = "" THEN
    LOCATE 28, 1: PRINT SPACE$(80): COLOR 12
    LOCATE 28, 1: PRINT "Finished Processing...Press Any Key"
    WHILE INKEY$ = "": WEND
END IF: SCREEN 0: CLS : END




SUB BuildImage (J AS INTEGER, FileNum AS INTEGER, Value.Now AS SINGLE)

    '-------------------------------------------------------------
    ' Subroutine to determine view area of beam and assign the data value
    ' associated with the beam to the grid node (or update the average of
    ' all beams to this point that view a given grid node)
    '-------------------------------------------------------------

    DIM x AS LONG, y AS LONG
    DIM xLo AS INTEGER, xHi AS INTEGER
    DIM yLo AS INTEGER, yHi AS INTEGER
```

```
'---Determine view radius of current PBMR beam.
SELECT CASE J
    CASE 1: Rng = (.34 * Alt) / 2: col = 9
    CASE 2: Rng = (.29 * Alt) / 2: col = 12
    CASE 3: Rng = (.29 * Alt) / 2: col = 10
    CASE 4: Rng = (.34 * Alt) / 2: col = 14
    CASE 5: Rng = .04 * Alt: col = 15
END SELECT

'---Display current beam's nominal view area on graphics screen.
CIRCLE (xBeam(J), yBeam(J)), Rng, col

'---Skip if beam information is outside desired image area.
IF (xBeam(J) + Rng) < xMin OR (xBeam(J) - Rng) > xMax THEN EXIT SUB
IF (yBeam(J) + Rng) < yMin OR (yBeam(J) - Rng) > yMax THEN EXIT SUB

'----Identify "search box" about the current beam view area.
xLo = (INT(ABS(xBeam(J) - Rng - Grd)) - (INT(ABS(xBeam(J) - Rng - Grd)) MOD Grd)) * SGN(xBeam(J) - Rng - Grd)
xHi = (INT(ABS(xBeam(J) + Rng + Grd)) - (INT(ABS(xBeam(J) + Rng + Grd)) MOD Grd)) * SGN(xBeam(J) + Rng + Grd)
yLo = (INT(ABS(yBeam(J) - Rng - Grd)) - (INT(ABS(yBeam(J) - Rng - Grd)) MOD Grd)) * SGN(yBeam(J) - Rng - Grd)
yHi = (INT(ABS(yBeam(J) + Rng + Grd)) - (INT(ABS(yBeam(J) + Rng + Grd)) MOD Grd)) * SGN(yBeam(J) + Rng + Grd)

'---If necessary, trim search box to image's edge.
IF xLo < xMin THEN xLo = xMin
IF xHi > xMax THEN xHi = xMax
IF yLo < yMin THEN yLo = yMin
IF yHi > yMax THEN yHi = yMax

'---Inspect all grid nodes inside the search box.
'---   NOTE: Y-coordinate axis direction is reversed in the image file
'---   to maintain compatiblity with IDRISI conventions.
FOR y = yLo TO yHi STEP Grd
    FOR x = xLo TO xHi STEP Grd
        '---Euclidian distance, current beam center to current grid node.
        Dist = SQR((xBeam(J) - x) ^ 2 + (yBeam(J) - y) ^ 2)
        '---Is radial distance <= range? If so, record.
        IF Dist <= Rng THEN
            '---Current binary file position.
            Byte& = ((yMax - y) / Grd) * xSize + ((x - xMin) / Grd)
            Byte& = 4 * Byte& + 1
            '---Call up current image data.
            GET FileNum, Byte&, Value.Old
            GET FileNum + 1, Byte&, Obs
            '---Average node value; weight according to number
            '---of observations of this node up to this point.
            Obs = Obs + 1
            Value.New = ((1 / Obs) * Value.Now) + (((Obs - 1) / (Obs)) * Value.Old)
            '---Update binary image file.
            PUT FileNum, Byte&, Value.New
            PUT FileNum + 1, Byte&, Obs
```

```
            END IF
        NEXT x
    NEXT y

END SUB



SUB Explain

    '-------------------------------------------------------------
    ' Subroutine to explain DISTRIB to user.  This subroutine is invoked
    ' by typing "DISTRIB ? [ENTER]" at the DOS command prompt.
    '-------------------------------------------------------------

    '---Initialize user interface.
    CLS : COLOR Banner.Color: BOX 1, 80, 1, 3, 2: COLOR Dialog.Color
    LOCATE 2, 3: PRINT "IDRISI : Distribute PBMR data to binary image file                v.3.00"
    VIEW PRINT 5 TO 24

    '---Provide information about DISTRIB program.
    COLOR Banner.Color: BOX 5, 76, 5, 8, 1
    LOCATE 6, 11: PRINT "          Developed by  William E. Nichols, 1989          "
    LOCATE 7, 11: PRINT "Water Resources Engineering Team  /  Oregon State University"
    LOCATE 10, 1: COLOR Dialog.Color
    PRINT "DISTRIB distributes PBMR data to a binary image file.  POINT must first be"
    PRINT "used to create a ground coordinate registered PBMR data file(s), after which"
    PRINT "DISTRIB may be invoked to image the data."
    PRINT
    PRINT "To aid in visualizing the image creation process the PBMR beams are mapped"
    PRINT "on a VGA graphics screen as data are processed.  The image area is indicated"
    PRINT "as a highlighted rectangle.  The dimensions of the viewing area can be "
    PRINT "customized to meet user needs by adjusting the DISTRIB.CFG configuration file."
    PRINT "DISTRIB.CFG contents are: Minimum X; Maximum X; Minimum Y; Maximum Y; and."
    PRINT "tick spacing."
    PRINT
    PRINT "DISTRIB assumes a .REG extension for input data files and assigns a .IMG"
    PRINT "extension to the binary image file it creates."
    LOCATE 22, 1: END

END SUB
```

```
SUB InitializeFile (FileNum AS INTEGER, Out.File$, Tmp.File$)

    '-------------------------------------------------------------
    '   Subroutine to initialize binary image file and a corresponding
    '  "shadow file" used to track number of times a given grid node is
    '   viewed by a given sensor (used to prevent weighted averaging).
    '-------------------------------------------------------------

    '---Open image and shadow files in binary mode.
    OPEN Out.File$ FOR BINARY AS (FileNum)
    OPEN Tmp.File$ FOR BINARY AS (FileNum + 1)

    Zero = 0!                                   '---Initial value of zero
    rowStr$ = SPACE$(4 * xSize)                 '---Complete row of values

    '---Write first row of values.
    FOR I = 1 TO xSize STEP 4
        PUT FileNum, , Zero
    NEXT I

    '---Read the row back into a string and set pointer to start of file.
    GET FileNum, 1, rowStr$: SEEK FileNum, 1

    '---Write string value for all rows in both image & shadow files.
    FOR I = 1 TO ySize
        PUT FileNum, , rowStr$
        PUT FileNum + 1, , rowStr$
    NEXT I

    '---Initialization completed.

END SUB



SUB InitializeGraf

    '-------------------------------------------------------------
    ' Subroutine to initialize graphics display screen used to display
    ' in a map format the programs progress in PBMR/PRT-5 data processing.
    ' Values for display area are read from a DISTRIB configuration file.
    '-------------------------------------------------------------
    ' NOTE TO PROGRAMMERS:  Only this subroutine needs changed to adjust
    '    the program to use a different graphics standard than VGA.
    '-------------------------------------------------------------
```

```
    '---Get DISTRIB graphics configuration information.
    OPEN "DISTRIB.CFG" FOR INPUT AS #1
    INPUT #1, Min.X.View, Max.X.View, Min.Y.View, Max.Y.View, Inc.Axis
    CLOSE #1

    '---Graphics display initialization.
    SCREEN 12: CLS : VIEW (5, 20)-(635, 425), , 7
    WINDOW (Min.X.View, Min.Y.View)-(Max.X.View, Max.Y.View): COLOR 7
    LINE (Min.X.View, 0)-(Max.X.View, 0): LINE (0, Min.Y.View)-(0, Max.Y.View)
    FOR x% = (Min.X.View + Inc.Axis) TO (Max.X.View - Inc.Axis) STEP Inc.Axis
        LINE (x%, -(Inc.Axis / 4))-(x%, (Inc.Axis / 4))
    NEXT x%
    FOR y% = (Min.Y.View + Inc.Axis) TO (Max.Y.View + Inc.Axis) STEP Inc.Axis
        LINE (-(Inc.Axis / 4), y%)-((Inc.Axis / 4), y%)
    NEXT y%
    LINE (xMin, yMin)-(xMax, yMax), 7, BF: COLOR 2
    LOCATE 1, 70: PRINT "DISTRIB 1.0"
    LOCATE 1, 1: PRINT "Day of Year:      Alt:          Pass:     Site: "

END SUB
```

```
'
'  UNPACK.BAS
'                                        Last Modified: 29 Aug 1989 (WEN)
'
'  Program to convert binary image files created with QuickBASIC 4.5
'  programs (i.e. IEEE Binary) to ASCII files.  UNPACK is an add-on
'  IDRISI Version 3.0 module.
'
'  MAKEMASK was written and compiled in Microsoft QuickBASIC 4.5 using
'  IBM PS/2 computers (Models 30-286, 50, and 70).
'
'  Developed by : William E. Nichols, 1989
'  Organization : Water Resources Engineering Team
'                 Oregon State University, Corvallis, Oregon
'  Project :      USDA-ARS Cooperative Research Project
'

'---Initialize program environment.
REM $INCLUDE: 'IDRISI.ICL'          'IDRISI User Library
CALL Read.ENV.File

'---Obtain available operation information from command line.
cTot$ = COMMAND$
FOR I = 1 TO LEN(cTot$)
    c$ = MID$(cTot$, I, 1)
    IF c$ <> " " THEN
        J = J + 1: IF J = 1 THEN k = k + 1
        SELECT CASE k
            CASE 1: Old.Image$ = Old.Image$ + c$
            CASE 2: New.Image$ = New.Image$ + c$
        END SELECT
    ELSE
        J = 0
    END IF
NEXT I

'---Check if required information was found.
IF Old.Image$ = "" OR New.Image$ = "" THEN
    CLS : COLOR Banner.Color: BOX 1, 80, 1, 3, 2
    COLOR Dialog.Color: LOCATE 2, 3
    PRINT "IDRISI : IEEE Binary to ASCII file conversion                    v.3.00"
    VIEW PRINT 5 TO 23
    COLOR Dialog.Color
    PRINT "Enter the name of the binary file to convert"; TAB(55); ": ";
    INPUT "", Old.Image$
    PRINT "Enter the name of the ASCII file (may be the same)"; TAB(55); ": ";
    INPUT "", New.Image$
```

```
        PRINT : PRINT "Does this image have a .DOC file yet?"; TAB(55); ": ";
        INPUT "", resp$
    END IF

    '---Make a documentation file if necessary.
    IF UCASE$(resp$) <> "Y" THEN
        PRINT
        PRINT "Are data integer [0] or real [1]?"; TAB(55); ": ";
        INPUT "", New.Data.Type
        New.File.Type = 3            '---Indicate IEEE Binary storage
        PRINT
        INPUT "Enter the number of rows    : ", rows
        INPUT "Enter the number of columns : ", cols
        INPUT "Enter the cell x dimension  : ", cellX
        INPUT "Enter the cell y dimension  : ", cellY
        PRINT
        PRINT "Please enter a title for this image : "
        INPUT "", Title$: IF Title$ = "" THEN Title$ = "<none>": PRINT
        CALL Make.DOC.File
        IF Old.Image$ <> New.Image$ THEN
            NAME (Drive$ + Path$ + New.Image$ + Image.DocFile.Extension$) AS (Drive$ + Path$ + Old.Image$ +
Image.DocFile.Extension$)
        END IF
    END IF

    '---Check if input file is correct (IEEE Binary).
    CALL Read.DOC.File
    IF Old.File.Type <> 3 THEN
        LOCATE , 1: PRINT SPACE$(40): COLOR Message.Color
        LOCATE 21, 1: PRINT "ERROR : This module for IEEE binary files only."
        PRINT : END
    END IF

    '---Open I/O files.
    Img.File.1$ = Drive$ + Path$ + Old.Image$ + Image.File.Extension$
    OPEN Img.File.1$ FOR BINARY AS #1
    IF Old.Image$ = New.Image$ OR New.Image$ = "" THEN
        Img.File.2$ = Drive$ + Path$ + "UNPACK00" + Image.File.Extension$
    ELSE
        Img.File.2$ = Drive$ + Path$ + New.Image$ + Image.File.Extension$
    END IF: OPEN Img.File.2$ FOR OUTPUT AS #2

    '---Input data from IEEE binary file and output to ASCII file.
    COLOR Message.Color: PRINT : PRINT "working ... ";
    SELECT CASE Old.Data.Type
        CASE 0                                   '---Integer data
            WHILE NOT EOF(1)
                GET #1, , Intgr%
                WRITE #2, Intgr%
                IF Intgr% > max THEN max = Intgr%
```

```
            IF Intgr% < min THEN min = Intgr%
        WEND
    CASE 1                                      '---Real data
        WHILE NOT EOF(1)
            GET #1, , Real!
            WRITE #2, Real!
            IF Real! > max THEN max = Real!
            IF Real! < min THEN min = Real!
        WEND
    CASE ELSE
        LOCATE , 1: PRINT SPACE$(40): COLOR Message.Color
        LOCATE 21, 1: PRINT "ERROR : Data must be real or integer."
        PRINT : END
END SELECT

'---Close I/O files.
CLOSE #1: CLOSE #2

'---Open I/O files.
IF Old.Image$ = New.Image$ OR New.Image$ = "" THEN
    KILL (Drive$ + Path$ + Old.Image$ + Image.DocFile.Extension$)
    KILL Img.File.1$
    NAME Img.File.2$ AS Img.File.1$
END IF

'---Write new image documentation file.
New.Data.Type = Old.Data.Type
New.File.Type = 0
CALL Make.DOC.File

'---Exit to DOS.
LOCATE , 1: PRINT SPACE$(40)
IF Old.Image$ <> "" THEN
    COLOR Message.Color
    LOCATE 21, 1: PRINT "UNPACK execution completed."
END IF: PRINT : END
```

```
'
'   MAKEMASK.BAS
'                                          Last Modified:  7 Sep 1989 (WEN)
'
'   Program to generate a query mask for extracting image information
'   from within known linear boundaries.  MAKEMASK is an add-on IDRISI
'   Version 3.0 module.
'
'   MAKEMASK was written and compiled in Microsoft QuickBASIC 4.5 using
'   IBM PS/2 computers (Models 30-286, 50, and 70).
'
'   Developed by : William E. Nichols, 1989
'   Organization : Water Resources Engineering Team
'                  Oregon State University, Corvallis, Oregon
'   Project :      USDA-ARS Cooperative Research Project
'

'---Initialize program environment.
DECLARE SUB Set.Mask ()
REM $INCLUDE: 'IDRISI.ICL'              '---IDRISI User's Library

'---Initialize user interface.
CALL Read.ENV.File
CLS : COLOR Banner.Color: BOX 1, 80, 1, 3, 2
COLOR Dialog.Color: LOCATE 2, 3
PRINT "IDRISI : Query mask generation from linear boundaries                v.3.00"
VIEW PRINT 5 TO 24

'---Attempt to open a named query mask image .DOC file.  If not found,
'   ask user if he/she wishes to create it and proceed accordingly.
ON ERROR GOTO FileNotFound
INPUT "Enter the name of the mask image : ", Old.Image$
docName$ = Drive$ + Path$ + Old.Image$ + Image.DocFile.Extension$
OPEN docName$ FOR INPUT AS #1
CLOSE #1
ON ERROR GOTO 0

'---Read document file and display contents.
CALL Read.DOC.File
COLOR Dialog.Color: PRINT : PRINT "image title : "; Title$
PRINT "data type   : ";
    IF New.Data.Type = 0 THEN PRINT "integer"
    IF New.Data.Type = 1 THEN PRINT "real"
    IF New.Data.Type = 2 THEN PRINT "byte"
PRINT "file type   : ";
    IF New.File.Type = 0 THEN PRINT "ascii"
    IF New.File.Type = 1 THEN PRINT "binary"
    IF New.File.Type = 2 THEN PRINT "packed binary"
    IF New.File.Type = 3 THEN PRINT "IEEE Binary"
```

```
    PRINT "rows       : "; rows
    PRINT "columns    : "; cols
    PRINT "minimum    : "; min
    PRINT "maximum    : "; max
    PRINT "cell x     : "; cellX
    PRINT "cell y     : "; cellY
    PRINT : INPUT "Proceed with this image? <Y/N> : ", resp$
    IF UCASE$(resp$) = "N" THEN CLS : END

    '---Input query boundaries and modify binary image file accordingly.
    CALL Set.Mask

    END



FileNotFound:
    BEEP: CLS 2
    PRINT "File "; UCASE$(Old.Image$); " not found! . . . Create it? <Y/N> : ";
    INPUT "", resp$
    SELECT CASE UCASE$(resp$)
        CASE "Y":
            '---Record mask image .DOC file.
            New.Image$ = Old.Image$       '---New image base filename
            New.File.Type = 3             '---IEEE binary storage
            New.Data.Type = 0             '---Integer data
            PRINT
            INPUT "Enter the number of rows    : ", rows
            INPUT "Enter the number of columns : ", cols
            INPUT "Enter the cell x dimension  : ", cellX
            INPUT "Enter the cell y dimension  : ", cellY
            PRINT
            PRINT "Please enter a new title for the mask image being created : "
            INPUT "", Title$: IF Title$ = "" THEN Title$ = "<none>": PRINT
            CALL Make.DOC.File
            '---Initialize query mask .IMG file.
            COLOR Message.Color: PRINT
            PRINT "Initializing Binary Files..."
            OPEN (Drive$ + Path$ + Old.Image$ + Image.File.Extension$) FOR BINARY AS #2
            Zero% = 0: rowStr$ = SPACE$(2 * cols)
            FOR x = 1 TO cols
                PUT #2, , Zero%
            NEXT x
            GET #2, 1, rowStr$: SEEK #2, 1
            FOR y = 1 TO rows
                PUT #2, , rowStr$
            NEXT y
            CLOSE #2: CLS 2: RESUME NEXT
```

```
        CASE "N": CLS 2: INPUT "Enter the name of the mask image : ", Old.Image$
            CLS 2: RESUME
        CASE ELSE: GOTO FileNotFound
    END SELECT




SUB Set.Mask

    '_____________________________________________________________
    '  Subroutine to input query boundaries and modify binary image file
    '_____________________________________________________________

    'SUBROUTINE COMMENTS
    '
    '---VECTOR VARIABLES EXPLANATION
    '
    '  Points are stored in array P(,) where the first subscript
    '  identifies the point number (as entered by user), and the second
    '  subscript refers to axis (1 = x coordinate, 2 = y coordinate).
    '
    '  Lines information is stored in array L(,) where the first
    '  subscript refers to line number and the second subscript refers to
    '  constant (1 = slope, 2 = intercept).  The equation of any line is
    '  given by:
    '
    '        Y = mX + b,      where m = slope and b = intercept.
    '
    '  In this subroutine line numbers are assigned based on point order;
    '
    '     Line 1 = line between points 1 & 2
    '     Line 2 = line between points 2 & 3
    '     Line 3 = line between points 3 & 4
    '     Line 4 = line between points 4 & 5
    '
    '  Point 5 is assigned the coordinates of Point 1 for convienience
    '  in looping structures (and hence does not represent a new point).
    '
    '  The Bound(,) array is used to identify those polygon edges (lines)
    '  that bound a plane in which the current cell resides.  The first
    '  subscript is the line number, following the standard given above.
    '  The second subscript is the plane (1 = y plane, 2 = y plane).  A
    '  value of zero in the array indicates the given line does not bound
    '  the current cell in the given plane, while a value of one indicates
    '  that it is a boundary.
    '
    '
```

```
'---SEARCH ALGORITHM COMMENTS
'
'   The subroutine handles one four-sided polygon at a time, converting
'   the cell values of the image to the selected mask value for all
'   cells within the polygon.  The first step is to determine a "search
'   box" about the polygon.  This is done strictly for speed, since every
'   cell in the image could be tested also.  Next, for every cell in the
'   search box the cell's center coordinate is tested to determine if it
'   is inside the polygon (or on a line defining the polygon).  This
'   rasterization process requires computation of the equations of the
'   four lines defining the polygon, which are subsequently used to
'   construct maximum and minimum ranges in both axes in the plane of the
'   grid node in question; if the node is within the range, it is in the
'   polygon.  Positive search results in modification of the binary
'   image file in use.
'

DIM I AS INTEGER, J AS INTEGER, K AS INTEGER
DIM P(5, 2), L(4, 2), Bound(4, 2) AS INTEGER

OPEN (Drive$ + Path$ + Old.Image$ + Image.File.Extension$) FOR BINARY AS #2

CLS 2: COLOR Dialog.Color
PRINT "Select query windows that can be defined by linear boundaries between four   "
PRINT "SUCCESSIVE points.  For each query window, enter the new (nonzero) integer   "
PRINT "mask value and the four coordinates.  All grid cells within and on the       "
PRINT "boundaries will be assigned the mask value.  For more complex windows, repeat"
PRINT "this process using less complex sub-windows to complete the mask image.  To  "
PRINT "finish, enter a '-1' value for the mask value.  Use ACTUAL COORDINATES for"
PRINT "the points (not cell addresses); remember that IDRISI transposes the Y-axis."
PRINT : PRINT : PRINT


DO
    '---Input four points defining boundary lines.
    COLOR Dialog.Color
    INPUT "Assign a mask value of     : ", Mask%
    IF Mask% = -1 THEN EXIT DO
    PRINT "to cells within the polygon defined by these four successive point coordinates "
    FOR K = 1 TO 4
        PRINT
        PRINT USING "   Point No. #   x : "; K; : INPUT "", P(K, 1)
        PRINT "                 y : "; : INPUT "", P(K, 2)
    NEXT K: PRINT
    COLOR Message.Color: PRINT "Processing . . . "
    P(5, 1) = P(1, 1): P(5, 2) = P(1, 2)
    GOSUB Modify
LOOP: CLOSE #2

EXIT SUB
```

```
Modify:
    '---Define a "search box" of within image.
    FOR K = 1 TO 4
        IF P(K, 1) > xMax THEN xMax = P(K, 1)       '---Maximum x point
        IF P(K, 2) > yMax THEN yMax = P(K, 2)       '---Maximum y point
    NEXT K: xMin = xMax: yMin = yMax
    FOR K = 1 TO 4
        IF P(K, 1) < xMin THEN xMin = P(K, 1)       '---Minimum x point
        IF P(K, 2) < yMin THEN yMin = P(K, 2)       '---Minimum y point
    NEXT K

    '---Determine cell ranges of search box.
    x.Min.Cell = INT(xMin / cellX)
    x.Max.Cell = INT(xMax / cellX) + 1
    y.Min.Cell = INT(yMin / cellY)
    y.Max.Cell = INT(yMax / cellY) + 1

    '---Determine slopes & intercepts of four polygon boundary lines.
    FOR K = 1 TO 4
        '---If a vertical line occurs the slope is undefined and would
        '   cause an error, so a vertical line is adjusted to a slightly
        '   non-vertical slope to prevent this problem.
        IF P(K + 1, 1) - P(K, 1) = 0 THEN
            L(K, 1) = .0001
        ELSE
            L(K, 1) = (P(K + 1, 2) - P(K, 2)) / (P(K + 1, 1) - P(K, 1))
        END IF
        L(K, 2) = (P(K, 2) - L(K, 1) * P(K, 1))
    NEXT K

    '---Replace background image cells on and within boundaries
    '   with new query mask value specified by user.
    FOR J = y.Min.Cell TO y.Max.Cell

        y = J * cellY - (cellY / 2)

        FOR I = x.Min.Cell TO x.Max.Cell

            x = I * cellX - (cellX / 2)

            '---Reset Bound(,) array.
            FOR K = 1 TO 4: Bound(K, 1) = 0: Bound(K, 2) = 0: NEXT K

            '---Which lines are bounding in planes of current cell?
            FOR K = 1 TO 4
                '---Lines bounding in y-direction
                IF ABS(x - P(K, 1)) < ABS(P(K + 1, 1) - P(K, 1)) THEN
                    IF ABS(x - P(K + 1, 1)) < ABS(P(K + 1, 1) - P(K, 1)) THEN
                        Bound(K, 1) = 1
                    END IF
```

```
    END IF
    '---Lines bounding in x-direction.
    IF ABS(y - P(K, 2)) < ABS(P(K + 1, 2) - P(K, 2)) THEN
        IF ABS(y - P(K + 1, 2)) < ABS(P(K + 1, 2) - P(K, 2)) THEN
            Bound(K, 2) = 1
        END IF
    END IF
NEXT K

'---If not bounded by two lines, then skip to next cell.
xTot = 0: yTot = 0
FOR K = 1 TO 4
    xTot = xTot + Bound(K, 1)
    yTot = yTot + Bound(K, 2)
NEXT K
IF xTot <> 2 OR yTot <> 2 THEN GOTO NextCell

'---Determine points on bounding lines in the x-dimension
'   of the current cell (the line connecting opposite
'   points on the polygon in this plane is the 'x-range')
y.Limit.Lo = yMax: y.Limit.Hi = yMin
FOR K = 1 TO 4
    IF Bound(K, 1) = 1 THEN
        '---For known x, find y; (Y = mX + b).
        y.Limit = (L(K, 1) * x) + L(K, 2)
        IF y.Limit < y.Limit.Lo THEN y.Limit.Lo = y.Limit
        IF y.Limit > y.Limit.Hi THEN y.Limit.Hi = y.Limit
    END IF
NEXT K

'---Determine points on bounding lines in the y-plane
'   of the current cell (the line connecting opposite
'   points on the polygon in this plane is the 'y-range')
x.Limit.Lo = xMax: x.Limit.Hi = xMin
FOR K = 1 TO 4
    IF Bound(K, 2) = 1 THEN
        '---For known y, find x; (X = Y/m - b).
        x.Limit = (y - L(K, 2)) / L(K, 1)
        IF x.Limit < x.Limit.Lo THEN x.Limit.Lo = x.Limit
        IF x.Limit > x.Limit.Hi THEN x.Limit.Hi = x.Limit
    END IF
NEXT K

'---Perform logical consistency tests on planar limits.
IF x.Limit.Hi < x.Limit.Lo THEN
    COLOR Message.Color: PRINT
    PRINT "ERROR: failure computing polygon x range."
    STOP
ELSEIF y.Limit.Hi < y.Limit.Lo THEN
    COLOR Message.Color: PRINT
```

```
            PRINT "ERROR: failure computing polygon y range."
            STOP
        END IF

        '---Check if current grid node is within both ranges;
        '   if so (ie. if grid cell is inside polygon) then
        '   continue.  Otherwise proceed to next grid cell.
        IF x < x.Limit.Lo OR x > x.Limit.Hi THEN GOTO NextCell
        IF y < y.Limit.Lo OR y > y.Limit.Hi THEN GOTO NextCell

        '---Cell is within query window; replace value with
        '   query value specified by the user.
        Byte& = (J - 1) * cols + (I - 1)
        Byte& = 2 * Byte& + 1
        PUT #2, Byte&, Mask%

NextCell:
        NEXT I
    NEXT J: PRINT : PRINT : PRINT
    RETURN

END SUB
```

```
'
'    IDRISI LIBRARY                                  Last Update: 28 Aug 1989
'
'    QuickBASIC 4.5 software development tool kit for use in building
'    new IDRISI 3.0 modules.
'
'    Developed by.....William E. Nichols, 1989
'    Organization.....Water Resources Engineering Team
'                     Oregon State University, Corvallis, Oregon
'    Project.....USDA-ARS Cooperative Agreement
'
```

```
    REM $INCLUDE: 'IDRISI.ICL'
```

```
SUB BOX (leftCol%, rightCol%, topRow%, bottomRow%, Lines%)

    '-----------------------------------------------------------
    '  Routine to draw a box using ASCII extended characters, given the
    '  top & bottom row and the left & right columns and number of lines
    '-----------------------------------------------------------

    '----Print the four corners;
    LOCATE topRow%, leftCol%:     IF Lines% = 1 THEN PRINT CHR$(218) ELSE PRINT CHR$(201)
    LOCATE topRow%, rightCol%:    IF Lines% = 1 THEN PRINT CHR$(191) ELSE PRINT CHR$(187)
    LOCATE bottomRow%, leftCol%:  IF Lines% = 1 THEN PRINT CHR$(192);  ELSE PRINT CHR$(200);
    LOCATE bottomRow%, rightCol%: IF Lines% = 1 THEN PRINT CHR$(217);  ELSE PRINT CHR$(188);

    '----Print the vertical lines;
    FOR vertLine% = topRow% + 1 TO bottomRow% - 1
        LOCATE vertLine%, leftCol%:  IF Lines% = 1 THEN PRINT CHR$(179);  ELSE PRINT CHR$(186);
        LOCATE vertLine%, rightCol%: IF Lines% = 1 THEN PRINT CHR$(179);  ELSE PRINT CHR$(186);
    NEXT vertLine%

    '----Print the horizontal lines;
    horizLength% = rightCol% - leftCol% - 1
    IF Lines% = 1 THEN
        horizline$ = STRING$(horizLength%, 196)
    ELSE
```

```
        horizline$ = STRING$(horizLength%, 205)
    END IF: LOCATE topRow%, leftCol% + 1: PRINT horizline$
    LOCATE bottomRow%, leftCol% + 1: PRINT horizline$;

END SUB




SUB Make.DOC.File

    '-------------------------------------------------------------
    '     Subroutine to create new IDRISI .DOC (Documentation) file
    '-------------------------------------------------------------

    DocName$ = Drive$ + Path$ + New.Image$ + Image.DocFile.Extension$
    OPEN DocName$ FOR OUTPUT AS #1

    PRINT #1, "image title : "; Title
    IF New.Data.Type = 0 THEN PRINT #1, "data type   : integer"
    IF New.Data.Type = 1 THEN PRINT #1, "data type   : real"
    IF New.Data.Type = 2 THEN PRINT #1, "data type   : byte"
    IF New.File.Type = 0 THEN PRINT #1, "file type   : ascii"
    IF New.File.Type = 1 THEN PRINT #1, "file type   : binary"
    IF New.File.Type = 2 THEN PRINT #1, "file type   : packed binary"
    IF New.File.Type = 3 THEN PRINT #1, "file type   : IEEE binary"
    PRINT #1, "rows        : "; rows
    PRINT #1, "columns     : "; cols
    PRINT #1, "minimum     : "; min
    PRINT #1, "maximum     : "; max
    PRINT #1, "cell x      : "; cellX
    PRINT #1, "cell y      : "; cellY
    PRINT #1, "legend      : "; Legend

    IF Legend <> 0 THEN
        REDIM Legend.Text(Legend) AS STRING
        FOR I = 1 TO Legend
            PRINT #1, "category";
            PRINT #1, USING "###"; I;
            PRINT #1, " : "; Legend.Text(I)
        NEXT I
    END IF

    CLOSE #1

END SUB
```

```
SUB Read.DOC.File

    '-------------------------------------------------------------
    '  Subroutine to read contents of the IDRISI .DOC (Documentation) file
    '-------------------------------------------------------------

    DocName$ = Drive$ + Path$ + Old.Image$ + Image.DocFile.Extension$
    OPEN DocName$ FOR INPUT AS #1

    LINE INPUT #1, description$
        Title$ = RIGHT$(description$, LEN(description$) - 14)
    LINE INPUT #1, description$
        description$ = RIGHT$(description$, LEN(description$) - 14)
        IF description$ = "integer" THEN Old.Data.Type = 0
        IF description$ = "real" THEN Old.Data.Type = 1
        IF description$ = "byte" THEN Old.Data.Type = 2
    LINE INPUT #1, description$
        description$ = RIGHT$(description$, LEN(description$) - 14)
        IF description$ = "ascii" THEN Old.File.Type = 0
        IF description$ = "binary" THEN Old.File.Type = 1
        IF description$ = "packed binary" THEN Old.File.Type = 2
        IF description$ = "IEEE binary" THEN Old.File.Type = 3
    LINE INPUT #1, description$
        rows = VAL(RIGHT$(description$, LEN(description$) - 14))
        LINE INPUT #1, description$
        cols = VAL(RIGHT$(description$, LEN(description$) - 14))
    LINE INPUT #1, description$
        min = VAL(RIGHT$(description$, LEN(description$) - 14))
    LINE INPUT #1, description$
        max = VAL(RIGHT$(description$, LEN(description$) - 14))
    LINE INPUT #1, description$
        cellX = VAL(RIGHT$(description$, LEN(description$) - 14))
    LINE INPUT #1, description$
        cellY = VAL(RIGHT$(description$, LEN(description$) - 14))
    LINE INPUT #1, description$
        Legend = VAL(RIGHT$(description$, LEN(description$) - 14))

    IF Legend <> 0 THEN
        REDIM Legend.Text(Legend) AS STRING
        FOR I = 1 TO Legend
            LINE INPUT #1, description$
            Legend.Text(I) = RIGHT$(description$, LEN(description$) - 14)
        NEXT I
    END IF

    CLOSE #1

END SUB
```

```
SUB Read.ENV.File

    '-------------------------------------------------------------
    '  Subroutine to read contents of the IDRISI .ENV (Environment) file
    '-------------------------------------------------------------

    OPEN "IDRISI.ENV" FOR INPUT AS #1

    LINE INPUT #1, description$
    LINE INPUT #1, description$
    LINE INPUT #1, description$
        Drive$ = RIGHT$(description$, LEN(description$) - 40)
    LINE INPUT #1, description$
        Path$ = RIGHT$(description$, LEN(description$) - 40)
    LINE INPUT #1, description$
        Vector.DocFile.Extension$ = RIGHT$(description$, LEN(description$) - 40)
    LINE INPUT #1, description$
        Image.DocFile.Extension$ = RIGHT$(description$, LEN(description$) - 40)
    LINE INPUT #1, description$
        Image.File.Extension$ = RIGHT$(description$, LEN(description$) - 40)
    LINE INPUT #1, description$
        Vector.File.Extension$ = RIGHT$(description$, LEN(description$) - 40)
    LINE INPUT #1, description$
        units$ = RIGHT$(description$, LEN(description$) - 40)
    LINE INPUT #1, description$
        Values.DocFile.Extension$ = RIGHT$(description$, LEN(description$) - 40)
    LINE INPUT #1, description$
        Values.File.Extension$ = RIGHT$(description$, LEN(description$) - 40)
    LINE INPUT #1, description$
        Banner.Color = VAL(RIGHT$(description$, LEN(description$) - 40))
    LINE INPUT #1, description$
        Dialog.Color = VAL(RIGHT$(description$, LEN(description$) - 40))
    LINE INPUT #1, description$
        Message.Color = VAL(RIGHT$(description$, LEN(description$) - 40))
    LINE INPUT #1, description$
        'TabletPort
    LINE INPUT #1, description$
        'PlotterPort

    CLOSE #1

END SUB
```

```
'
'   EVAPVIEW Version 1.0
'                                                  Last Update: 13 Sep 1989
'
'   EVAPVIEW is a graphically based program for use in data analysis &
'   selection.  EVAPVIEW imports 15-minute evaporative flux and
'   evaporative fraction data downloaded with SAMTRAN and presents the
'   data for inspection.
'
'   EVAPVIEW was written and compiled with Microsoft QuickBASIC 4.5 on
'   IBM PS/2 computers (Models 30/286, 50 and 70).
'
'   Developed by.....William E. Nichols, 1989
'   Organization.....Water Resources Engineering Team
'                    Oregon State University, Corvallis, Oregon
'   Project..........USDA-ARS - OSU Cooperative Research Project
'

DIM hour%(96), minute%(96), Rn(96), H(96), LE(96), G(96), evapFrac(96)

SCREEN 12
COLOR 12: LOCATE 1, 22: PRINT "SAMER Evaporative Fraction Data Check"
VIEW (5, 25)-(310, 225), , 15
VIEW (330, 25)-(635, 225), , 15
VIEW (430, 265)-(635, 465), , 15
VIEW (5, 50)-(310, 225), , 15
VIEW (330, 50)-(635, 225), , 15
VIEW (430, 290)-(635, 465), , 15
WINDOW (0, 0)-(1, 1): LINE (0, 0)-(1, 1), 7, , &H8888
LOCATE 3, 13:  PRINT "Energy Balance"
LOCATE 3, 51: PRINT "Evaporative Fraction"
LOCATE 18, 61: PRINT "Scatter Plot"

'---Open output files.
COLOR 2
LOCATE 19, 1: INPUT "Record all selected data in : ", Out.1$
LOCATE 21, 1: INPUT "Record cloud-free data in   : ", Out.2$
LOCATE 23, 1: INPUT "Input data file names       : ", BatchFile$
FOR I = 19 TO 21: LOCATE I, 1: PRINT SPACE$(45): NEXT I
LOCATE 16, 1: COLOR 7: PRINT "All-Weather : "; : COLOR 2: PRINT UCASE$(Out.1$)
LOCATE 17, 1: COLOR 7: PRINT "Cloud-Free  : "; : COLOR 2: PRINT UCASE$(Out.2$)
OPEN Out.1$ FOR OUTPUT AS #1
OPEN Out.2$ FOR OUTPUT AS #2
OPEN BatchFile$ FOR INPUT AS #3

WHILE NOT EOF(3)

    '---Get next input data file name.
    LINE INPUT #3, InFile$
```

```
        InFile$ = MID$(InFile$, 1, 12)
        COLOR 6: LOCATE 16, 68: PRINT UCASE$(InFile$);
        day% = VAL(MID$(InFile$, 5, 2))
        month% = VAL(MID$(InFile$, 7, 2))

        '---Input file contents.
        N = 1
        OPEN InFile$ FOR INPUT AS #4
        WHILE NOT EOF(4)
            INPUT #4, hour%(N), minute%(N), Rn(N), H(N), LE(N), G(N), evapFrac(N)
            N = N + 1
        WEND: CLOSE #4

        '---Remove data for periods where Rn ≤ 0 (Concentrate on daylight).
        FOR I = 1 TO N
            IF Rn(I) <= 0 THEN
                Rn(I) = -99
                LE(I) = -99
                H(I) = -99
                G(I) = -99
                evapFrac(I) = -99
            END IF
        NEXT I

        GOSUB ShowData

        '---Select this date?
Again:
        COLOR 2
        LOCATE 22, 1: PRINT "Choose appropriate option:"
        LOCATE 23, 1: PRINT "  [-1] = Reject; unsuitable for analysis"
        LOCATE 24, 1: PRINT "   [1] = Cloudfree database only"
        LOCATE 25, 1: PRINT "   [2] = Cloud-free & total databases"
        LOCATE 26, 1: PRINT "   [3] = Modify data"
        LOCATE 28, 1: INPUT "Action : ", choice%
        FOR I = 19 TO 28: LOCATE I, 1: PRINT SPACE$(40): NEXT I

        SELECT CASE choice%
            CASE -1
            CASE 1
                PRINT #1, month%, day%, Evap.Frac.Mid, Evap.Frac.Day
            CASE 2
                PRINT #1, month%, day%; Evap.Frac.Mid, Evap.Frac.Day
                PRINT #2, month%, day%, Evap.Frac.Mid, Evap.Frac.Day
            CASE 3
                LOCATE 23, 1: PRINT "Data Modification:"
                LOCATE 24, 1: PRINT "   No. of Points: "; N
                LOCATE 25, 1: PRINT
                LOCATE 26, 1: INPUT "Specify Point to remove: ", M
                IF M > N THEN GOTO Again
```

```
                FOR I = 20 TO 28: LOCATE I, 1: PRINT SPACE$(40): NEXT I
                Rn(M) = -99
                H(M) = -99
                LE(M) = -99
                G(M) = -99
                evapFrac(M) = -99
                GOSUB ShowData
                GOTO Again
            CASE ELSE
                GOTO Again
        END SELECT

        IF choice% = 1 OR choice% = 2 THEN
            VIEW (430, 290)-(635, 465), , 15: WINDOW (0, 0)-(2, 2)
            IF choice% = 1 THEN CIRCLE (Evap.Frac.Mid, Evap.Frac.Day), .02, 12
            IF choice% = 2 THEN CIRCLE (Evap.Frac.Mid, Evap.Frac.Day), .02, 10
        END IF

Next.Rec:

    WEND

    SCREEN 0: END



ShowData:

    '---Find evapFrac maximum and minimum for graphing.
    max = -100: min = 100
    FOR I = 1 TO N
        IF evapFrac(I) <> -99 THEN
            IF evapFrac(I) > max THEN max = evapFrac(I)
            IF evapFrac(I) < min THEN min = evapFrac(I)
        END IF
    NEXT I: range = max - min
    max = max + (range / 10): min = min - (range / 10)
    IF max = 0 THEN max = 1
    IF min >= max THEN max = min + 1

    '---Display energy balance terms in left side window.
    VIEW (5, 50)-(310, 225), , 15: WINDOW (0, -200)-(24, 800): CLS 1
    LINE (0, 0)-(24, 0), 7
    FOR I = 1 TO (N - 1)
        '---Compute current variable time.
        dt = hour%(I) + (minute%(I) / 60)
        '---Net radiation (Rn)
        IF Rn(I) <> -99 AND Rn(I + 1) <> -99 THEN
            LINE (dt - .25, Rn(I))-(dt, Rn(I + 1)), 12
        ELSEIF Rn(I) <> -99 AND Rn(I + 1) = -99 THEN
```

```
        CIRCLE (dt, Rn(I)), .1, 12
    END IF
    '---Sensible Heat Flux (H)
    IF H(I) <> -99 AND H(I + 1) <> -99 THEN
        LINE (dt - .25, H(I))-(dt, H(I + 1)), 14
    ELSEIF H(I) <> -99 AND H(I + 1) = -99 THEN
        CIRCLE (dt, H(I)), .1, 14
    END IF
    '---Latent Heat Flux (LE)
    IF LE(I) <> -99 AND LE(I + 1) <> -99 THEN
        LINE (dt - .25, LE(I))-(dt, LE(I + 1)), 9
    ELSEIF LE(I) <> -99 AND LE(I + 1) = -99 THEN
        CIRCLE (dt, LE(I)), .1, 9
    END IF
    '---Ground Heat Flux (G)
    IF G(I) <> -99 AND G(I + 1) <> -99 THEN
        LINE (dt - .25, G(I))-(dt, G(I + 1)), 11
    ELSEIF G(I) <> -99 AND G(I + 1) = -99 THEN
        CIRCLE (dt, G(I)), .1, 11
    END IF
NEXT I

'---Display evaporative fraction in right side window.
VIEW (330, 50)-(635, 225), , 15: WINDOW (0, min)-(24, max): CLS 1
LINE (0, 0)-(24, 0), 7
FOR I = 1 TO N
    dt = hour%(I) + (minute%(I) / 60)
    IF evapFrac(I) <> -99 AND evapFrac(I + 1) <> -99 THEN
        LINE (dt - .25, evapFrac(I))-(dt, evapFrac(I + 1)), 12
    ELSEIF evapFrac(I) <> -99 AND evapFrac(I + 1) = -99 THEN
        CIRCLE (dt, evapFrac(I)), .1, 12
    END IF
NEXT I

'---Compute All-day evaporative fraction value.
K = 0: L = 0
FOR I = 1 TO (N - 1)
    dt = hour%(I) + (minute%(I) / 60)
    IF evapFrac(I) <> -99 THEN
        IF dt < 11 OR dt > 13 THEN
            Evap.Frac.Day = Evap.Frac.Day + evapFrac(I)
            K = K + 1
        ELSEIF dt >= 11 AND dt <= 13 THEN
            Evap.Frac.Mid = Evap.Frac.Mid + evapFrac(I)
            L = L + 1
        END IF
    END IF
NEXT I
IF K <> 0 THEN Evap.Frac.Day = (Evap.Frac.Day / K) ELSE GOTO Next.Rec
IF L <> 0 THEN Evap.Frac.Mid = (Evap.Frac.Mid / L) ELSE GOTO Next.Rec
```

```
'---Display Statistics.
COLOR 7: LOCATE 19, 1: PRINT "All-Day EF: "; : COLOR 6: PRINT Evap.Frac.Day
COLOR 7: LOCATE 20, 1: PRINT "Mid-Day EF: "; : COLOR 6: PRINT Evap.Frac.Mid

RETURN
```

INDEX